Stitching interferometry for accurate measurement of curved surfaces

Citation for published version (APA):
Fan, Y. J. (1998). *Stitching interferometry for accurate measurement of curved surfaces*. [Phd Thesis 1 (Research TU/e / Graduation TU/e), Mechanical Engineering]. Technische Universiteit Eindhoven. https://doi.org/10.6100/IR512441

DOI:
10.6100/IR512441

Document status and date:
Published: 01/01/1998

Document Version:
Publisher's PDF, also known as Version of Record (includes final page, issue and volume numbers)

Please check the document version of this publication:

• A submitted manuscript is the version of the article upon submission and before peer-review. There can be important differences between the submitted version and the official published version of record. People interested in the research are advised to contact the author for the final version of the publication, or visit the DOI to the publisher's website.
• The final author version and the galley proof are versions of the publication after peer review.
• The final published version features the final layout of the paper including the volume, issue and page numbers.

Link to publication

General rights
Copyright and moral rights for the publications made accessible in the public portal are retained by the authors and/or other copyright owners and it is a condition of accessing publications that users recognise and abide by the legal requirements associated with these rights.

- Users may download and print one copy of any publication from the public portal for the purpose of private study or research.
- You may not further distribute the material or use it for any profit-making activity or commercial gain
- You may freely distribute the URL identifying the publication in the public portal.

If the publication is distributed under the terms of Article 25fa of the Dutch Copyright Act, indicated by the "Taverne" license above, please follow below link for the End User Agreement:

www.tue.nl/taverne

Take down policy
If you believe that this document breaches copyright please contact us at:

openaccess@tue.nl

providing details and we will investigate your claim.

Download date: 04. Oct. 2023

Stitching Interferometry for Accurate Measurement of Curved Surfaces

Yu Jian Fan

Stitching Interferometry for Accurate Measurement of Curved Surfaces

Yu Jian Fan

Stitching Interferometry for Accurate Measurement of Curved Surfaces

Proefschrift

ter verkrijging van de graad van doctor aan de
Technische Universiteit Eindhoven,
op gezag van de Rector Magnificus, prof.dr. M. Rem
voor een commissie aangewezen door het
College voor Promoties in het openbaar te verdedigen op
dinsdag 9 juni 1998 om 16.00 uur

door

Yu Jian Fan

geboren te Shaanxi, China

Dit proefschrift is goedgekeurd door de promotoren:

prof.dr.ir. P.H.J. Schellekens
en
prof.dr.ir. H. F. van Beek

en de copromotor:
dr.ir. C.H.F. Velzel

CIP-DATA LIBRARY TECHNISCHE UNIVERSITEIT EINDHOVEN

Fan, Yu Jian

Stitching interferometry for accurate measurement of curved surfaces /
by Yu Jian Fan. - Eindhoven : Technische Universiteit Eindhoven, 1998
Proefschrift. - ISBN 90-386-0660-5
NUGI 841

Trefw.: interferometrie, asferisch oppervlak, metrologie, koppeling oppervlakken
Subject headings: interferometry, aspheric surface, measurement, surface stitching

Druk: Universiteitsdrukkerij Technische Universiteit Eindhoven

To my wife and parents

献给我的父母和妻子

范 裕健

一九九八年四月 于 荷兰

Summary

Commercial optical interferometers are often not suitable for measuring curved aspheric surfaces because of the high fringe density and the aberrations due to the surface asphericity. The aim of this research is to develop a measurement technique suitable for the accurate measurement of aspheric surfaces which overcomes these problems.

A novel method named stitching interferometry has been developed, that is capable of measuring steep aspheric curved surfaces precisely. This thesis describes the development of this innovative technique for the measurement of curved surfaces having large aspheric departures.

The principle of stitching interferometry is as follows. A series of measurements of overlapping surface segments is made which is subsequently stitched together to obtain an entire surface profile. Using regions of overlap and knowing the transformations between the measured profiles the surface topography can be obtained. This was implemented by modifying a commercial phase shifting interferometer with a self-designed precise mechanical manipulator for shifting and/or rotating the object under test.

We describe the stitching procedure as follows. Firstly, two interferograms of the object in two successive positions in space are recorded in such a way that the two pictures have a surface region in common where the fringes are well resolved. Between the two positions, the object under test is shifted along a common optical axis of the interferometer and the aspheric test surface. Secondly, the surface profiles in the two positions are obtained by analysing and calculating the two interferograms. Next, the two surface profiles in the region of overlap are superposed by making use of the transformations between these two positions. Applying this procedure recursively, a completely surface profile can be acquired.

Stitching interferometry is different in procedure from other existing techniques. It firstly interprets the interferograms into geometrical topographies and then stitches the topographic profiles together so as to obtain the overall shape of a surface. This makes it more universal to use. Whereas the majority of commercial interferometers employ only one fixed reference wavefront, stitching interferometry employs a family of reference wavefronts. This is realised by means of varying the relative position of the tested surface with respect to the reference surface.

A five-axis precision manipulator is designed to realize three translations and two rotations. The principal motion, translation along the vertical optical axis, is realised in virtue of three symmetric elastic leaf springs. High accuracy is achieved at 0.1 μm/mm in straightness and 1″/mm in rotation deviation over the 2 mm central part of the translation stroke. Two offset translations and two rotations are realised by means of elastic pivots.

Experimental results have shown that stitching interferometry is capable of measuring complicated surfaces having large aspheric departures precisely. As a result, it is possible to extend the measuring range of aspheric departures from a few micrometres up to several tens of micrometres.

The technique of stitching interferometry offers considerable potential for testing curved surfaces having aspheric departures. Furthermore, the concept and method may be used to upgrade commercial interferometers.

Contents

Summary i

Contents iii

1. General Introduction 1

1.1 Manufacturing metrology and production 1
1.2 Interferometry for curved surface measurements 3
1.3 Aim and outcomes of this research 7
1.4 Outline of the thesis 8

2. Curved Surfaces and Their Measurement Problems 10

2.1 Literature review and survey 10
2.2 The aspheric surfaces to be tested 16
2.3 Interferometry of the curved surfaces 20
2.4 Problem description 21

3. Improvement of the Interferometry 23

3.1 Optical interference and interferometry 23
3.2 Fizeau interferometry used 28
3.3 The stitching strategy 31

4. Stitching Interferometry 34

4.1 Stitching procedure 34
4.2 Mathematical models and algorithms 36
4.3 Correction of the misalignment 40

4.4 Rectification of data misregistration 49
4.5 The overlap regions 60

5. Realisation and Experiments 64

5.1 Measuring scheme 64
5.2 The interferometer 65
5.3 The five-axis manipulator 67
5.4 Experimental setup 71
5.5 Experiments 75

6. Accuracy Analysis and Validation 79

6.1 Terminology about accuracy 79
6.2 Errors with a single measurement 80
6.3 Stitching processing errors 84
6.4 Short summary 89
6.5 Validation 90

7. Conclusions and Recommendations 95

7.1 Conclusions 95
7.2 Recommendations 96

Appendixes 97

Bibliography 102

Samenvatting 109

Acknowledgements 111

Curriculum Vitae 113

1.

General Introduction

1.1 Manufacturing metrology and production

1.1.1 Manufacturing and quality

In today's increasingly competitive environment, the ability to control product quality in the manufacturing process is crucial. Ensuring customer satisfaction through proper manufacturing metrology and effective quality management is widely recognised to be a key business strategy and fundamental to a successful manufacturing operation [Tannock 1992].

In order to obtain enough information and to perform manufacturing metrology, we make use of all our senses. However, we cannot rely only on our physical senses because of their limitations and unavailability in certain cases. Therefore, we must make use of a great variety of measuring machines and instruments. It has taken many decades to provide manufacturers with the suitable measurement techniques needed to create better products and the standards for reproducing quality in a consistent way.

In recent years, the vital importance of the manufacturing metrology and quality function has been recognised widely. Greater scope has been achieved because manufacturing metrology roles have been supplemented by a responsibility for management leadership in quality improvement.

1.1.2 Manufacturing metrology

In the world of metrology, meaning the science of measurement, dimensional and mechanical measurements are fundamental to manufacturing industry, trade, and the many scientific and technical activities affecting modern life. Metrology for engineering, ranging from the measurement of irregularly shaped small components to whole structures makes use of a number of different mechanical, electronic and optical techniques.

Manufacturing metrology and quality control within manufacturing industry may be exercised in such ways as laboratory testing, non-destructive inspection, in-process monitoring, post-process measurement and product test. Metrology should be in phase with manufacturing rhythm and the high accuracy tolerances of manufacturing equipment. To develop metrology and to provide industry with suitable measurement techniques and the instruments needed, a great deal of research and development has been carried out continuously in many research institutes.

Engineers have been measuring and characterising the shape and microtopography of surfaces for many years. Most of this work has been based on two-dimensional profiles of surfaces obtained with the use of stylus instruments.

In the last two decades, both theoretical and experimental investigations have been undertaken to determine the feasibility of using non-contact and field-sensing optical means such as laser interferometry to measure precision shape and surface microgeometry quantitatively [Brown 1993, Kunzmann 1993]. One of the motivations for this new direction is the increasing effort to use non-contact and field-sensing rather than the traditional contact and point-sensing stylus instruments for quality control and inspection. Another motivation is due to the rapidly increasing demands from modern flexible manufacturing patterns and precision engineering development for better and more accurate measurement techniques over an area.

Precision engineering is the multidisciplinary science underlying the development and realisation of high precision machines, instruments and communication devices. It is firmly based on accurate measurement technology. In the last decade, we have witnessed dramatic progress in precision engineering, especially the innovations of new measurement techniques and measuring instruments.

It is an important trend to develop precision engineering in the interdisciplinary integration of precision metrology, precision manufacturing, and design for precision, instead of in each of those fields separately. Such integration and development of precision engineering activities make it possible to manufacture complicated curved surfaces and therefore result in higher requirements for new measurement techniques.

1.2 Interferometry for curved surface measurements

1.2.1 Curved aspheric surfaces and their applications

Curved aspheric surfaces have been more and more used or suggested for application in a variety of fields. One aspheric part can replace several spherical components in an optical system to correct aberrations, and therefore the use of aspheric surfaces allows drastic improvements of performance, space, weight, and cost [Schulz 1988]. The use of lenses, mirrors and precision products with aspheric surfaces, as well as with other kinds of curved surfaces is increasing with required high precision. As examples we mention contact lenses and moulds, optical aspheric elements in compact disc (CD) players, magnetic storage devises, recorders and laser printers. We have also witnessed an increasing application of curved surfaces in diverse precision machines and astronomical equipment, such as precision air bearing elements, engine parts and textured plastic surfaces. The innovative single point diamond turning method, using advanced control of tools and workpiece position, makes it possible to manufacture complex-shaped surfaces and therefore stimulates a wider use of curved surfaces greatly.

Nevertheless, the use of curved surfaces is often limited by the difficulty of finding an accurate and low-cost method to test them. The requirements in terms of performance and reliability in numerous fields mean that a growing number of optical and mechanical systems use components designed and manufactured with submicron tolerances. As the design and manufacturing of precision objects with curved surfaces, e.g., contact lenses, become more sophisticated it also becomes desirable to have an accurate measure of the shape of the lens surfaces [Brown 1993, Greivenkamp 1987]. A major need is to test aspheric surfaces that have large departures from a best-fit reference sphere.

1.2.2 Interferometrical measurements

Surface characteristics, such as geometry, roughness and waviness, are important parameters in the determination of the performance of an element. Despite of the wide use of mechanical methods, optical methods are becoming interesting tools for high accurate surface topography measurement. Micro- and macrostructure measurement techniques were developed to measure the surface topography, resolutions of two nanometres or better can be obtained.

Shape measurements of curved surfaces are essential for precision manufacturing of spherical or aspherical workpieces. Conventional measurements are based on point sensing methods and possess some inherent drawbacks, which limit their application in the measurement of curved surfaces. Interferometric methods seem to be suitable for the measurement of precision curved surfaces because the whole shape of the workpiece can be visualised with high resolution and without physical contact on the tested surface.

Since its discovery, interferometry has grown into a powerful technique for the characterisation and evaluation of optical surfaces. With the advent of laser, solid state detector and phase measuring algorithms, it provides extremely helpful tools in science and engineering for the accurate surface measurement, accuracies of tens of nanometres or even better being achievable [Massie 1988, Schlewitt 1994]. Interferometry has played a major role in greatly improving the quality of optical and other precision engineered components manufactured.

1.2.3 A dilemma between measurement range and accuracy

- **general consideration**

The accuracy of measurement techniques in dimensional measurement is limited by a number of factors that must be considered in planning and performing measurements. In general manufacturing circumstances, measurement accuracies in the order of a few micrometres can be reached if all setup parameters are under control, while typically an accuracy order of a few tens of micrometres can be expected in most applications. In the worst situation, deviations as high as approximate 30 micrometres may be experienced [Chiffre 1995].

Instruments differ widely in performance, in both vertical (i.e., normal to the surface) range and resolution, and in the range of surface wavelengths. The performances of instruments are limited mainly by the specifications of a number of critical components. A range of parameters is needed to define the capabilities and limitations of the instrument [Stedman 1987].

Interferometry is a technique offering rapid full field measurement. As for the interferometric measurement, the specifications of critical components are as follows: the quality of the cavity between the reference surface and a tested surface; the signal-to-noise ratio (SNR) on the charge-coupled-detector (CCD) camera employed; and the effects due to ambient errors.

The accuracy of a length interferometer for absolute measurement in air depends on the accuracy of the refractometer used [Kunzmann 1993]. However, in the case of most common applications, an optical reference surface is used that yields a virtual reference wavefront in the interferometric measurement. The measurement accuracy for relative measurements then depends primarily on the quality of cavity between the reference surface and a tested surface. Typically, it is of the order of tenths of wavelength [Möller-Wedel 1994]. The resolution of an interferometer today is of the order of nanometres, which is mainly subject to the signal-to-noise ratio (SNR) on a CCD array employed.

A fundamental limitation of conventional interferometry is its inability to measure surfaces with large aspheric departures from the reference wavefront. The asphericity of the surface is evaluated by subtracting a fitting spherical surface from the measured relief. The main problem to measure aspheric surfaces generally is that the fringe density is too high to be detected when both high accuracy and large measuring range are desired.

From a testing point of view, the prime characteristic of an aspheric surface is that it has a large departure from a best fitting reference sphere, and an interferogram made without some sort of aspheric null elements contains too many fringes. In other words, the fringe frequency is over the Nyquist frequency [Greivenkamp 1987, Malacara 1993].

The Nyquist condition of having at least two pixels per fringe provides a limit to the measurement range of asphericity with an interferometric system. Moreover, in order to maintain a desirable accuracy, it is customary in practice to accept a folding frequency twice as high as the Nyquist condition requires and to accept a sampling frequency twice the folding frequency [Fan 1994-a]. In other words, a condition of preferably having eight pixels per fringe should be kept, which limits the measurement range of aspheric departures.

• measurement degree of freedom analysis

Now we are going to analyse the relationship between the capability of an interferometer to perform a measurement of the curved surfaces and the requirement for an interferometer to be used to fulfil the measurement. In the following, we shall use a term, “measurement degree of freedom”, for the analysis. This term, however, has nothing to do with the meaning of degree of freedom used in mechanical design and kinematic analyses.

From the measurement viewpoint of degree of freedom, the capability of an interferometer is restricted proportionally by the ratio of degrees of freedom available with the instrument to the degrees of freedom needed to perform a measurement.

Taking advantage of symmetry, we could analyse the problem in a line along an axis-symmetrical section. The total degrees of freedom available with an instrument, DOF_a, is proportional to the number of detecting pixels (NP) and the SNR of the CCD, the latter is defined as a ratio of the phase measurement range (2π) to the phase resolution $\Delta\varphi$ in an interferometric measurement. Therefore, we have

$$DOF_a = NP \times SNR / k = NP \times 2\pi / k\Delta\varphi \,, \tag{1-1}$$

where k represents the least number of pixels to detect each fringe unambiguously. According to the foregoing discussion, as for the minimum requirement of the Nyquist condition, k is 2, for a normal condition 4 and for a very precise measurement 8.

The total degrees of freedom needed, DOF_n, is related to the maximum asphericity $d_{r,max}$, the number of fringes (NF) with a given wavelength of measuring light λ, and therefore to the Nyquist sampling condition above-mentioned.

$$DOF_n = NF / \delta = 2td_{r,\,max} / \lambda\delta, \tag{1-2}$$

where t is an evenness factor ($t > 1$) regarding fringe distribution over the line in question, δ is a utility factor of detecting pixels ($\delta < 1$). Actually, δ is proportional to the 1/SNR, and is in practice about 1/100.

As a result, the measurement capability ξ, which is a function of measurement error or uncertainty ε, can be expressed as

$$\xi(\varepsilon) \propto \{k\, t\, \Delta\varphi\, d_{r,\,max} / \lambda\, \delta\, NP\}^{1/2}, \tag{1-3}$$

The larger the aspheric departures d_r with a given dimension, the poorer the accuracy achieved. Actually, even a "mild" aspheric surface with only a few micrometres asphericity will violate the common Nyquist condition when the required measurement accuracy is of the order of submicrometres with a commercial interferometer available today.

As a result, there is a dilemma between measurement range and accuracy in interferometric measurement of aspheric surfaces. How to make a satisfactory trade-off requires particular thoughts and skills. If the trade-off dilemma could not be settled internally in an ordinary method, some extra degrees of freedom must be introduced externally into the interferometrically measuring system.

1.2.4 Demands for new accurate measurement techniques

Aspheric surfaces are often manufactured by computer numerical control (CNC) machines based on precision processes. Therefore, precision measurement of such kind of curved shapes is a necessity to process control and product quality validation in manufacturing processes such as diamond turning and ductile grinding. However, there are limitations in using aspheric elements mainly because of the difficulty of measuring these elements.

While much work has been done on the measurements of aspheric surfaces, no outstanding technique has yet been developed [Brown 1993, Lowman 1996]. The actual measurement techniques to inspect these product ranges are insufficient to satisfy the increasing demands of industry, especially to the required measurement range, accuracy and convenience. The use of stylus instruments may be undesirable because of the possible risk of leaving permanent marks or damage to the surface and the relatively slow speed of measurement. Also the dimensions and gradients of the lenses are out of range for most commercially available optical based relief measuring instruments.

Up to now, the most commonly used measurements present at least one of the following drawbacks [Durand 1992]:
- non-versatility (null test and holography)
- relatively high measurement uncertainty (coordinate measuring machines (CMMs))
- limited measurement ranges of sag and diameter (profilometers)
- time-consuming measurement (point-sensing methods)
- surface contact with the risk of deformation and damage (contact measurements)

Even for interferometry, while it is easy to test a flat or a sphere, it is not as simple to test a curved aspheric surface. It requires innovative thought and effort to develop a suitable and accurate technique for the measurement of curved surfaces.

1.3 Aim and outcomes of this research

The aim of this research is to develop a measurement technique suitable for the accurate shape and surface measurement of curved aspheric surfaces with submicrometre accuracy. This research results in the development of an innovative high precision instrument using the principle referred to as "Stitching Interferometry" for the measurement of curved surfaces having large aspheric departures [Fan 1996 & 1997].

Stitching interferometry is a method to overcome the problem of limited measuring range and aberrations due to asphericity in optical interferometric testing for curved surfaces. A series of measurements of overlapping surface segments is made which is subsequently stitched together to obtain an entire reconstructed profile. In order to correct the misalignment and to rectify the data misregistration between two successive submeasurements, stitching algorithms have been developed. An instrument is built with which experiments have been conducted. The technique offers numerous possible applications for testing deep wave fronts and surfaces.

The key points of this technique are the following. First of all, stitching interferometry is different in the procedure from all other existing techniques. It firstly interprets the sub-interferograms into geometrical topographies and then stitches the topographic segments together so as to obtain the overall shape of a surface. This makes it more universal to use. Secondly, whereas the majority of commercial interferometers employ only one fixed reference wavefront, stitching interferometry employs a family of reference wavefronts. This is realised by means of varying the relative position of the tested surface with respect to the reference surface. Furthermore, another key point is the design of a unique precision manipulator for shifting and/or rotating the workpiece under test.

1.4 Outline of the thesis

A novel technique, named stitching interferometry, that is capable of measuring steep aspheric surfaces precisely, is described in this thesis. The configuration of this thesis is as follows.

In Chapter 2, following Chapter 1 regarding the background and general introduction to this research, an overview on the relevant research and literature review is given. The aspheric surfaces to be tested are described in geometric detail. The next content concerns the principles of interferometry utilised in this research. Furthermore, the problems and difficulties with the interferometrically accurate measurement of curved aspheric surfaces are presented and discussed.

Chapter 3 provides firstly some necessary basics of interferometry with the emphasis on the Fizeau interferometry, including Fizeau fringe patterns, phase shifting interferometry and fringe interpretation. The second part of this chapter demonstrates concisely the stitching strategy we proposed to solve the problems described in Chapter 2.

Chapter 4 is the theoretical core of this thesis. To fulfil the stitching interferometry for the measurement of curved surfaces customarily, careful analyses must be executed on the following items. The first one is to correct errors introduced by the misalignment of the series of measurements. Another one is to rectify the misregistration errors of the individual data sets introduced by surface asphericity and object shift due to optical path variation. These will be explored in this chapter. Also, more considerations on the overlap region in the stitching interferometry are discussed.

Chapter 5 illustrates the measuring scheme and experimental setup, including the modification of the Möller-Wedel V100/P interferometer used and the self-designed five-axis manipulator with which an object under test is shifted and/or rotated in the stitching measuring procedure. Experimental results are demonstrated together with further discussions.

A group of accuracy analyses is carried out in Chapter 6. Errors in stitching interferometers for the accurate measurement of curved surfaces may result from single measurement error sources and stitching processing error sources. The first analysis is associated with the quality of optical cavity, data acquisition process and the ambient effects. The second analysis is associated with the residual defocus errors, positioning and misalignment errors, as well as temperature changes. Another important part of Chapter 6 concerns the cross check and validation for the stitching method.

Finally, Chapter 7 will complete this thesis with conclusions and recommendations.

2.

Curved Surfaces and Their Measurement Problems

2.1 Literature review and survey

Measuring curved aspheric surfaces is one of the more challenging and interesting testing applications. Many techniques exist for examining curved surfaces [Fan 1994-b]. Each of these methods has its own merits and weaknesses. We shall briefly review and discuss various possible methods for testing aspheric. Although surface profilometry and geometric ray test are mentioned, the primary focus is interferometry.

2.1.1 Interferometric methods

Interferometers can measure the departure of a surface relative to some reference surface. When testing flat surfaces, errors are measured relative to a plane surface. When testing curved spherical or aspheric surfaces, the surface is tested relative to a reference sphere (non-null test), or relative to the desired ideal aspheric shape (null test) [Stahl 1990, Wyant 1987].

- **interferometric null test**

The principle behind interferometry null test is to compensate or correct wavefront shape of aspheric aberration individually by means of either material null elements or simulation.

The aberration compensation null test uses a null lens to introduce enough aberration into the test beam such that eliminates the aberration produced by testing aspheric surface at its center of curvature. Another method is the aberration matching null test or holography. It utilises a hologram to produce a reference aspheric wavefront that is then compared interferometrically with the wavefront from the object under test. In case that a real master is not available for making, a synthetic computer-generated-hologram can be made. Positioning error, distortion in the hologram plotter and costliness are its problems [Pfeiffer 1992].

Besides, a zone-plate can be used too. A zone-plate can be made as a photo plate with a circle grating that has a pattern calculated to reproduce the shape of the designed surface. Therefore a symmetrical spheric or aspheric shape can be measured [Nomura 1993].

The primary disadvantage of interferometric null test is that requires a precision tailored null lens or a custom-designed hologram as well as careful adjustment and precision alignment.

- **shearing interferometry**

Another approach is to use the shearing interferometry in which two shifted images of the wavefront under test are superimposed to interfere with each other [Yatagai 1987]. The surface slope is measured with shearing interferometry, and the actual surface then is reconstructed by integration. The attractive feature of using shearing interferometry for aspheric surface testing is that the sensitivity of the test can be varied by changing the shear distance.

The most important shearing interferometry is of lateral shearing one, although other kinds of shearing interferometry such as radial, rotational and reversal shearing interferometry are used at the same time. Basically, the method of lateral shearing interferometry consists of displacing the defective wavefront laterally by a small amount and obtaining the interference pattern between the original wavefront and the displaced or shifted version of itself. It has been reported that aspheric surfaces can be measured using lateral shearing interferometry to an accuracy of 1% to 0.1% of the asphericity [Cho 1997, Hardy 1987].

The biggest problem with using lateral shearing interferometry for measuring aspheric surface is that it reduces the number of fringes least where the density is highest, working not so effectively as desired.

- **sub-Nyquist interferometry**

Sub-Nyquist interferometry (SNI) is a data collection and analysis method that is capable of extending the measuring range of an interferometer through the use of a priori information about the tested surface [Greivenkamp 1987]. It is based on the assumption that the surface at any point is differentiable. This additional information allows the analysis to interpret fringes that occur at frequencies well in excess of the Nyquist frequency so as to under-sample the wavefront and still performs an adequate measurement. The fundamental limit to the measuring range of an SNI system is in the ability of the sensor to respond to the high-frequency. To put this technique into practice needs a kind of sensor with a small width-to-pitch ratio or even a point-typed detector.

- **small- or sub-aperture interferometry**

The basic idea behind this kind of testing of aspheric surfaces is to divide the wavefront up into small sections; the wavefront departure in each subaperture is within the measuring range of the instrumentation. The maximum fringe frequency is kept below the Nyquist frequency of the sensor. The problem becomes then that to fit all of these separate measurements, which can contain different amounts of tilt, piston, and sometimes defocus, so as to obtain a complete map of the aspheric surface.

From the viewpoint of optical wavefront test, Zernike polynomial wavefront representation is generally common way to treat the measurements of small- or sub-aperture data [Evans 1995, Liu 1988, Melozzi 1993, Nergo 1984]. The overall surface is represented by a polynomial expansion, and the subaperture data is analysed to determine the expansion coefficients. The Zernike polynomials with a limited number of terms are used.

The same principles can be used also in the measurement of a large plane surface, a ball and photomasks in lithography [Otsubo 1994, Sullivan 1996, Sandstorm 1995].

The principal difficulties of the subaperture testing method are that the results of many subaperture measurements must be combined to yield the full aperture aberrations accurately, and that variable and imprecise amount of focus errors and other misalignment errors must be removed from the data properly.

- **two-wavelength or multiple-wavelength interferometry**

The additional information that two-wavelength interferometry uses to extend the interferometric measurement beyond the Nyquist frequency is a separate measurement at different wavelength [Creath 1985, Ho 1992, Tiziani 1996]. Multiple-wavelength one is based on the same principle. In this way, a tuneable resolution can be conducted in respect to the fringe alias.

A practical problem with such kind of measurements is chromatic aberration in the reference optics and the interferometer.

- **grating interferometry**

A grating interferometer can be used to test flat surfaces that are either too rough or deformed for conventional visible-wavelength interferometer. It uses a diffractive optical assembly to illuminate the test piece at two incident angles. The reflected beams recombine to generate an interference pattern with an equivalent wavelength [de Groot 1996]. In order to employ such kind of a method for testing curved surfaces, some suitable curved diffractive optics must be developed.

2.1.2 Surface profilometry

Surface profilometry types can be split into contact and noncontact devices. A contact profiler scans a probe across the surface and determines height by looking at the height variations of the probe as it scanned. This implies a possible risk to leave scratch or damage the tested surface. Noncontact devices measure surface height without coming in contact with the surface. Most of them are optical microscopes, being used to determine surface roughness or geometry of small features [Blakley 1994, Cochran 1988, Sasaki 1990, Yoshizumi 1987]. Although they are very sensitive and can measure heights with a precision of submicrons, the fact that they hold much smaller field of measurement than what we desire downgrades their position in our selection. Scanning probe microscopes such as scanning tunnelling microscopes (STM) and atomic force microscopes (AFM) have the same picture because of the limited measuring ranges of sag and diameter [Vorburger 1997].

The primary disadvantage of this technique is that in order to produce a complete picture of the surface many scans are required. Furthermore, its accuracy can be effected by mechanical alignment errors between the probe and surface. There are also problems with measuring steep surface slopes. Its field of view is limited to only a few millimetres. Furthermore, high resolution asks for small stylus but due to Hertzian contact limits a low measurement pressure is required. Therefore it results in also dynamic problems.

One possibility to improve the limitation to the field of view of a microscope or an optical profilometer is to make use of the small- or sub-aperture interferometry [Cochran 1988, Wyant 1997]. Other possible means might be a combination of a coordinate measuring machine (CMM) with an optical probing detector.

2.1.3 Moiré topography and projection fringe methods

In addition to interferometric and profilometric tests, aspheric surfaces can be contoured directly using techniques such as mechanical and optical probes. Among of those, moiré techniques and projection fringe techniques are widely used.
Moiré technique and its derivatives, as a kind of field-sensing methods, have getting many developments in recent years. Moiré topography can be used to determine the shape of an object by interpreting the moiré fringe patterns that are the contour lines of

surfaces in specific geometrical conditions [Kim 1992, Matsumoto 1995, Papp 1993, Patorski 1993, Post 1991].

Moiré deflectometry and appropriate instruments have been used for the measurements of such specular or optical surfaces as buttons of contact lenses [Glatt 1988, Kreske 1988]. The information provided by moiré deflectometry is a ray deflection map of a light beam. The most important factors to determine the sensitivity or accuracy in moiré technique are the grating pitch, quality of gratings, as well as the availability to divide the fringe patterns as fine as possible. The accuracy with this method generally is within the range of a few microns, for example 5 micron-accuracy of Rotlex OMS 101 system, which would be insufficient for this application.

Projection fringe methods are becoming more and more popular in 3D shape measurement [Betend-Bon 1992, Igarashi, 1992], with their virtues of simple in construction and wider in dynamic range.

However, such projection fringe methods with either laser sources or white-light sources may be an unsuitable choice when submicron accuracy is required in curved surface measurement.

2.1.4 Geometric ray methods

Before the advent of interferometry, optical components were characterised using geometric ray tests. Geometric ray test such as the Foucault and Ronchi tests can be used to test aspheric surfaces, too. Geometric ray tests measure the slope or height of a surface based upon how light rays travel after being reflected by the surface. This is accomplished by placing a physical obscuration between the object under test and the observer. Then by observing the patterns that are formed, it is possible to deduce information about the surface's ray aberrations.

In a Ronchi test, a binary grating with equal spacing of transparent and opaque strips, called a Ronchi grating, is positioned near the focal plane. Through the grating the exit pupil is observed so that a pattern corresponding to the aberration of the surface or system under test is observed. The phase of the Ronchigram measures the first derivative of the surface aberration. By numerical integration of the phase, the shape of the surface can be reconstruct [Blakley 1994, Omura 1988].

A so-called phase detection deflectometry is an application of phase detection to the Ronchi method. It is based on the measurement of the deflection of light rays, after reflection on every point of the surface under test [Durand 1992, Lin 1991].

Aspheric surfaces can also be measured by Schlieren methods [Gestel 1997, Malacara 1993, Prast 1987]. By mean of geometrical ray tracing analysis, surface geometry can be defined by the retroreflection or deflection beam; slope of the surface can be found by analysing components of the surface normal. As long as retroreflection or deflection information on the direction of the surface normal at special points is acquired, the profile shape can be determined mathematically.

The accuracy will be restricted mainly by the resolution of detecting system and positioning accuracy.

2.1.5 Short summary

Aspheric surfaces of optical elements and other high-precision objects are generally tested using profilometer or interferometer, although other kinds of measurements are also being accepted simultaneously.

For such measurements in a large-sized surface area with an accuracy order of submicrons, an interferometric measurement method is recommended and preferentially accepted due to its noncontact nature, field-sensing virtue and higher accuracy possible achieved.

However, the interferometric measurement of aspheric surfaces may be very hard to perform with existing commercial interferometers if the aspheric departure from the best fitting reference surface exceeds a few micrometres.

As for the light sources, we point out that besides the laser sources, the white-light sources have been more and more employed in optical measuring arrangements. They can be used, for example, to produce a separate fringe system for each wavelength, and the resultant intensity at any point in the plane of observation is obtained by summing these individual patterns [Hariharan 1992, Tolansky 1973].

2.2 The aspheric surfaces to be tested

2.2.1 Shaping and fabrication

Aspheric surfaces, or “aspherics”, are optical precision surfaces that are neither spherical nor plane. Although they have been used or suggested for application in a variety of fields the fabrication of aspheric surfaces is much more complicated than that of spherical surfaces. A spherical surface has the same curvature everywhere and in all directions so that it can be worked everywhere in the same manner. A sphere has only one shape parameter, the radius of curve. An aspheric surface, however, in principle, may have an infinite number of, in practice several, shape parameters.

There are several kinds of shaping and fabrication methods, including moulding and casting, as well as the utilization of elastic deformations. However, the innovation of single point diamond turning methods has brought a revolution in the aspheric fabrication. A high speed rotary spindle is incorporated with a precision linear slider on that a diamond tool is mounted. A typical feed rate with such diamond turning machines is approximately 50 micrometres per revolution, and the spindle rotation accuracy is of the order of submicrons at 3000 rpm (revolution per minute).

2.2.2 Geometry and surface parameters

Regarding aspheric surfaces in this thesis, we refer to symmetric and aspheric precision surfaces, especially to aspheric surfaces of contact lenses. Besides complete aspheric contact lenses, a type of half-completed lenses with the most important interior surface being ready shaped, so-called buttons, was tested most frequently.

The inner surface of such a lens or a button is machined with an ultra-precision diamond turning machine, with a resulting shape accuracy of 50~100 nm and a surface roughness R_a of 15~40 nm. The aspheric departures in the normal direction range from 25 up to 150 micrometres, corresponding to approximate 80 to 500 fringes.

The geometry of the lens or button is composed of several different diametrical zones. Each zone can then be specified as a surface of revolution that can be mathematically described. The types of these surfaces may range from spheres to aspheres that can be described by ellipses and polynomials.

The inner surface of the contact lens is composed of four portions from different kinds of surfaces. Figure 2-1 shows the shape of its axial cross-section.

Please note that the segment B, the most important part, is not simply depicted by one definite ellipse but by a family of varying ellipses, with variable parameters of eccentricity.

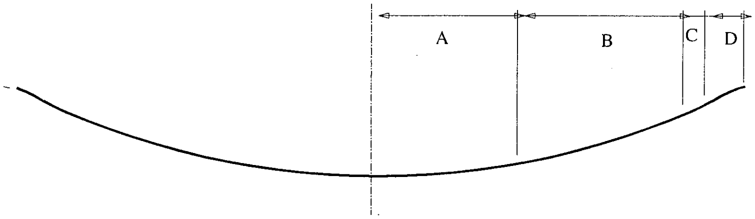

Figure 2-1 Axial cross-section of the inner surface of a contact lens

A: part of a circle; B: composition of varying ellipses;
C and D: parts of two different polynomials.

As an example, dimensions and shape types of the four different diametrical zones of an F.Ellipse 0.4 aspheric contact lens is shown in Table 2-1. The most important area of a contact lens is its optical zone, corresponding essentially to segments A and B, that is the inner portion with a maximum diameter of approximate 8.5 mm.

Table 2-1 Geometric parameters of EF0.4 contact lens inner surface

	A	**B**	**C**	**D**
shape	circle	varying ellipses	polynomial	polynomial
maximum diameter(mm)	3.871	8.234	8.794	9.802

The main factor that affects the quality of a lens is its aberration, namely variations in power across the lens. These in turn are due to deviations from shape imperfection on the lens surfaces. Current quality inspection is performed in such a way that only a small part of the entire surface is checked with a microscope with a 1 mm field of view.

2.2.3 Composition of the aspheric contact lens surface

The aspheric surface of this kind of contactlens is composed of four different kinds of surfaces. Since it has been formed by single-point diamond turning, it is of symmetric surface. As a result, we examine here only half part of its curve shape of the axial cross-section of the inner surface that consists of four different curves as well as a few discontinuous points. Figure 2-2 shows the cross-section of the curved shape.

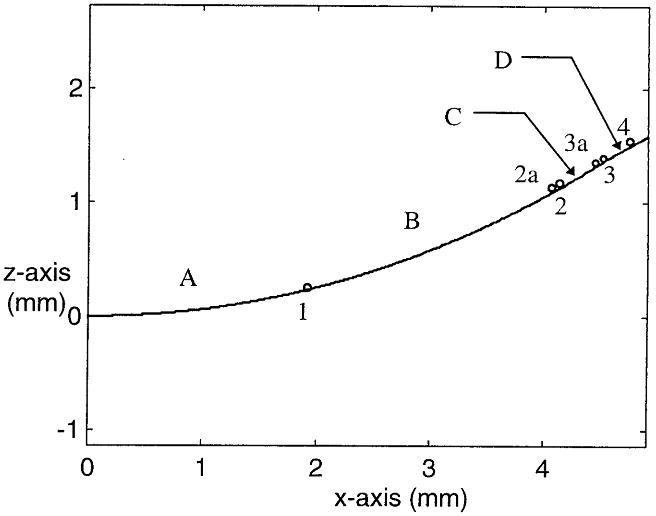

Figure 2-2 A half of the axial cross-section curved shape of the contact lens

Now we shall take the F.Ellipse 0.4 contact lens as an example to describe the composite curve shape of the surface. In terms of mathematics, the surface can be expressed in the forms of the segment functions as defined by the manufacturer.

$$Z(X, e(X)) = \begin{cases} r_0 - (r_0^2 - X^2)^{1/2}, & 0 \le X \le 1.9354; \\ \{r_0 / (1-e^2)\} \cdot \{1 - [1-(1-e^2)(X/r_0)^2]^{1/2}\}, & 1.9354 \le X \le 4.1173, \\ 1.4214 - 0.8598X + 0.2269X^2 - 0.008618X^3, & 4.1203 \le X \le 4.3970; \\ -4.0957 + 1.9532X - 0.1968X^2 + 0.0071X^3, & 4.4000 \le X \le 4.9012. \end{cases} \quad (2\text{-}1)$$

where r_0 is base radius of the spherical surface, and e is eccentricity that varies as the X-coordinate changes. In other words, $e = 0.1831X - 0.3544$, $0 \le e \le 0.4$. And both X and Z are one dimensional variables. The units of X and Z are all in millimetres.

Note there are two very small pieces of interim curves between point 2a (X = 4.1173) and point 2 (X = 4.1203), and between point 3a (X = 4.3970) and point 3 (X = 4.4000). This is owing to the requirement from the CNC diamond turning process designed by the manufacturer. For detailed description on the surface expression, please refer to the Appendix A.

Segment A is a circle part of the base surface, beginning at point 0 and ending at point 1. Segment B is of the most important piece in the optical zone, which is constituted of many different parts from a family of variable ellipses, starting from point 1 till point 2a. Segment C, from point 2 to point 3a, is a transitional piece of the surface while segment D is designed to just fit the shape of human eyes. Both segments C and D are quoted from some kinds of polynomial curves, but with opposite polarity of the curvature. For more details and mathematical descriptions of these segments, please see Appendix A of this thesis.

2.2.4 Aspheric departures of the contact lens surface

Figure 2-3 illuminates the geometric relationships between the aspheric surface of a contactlens curve and the reference spheric surface in an 8 mm radius. Where d_z and d_r stand for the aspheric departures in Z-direction and in the normal (spherically radial) direction respectively. The latter is much more important than the former because d_r has much to do directly with the fringe density in the Fizeau interferometry used.

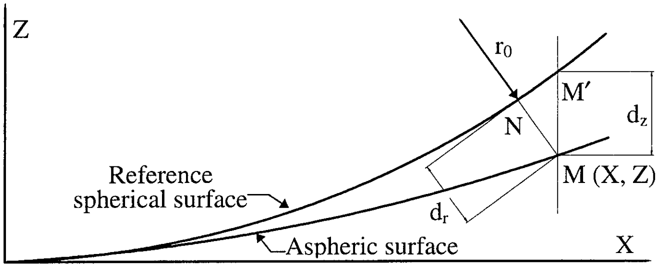

Figure 2-3 Geometric relationship between the aspheric surface and the reference spherical surface

The aspheric departures at point M (X, Z) are calculated as follows, according to the geometry shown in the figure, mathematical expression of Equation (2-1) as well as the description in Appendix A. In normal direction

$$d_r = \{X^2 + (r_0 - Z)^2\}^{1/2} - r_0 , \tag{2-2}$$

and in Z-direction

$$d_z = r - \{r_0^2 - X^2\}^{1/2} - Z\,. \qquad (2\text{-}3)$$

The maximum aspheric departures in segment B, with different eccentricities from 0.4 mm to 0.9 mm, span from 14.733 micrometres to 67.513 micrometres, exceeding far from a few micrometres that existing commercial interferometers can handle with. For details about the aspheric departures from the reference spheric surface of the contact lens surfaces, please refer to the three tables in Appendix B.

2.3 Interferometry of the curved surfaces

Figure 2-4 shows schematically Fizeau interferometer arrangement for testing a concave surface against a reference well-corrected focusing lens.

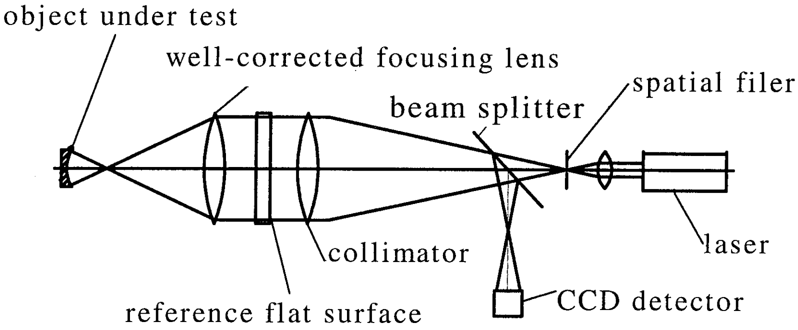

Figure 2-4 Schematic of the Fizeau interferometry

A HeNe laser is used which emits on a red beam with $\lambda = 632.8$ nm. After focusing by a microscope objective the beam passes a beam splitter and a collimating objective (collimator) which transforms the diverging light bundle again into an expanded parallel beam. For the measurement of curved aspheric surfaces the collimated light then passes a specially designed reference objective. The objective contains a reference surface from which part of the light is reflected back to form the reference wave. The transmitting light is focused again in order to create spherical wavefronts that can be reflected back by the aspheric sample surface. They are then imaged on the CCD array. The focal point of the collimator is located at the centre of curvature of the well-corrected converging reference lens. The concave surface under test is adjusted until its center of curvature almost coincides with the focal point of the collimator, too. The interferogram created by the superimposing wavefronts from reference and sample surface is detected by a CCD camera and displayed on a video monitor.

Evaluation of the interferogram can be done manually by the operator or automatically with a computer controlled evaluation system.

Our basic considerations are now as follows. Firstly we want to avoid the use of compensation elements. Secondly we prefer to using the noncontact field-sensing method. And finally we decided to accomplish this research by improving and modifying a commercial phase shifting interferometer with the aid of a fine 5-axis manipulator. This requires a smart measurement strategy and comprehensive algorithms to calculate the real surface shape.

2.4 Problem description

Aspheric surface testing would be greatly expedited by eliminating the need for a null condition. With modern commercial interferometers, high precision measurements can be made of flats and spheres. However, for precision topography measurements on aspheric surfaces, classic optical interferometers are often not suitable because of a too high fringe density and aberrations due to the aspheric departures [Fan 1997, Evans 1993, Malacara 1993]. To test in a non-null configuration, an interferometric technique must be capable of both measuring steep wavefronts and rectifying image deformation.

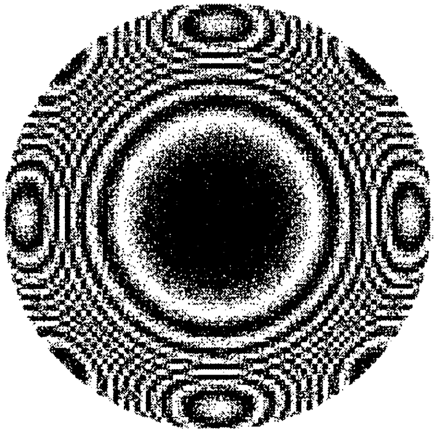

Figure 2-5 Simulated interferogram of an aspheric elliptical surface tested at its vertex centre of curvature

The first problem is that the fringe density is too high to be detected and interpreted. If an aspheric surface is tested at its center of curvature with a spheric reference, as shown in Figure 2-4, a very complicated interferogram with lots of fringes, acquired without some sort of aspheric null elements, is produced. This is because the stigmatic image points for an aspheric surface do not coincide. In other words, such an interferogram is unresolvable. Additionally, aliasing effects were found with such kinds of interferograms.

To manifest the situation, some simulation work with the measuring configuration shown in Figure 2-4 is done. Figure 2-5 illustrates the simulated interferogram of an elliptical surface, the same as segment B of the contact lens EF0.4 we tested, where the sampling density of points was 40 × 40 over the picture. It can be seen readily that frequencies above the Nyquist frequency of the CCD array are aliased in the outer zone of the interferogram.

The second problem is the different ray trajectories of incoming and outgoing rays. It can be seen from Figure 2-6 that in the case of an aspheric surface being measured in the scheme of Figure 2-4, the returning beams from the aspheric surface no longer follow the same path through the instrument's optical system as in the case of a spherical surface.

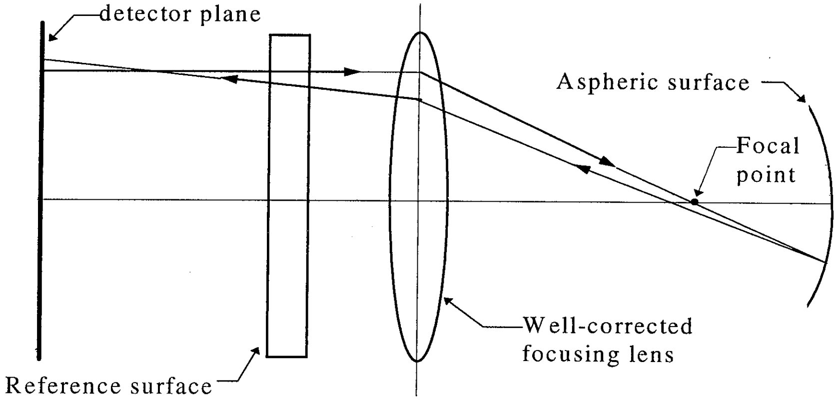

Figure 2-6 Different ray trajectories of incoming and outgoing rays

Therefore, the returning rays do not pass through the focal point of the well-corrected converging lens. In other words, a test wavefront suffers from aberrations due to the surface asphericity, that distort the interferogram [Fan 1997, Lowman 1996]. The fact that incoming and outgoing rays go different optical path due to the surface asphericity will result in data misregistration and interferogram deformation on the detector plane.

3.

Improvement of the Interferometry

3.1 Optical interference and interferometry

3.1.1 Historical

The roots of interferometry go back to the earliest studies of interference in optics and the interferometer by using conventional light sources. In 1678, Christiaan Huygens presented his principle of wave propagation through subsidiary wavelets. Later on, Isaac Newton had been conducting his researches in light, including the study on refraction, spectrum and the interference phenomena of Newton's rings. Thomas Young, in 1802, realised the principle of coherence and the principle of superposition and then provided the basis of interference. A most important step for the realisation of interferometry was taken by Armand Fizeau in 1862. He used a collimated light and studied the equal-thickness interfacing fringes. Albert Michelson was the first scientist who described the interferometer scientifically in 1882. It is probably correct to say that no single instrument has more profoundly affected modern interferometry than has the Michelson interferometer [Fowles 1968, Tolansky 1973].

The development of interferometer was restricted since then by the factors such as the limited coherence length of the light sources of that time, the very limited light intensity, the lack of photodetectors and electronics of today.

Lasers have removed many of the limitations imposed by conventional sources and have made possible many new interferometric techniques. Another development that has revolutionised interferometry is the increasing use of photodetectors and digital electronics for signal processing [Meyer-Arent 1984]. With the advent of phase measuring algorithms and solid state detector, as well as powerful computers, interferometry has undergone a timely and profound transformation during the last fifteen years. This change is driven both by technology and user requirements.

Perhaps the best known interferometric devices are the Michelson interferometer and its modification, Twyman-Green interferometer. However, for the purpose of practical use, most of the commercial interferometers are of Fizeau interferometers due to its generally versatile and common-path arrangement to prevent the influence due to ambient factors.

3.1.2 Interference and interferometry

One interesting fact about light is that it acts sometimes like a wave, other times more like a stream of very fast particles or quanta called photons. This wave/particle duality remains one of the mysteries of nature. Theoretically, at a point in empty space the electromagnetic state is said to be specified by two vectors, the electric field **E**, and the magnetic field **H**. However, in practice we emphasis and use whichever aspect makes our treatment easier and leads to a satisfactory result. In this thesis, light is treated as a kind of electromagnetic wave **E**, based on Maxwell's theory, as interference exhibits the wave character of light.

Interference arises from the superposition of two or more light waves satisfying certain conditions. The resultant intensity at any point depends on whether they reinforce or cancel each other.

- **optical interference**

The theory of optical interference is based essentially on the principle of linear superposition of electromagnetic fields. The complex amplitude at any point in the interference pattern is the sum of the complex amplitudes of the two waves, so that we can write [Fowles 1968, Hariharan 1992]

$$\mathbf{E} = \mathbf{E}_1 + \mathbf{E}_2, \tag{3-1}$$

where $\mathbf{E}_1 = E_{10}\exp(-i\varphi_1)$ and $\mathbf{E}_2 = E_{20}\exp(-i\varphi_2)$ are the complex amplitudes of the two waves. Suppose I_1 and I_2 be the intensities due to the two waves acting separately, and $\varphi(x, y) = k(\varphi_1 - \varphi_2)$ be the phase difference between them in the x-y plane where the waves are investigated, the resultant intensity is, therefore,

$$\begin{aligned} I &= C\,|\mathbf{E}|^2 = C\,(\mathbf{E}_1 + \mathbf{E}_2)\bullet(\mathbf{E}^*_1 + \mathbf{E}^*_2) \\ &= C\,(|\mathbf{E}_1|^2 + |\mathbf{E}_2|^2 + \mathbf{E}_1\bullet\mathbf{E}_2^* + \mathbf{E}_1^*\bullet\mathbf{E}_2) \\ &= I_1 + I_2 + 2(I_1 I_2)^{1/2}\cos\varphi(x, y), \end{aligned} \tag{3-2}$$

where $\mathbf{E}^*$ is the conjugate of **E** and C is a constant.

The term $2(I_1 I_2)^{1/2} \cos \varphi(x, y)$ is called the interference term. This term indicates that the intensity, I, in the region of superposition varies from point to point between maxima which exceed the sum of the intensity in the beams, and minima which may be near to zero.

If the two waves are derived from a common source, so that they have the same phase at the origin, the phase difference $\varphi(x, y)$ corresponds to an optical path difference

$$\Delta p = (\lambda / 2\pi) \times \varphi(x, y) . \tag{3-3}$$

If $\varphi(x, y)$, the phase difference between the beams, varies linearly across the field of view, the intensity varies cosinusoidally, giving rise to alternating light and dark bands or fringes.

With the aid of the interference pattern analyses, it is possible to achieve higher accuracy even up to nanometre order. The wavelength of the laser light is the unit of measurement (λ=0.6328 μm). The capability of showing fractions of a light wavelength by interferometry technique makes it possible to achieve very high measuring accuracy.

- **interference conditions for good fringes**

In general, when considering two-beam interference, five conditions must be met for good contrast fringes in an interferometric measurement:

1. The two interfering beams must be at approximately the same frequency;
2. The phase differences between the interfering beams must be constant over the measurement time;
3. The polarisation of the interfering beams must be equal;
4. The intensity of the interfering beams should be nearly identical, and;
5. The interfering beams must overlap to meet each other.

Any reduction in the conditions will reduce the fringe contrast and therefore reduce the sensitivity as well as the accuracy of the interferometry. Optics of the interference units are designed for maximum possible contrast of the interferograms.

- **Conceptual interferometry**

When light waves which meet the above-mentioned interference conditions are superposed, interference patterns can be observed in interferometers. Most interferometers are based on the principle shown schematically in Figure 3-1.

The light source can be either a laser or a monochromatic point source emits coherence beams. The light beam from the light source is guided to a device with which the beam is split into two. To make measurements using interference such an optical arrangement is usually need in which the two split beams travelling along separate paths are made to interfere. One of these is the reference path, while the other is the test or measurement path with the introduction of phase difference. After being guided to meet each other, the two beams interfere. The interference can be observed directly or can be recorded as so-called "interferogram" by a kind of detector. CCD array is of the most popular detector used in modern interferometers when visible wavelengths are employed.

Two methods are commonly used to obtain the two split beams from a single source. Wavefront division method uses apertures to isolate beam from separate portions of the primary wavefront while amplitude division derives two beams from the same portion of the original wavefront [Hariharan 1992].

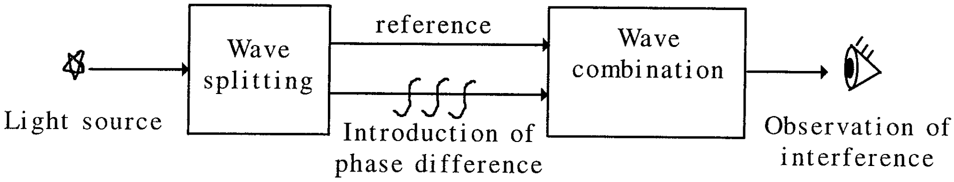

Figure 3-1 Conceptual schematics of interferometers

Naturally, to obtain a good interferogram, the forgoing-mentioned interference conditions should be satisfied. In addition, for a stationary interference pattern to be produced the phase difference between the two interfering waves should not change with time. The two interfering beams must, therefore, have the same frequency. Generally, this requirement can be met only if they are derived from the same source.

3.1.3 Phase shifting interferometry

- **phase shifting technique**

Phase measuring technique liberates people from arduous work with the interpretation of interference fringes. In any modern interferometric test of an aspheric optical surface some means is required to get the interferogram data into the computer for analysis. Phase shifting interferometry (PSI) is the best. The relatively simple concept behind PSI is that a time-varying phase shift is introduced between the reference wavefront and the test or sample wavefront in the interferometer. A time-varying signal is then produced at each measurement point in the interferogram, and the relative phase between the two wavefronts at that location is encoded in these signals.

In PSI, the phase different between the two interfering beams is made to vary in steps, and as the phase difference is varied the resulting intensity distribution is detected and fed into a computer. If three or more intensity measurements are made while the phase difference is varied, the phase variation across the interference pattern can be calculated. For more details on the phase shifting algorithm, please refer to Appendix C.

Virtues of phase measuring techniques include: interpretation of fringe patterns to better than $\lambda/100$, high speed measurement and automatic polarity determination, good results even with low-contrast fringes, results that are independent of intensity variations across the pupil and phase obtained at a fixed grid of data points [Creath 1988].

- **phase unwrapping**

There is one more operation that must be performed to the calculated phase $\varphi(x, y)$ before it is ready to be displayed and evaluated. Based on the four-step PSI algorithm described in Appendix C, the measured phase can be obtained from the following equation [Hariharan 1992, Malacara 1992]

$$\varphi(x, y) = \tan^{-1}[(I_2 - I_4)/(I_1 - I_3)] = \sin^{-1}(I_2 - I_4)/\cos^{-1}(I_1 - I_3). \qquad (3\text{-}4)$$

This simple equation is evaluated at each measurement point to obtain a map of the measured wavefront. However, the arctangent is defined only over the limited range of angles, $-\pi/2$ to $\pi/2$. Regardless of the actual value of the phase, only values of the phase within this range result from Equation (3-4). This limitation would appear to restrict us to measuring optical path differences to no more than half of a wavelength. Fortunately, there is sufficient information in the calculation to remedy the situation and to provide a usable measurement range. The facts that the wavefront or surface is actually continuous and that it extends over a much large range benefit the phase unwrapping work. .

The first correction is to extend the phase calculation range between 0 to 2π. This is possible because the signs of the sine and cosine are known independently of the tangent. Therefore, the maximum wavefront slope measurable is, in principle, limited to π per pixel. The second correction is to remove the 2π discontinuities that are present in the raw phase data generated. It converts the modulo 2π phase data into a continuous representation of the wavefront under test. Whenever one of the large discontinuities occurs in the reconstruction, 2π or multiples 2π are added to the adjoining data to remove the discontinuity.

- **requirements to specimens under test**

The application range of phase shift interferometry is independent on the fabrication brands. With a commercial interferometer, it can be measured of flat, spherical test specimen with following surface specifications:

- polished surfaces of glass, ceramics, metal, plastics or other comparable materials;
- coated or uncoated surfaces;
- diamond turned surfaces;
- Surfaces with minimum 4% direct reflecting light;
- reflectivity between 1% and 100%;
- deviation of shape accuracy to the reference element between 0.01μm to 3 μm.

3.2 Fizeau interferometry used

3.2.1 Principles and layout

An extremely useful and versatile interferometer is the Fizeau interferometer. The Fizeau interferometer is commonly employed for topographic testing when a test surface is compared with a reference one owing to its well-known characteristics: high stability, robust design, good sensitivity, and relatively low cost. We shall now describe a Fizeau interferometer used in this research for the measurement of curved aspheric surfaces. A schematic diagram is shown in Figure 3-2.

A helium-neon gas laser of about 1 mw power laser at 0.6328 μm in the single mode is employed. A very well corrected objective (collimator) serves to collimate the light from the pinhole, illuminated by a combination of the laser and a microscope objective. Laser light with a beam diameter of 0.6 mm goes through such a telescope system to be expanded by a factor of approximately 200. As a result a typical measuring field of 100 mm diameter is obtained.

Between the collimating objective and the pinhole (spatial filter), a beam splitter (BS) is placed so that the fringes can be observed from the side. The reference plane surface is adjusted so that the reflected image of the pinhole is autocollimated. The surface under test is adjusted until the image reflected from it also comes into coincidence with the pinhole.

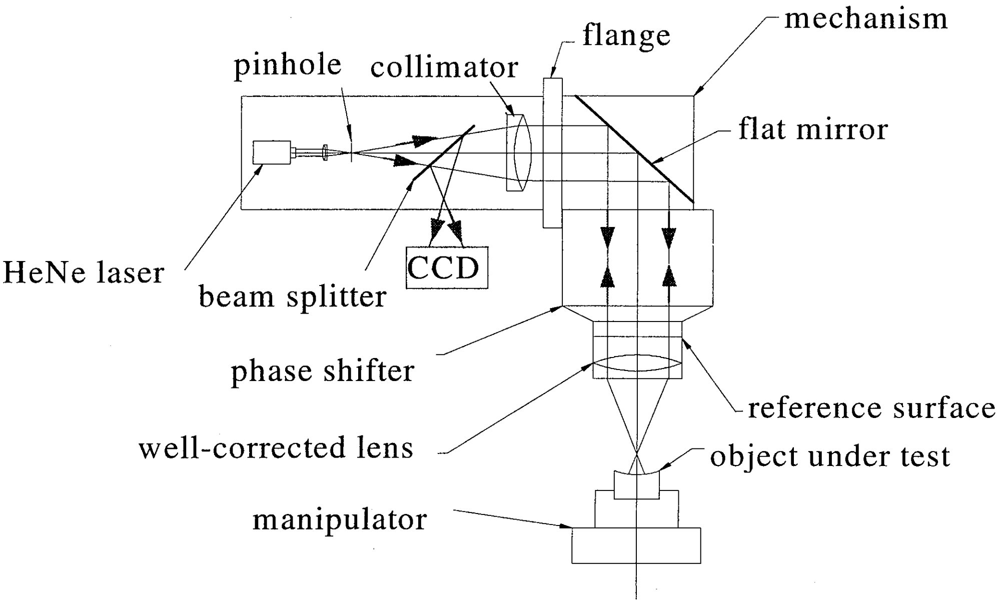

Figure 3-2 Schematic set up of the Fizeau interferometry used

Just as collimated light is employed for testing optical flats on the Fizeau interferometer, here an arrangement for testing a concave surface against a reference convex surface is used for testing our contact lenses. The point source of light is located at the centre of curvature of the convex reference surface. The concave surface under test is adjusted until its center of curvature almost coincides with the point source of light, too. We can also have an arrangement for testing convex surface against a concave reference surface.

The same setup can be used very easily for checking the uniformity of thickness (concentricity) of spherical shells. In this case the interfering beams are obtained from the front and back of the two spherical concentric surfaces.

3.2.2 Measurement accuracy and fringe interpretation

The accuracy of interferometric measurement is primarily determined by the optical cavity errors. The quality of all the optics of uncommon paths in the interferometer is very important. Among of that, the quality of the reference element determines essentially the accuracy of interferometric measurement. In the case of measuring a curved surface, the described accuracy is around $\lambda/20$ or 31 nanometres in peak-to-valley (PV). It is possible, anyhow, to remove such kind of systematic error by error separating techniques [Bendat 1986, Walker 1994]. The measurement accuracy depends on the system noise behaviour and includes errors caused by the internal optical setup, and errors introduced by the electronic elements like CCD camera and the influence of air turbulence and mechanical vibration.

The reproducibility of a phase shifting interferometer depends on the quality of the test specimen and the measuring conditions. Typical value, according to our experimental experience, under normal conditions is better than 30 nanometres. Under special conditions (well-controlled mechanical vibration and air turbulence) a reproducibility of 10 nanometres was achieved.

Apart from the above-mentioned all factors, the accuracy of fringe interpretation should be also taken into account. The most important limitation is the sampling interval. Referring to Appendix C, the optical phase between adjacent detector elements must not change by more than π in order to reconstruct the wavefront. This is because the phase measurements are modulo 2π owing to the arctangent calculation. This means that minimum two detector elements, or better in eight detector elements for one fringe ($\lambda/2$) are necessary (see Chapter 1.2.3).

The software with the Möller-Wedel V100/P interferometer, Intomatik, is used to control and calculate the phase measurement with respect to the reference wavefront generated by a reference object. Data points that do not contrast sufficiently are not accepted but indicated exclusively.

With the Fizeau phase shifting interferometer, the measured phase data are recorded to a map data file. They are scaled by the grey course of 256 and stored in phase integers. However, the measured data in such a map data file are encoded in a strange and special way therefore are unreadable in a normal way. A converting program to interpret the original data of phase integer into ordinary data referring to the height information was written, the basic algorithm used is given hereafter.

In our case that interference takes place with the reflected beams from the reference surface and the tested surface respectively, surface topographic height h can be calculated according to Equation (3-3),

$$h = (\lambda / 4\pi)\ \varphi(x, y)\,. \tag{3-5}$$

The relationship between real phase data, i.e., phase_real or $\varphi(x, y)$, and the stored integer phase data, phase_integer, in a measured data file is

$$\text{phase\_integer} = (\text{phase float} \times 256)_{\text{rounded}};\ \text{phase\_float} = \text{phase\_real} / 2\pi. \tag{3-6}$$

Therefore, we have got

$$h = (\text{phase\_integer} / 256) \times \lambda/2 \cong 1.2359 \times \text{phase\_integer}. \qquad (3\text{-}7)$$

3.3 The Stitching strategy

In order to solve the problems described in Chapter 2.4 with the accurate measurement of curved aspheric surfaces, a suitable measurement technique to overcome the fringe density and aberration difficulties must be developed. It has been found that, by analysing the interferograms of aspheric surfaces carefully, even in the case of too many fringes, such kinds of interferograms are still partially resolvable. Where and whether the fringe density is resolvable depends principally on the shape of the tested object, as well as the position of the object in the measuring frame in respect to a certain CCD array.

A novel technique is proposed for the accurate measurement of curved aspheric surfaces, named stitching interferometry. The essential considerations were to make use of a modified phase shifting interferometer with a tailored manipulator, without use of compensation elements. The method consists of varying the distance or position of a curved surface from the focus of an interferometry reference sphere with a precision manipulator.

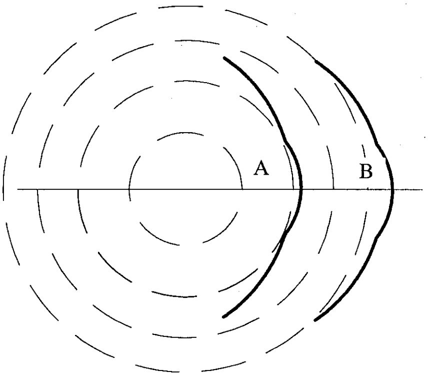

Figure 3-3 Comparing an aspheric surface(thick) with reference wavefronts(thin) varying in radius

It can be seen from Figure 3-3 that as the asphere is moved, the radius of curvature of the reference wavefront changes, matching different part of the aspheric surface on rings of increasing or decreasing diameter.

The basic idea behind the stitching interferometry is to divide the wavefront or the measured surface up into several segments so that the fringe density over a sub-interferogram from each sub-measurement remains resolvable. In other words, to shift the object with respect to the varying reference wavefronts, such that the differences between the reference wavefronts and the tested surface will be minimised. Figure 3-3 intuitively illustrates the concept of stitching interferometry. The inner portion of the measured surface is compared in position A with a befitting reference wavefront, while the outer portion is compared in position B with another wavefront. To accept the strategy implies that instead of using only one reference wavefront with fixed configuration parameters, a family of those, with variable configuration parameters such as radii, positions and orientations, must be employed.

Figure 3-4 shows the corresponding resultant interferograms of simulation which correspond to the position A and position B in Figure 3-3, respectively.

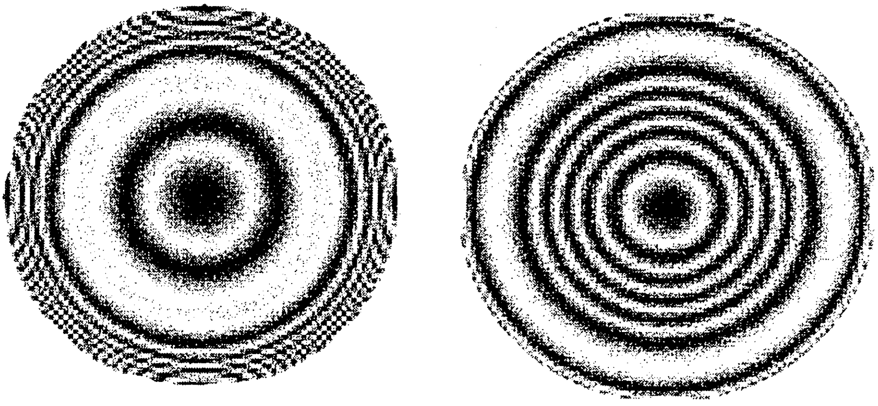

a) b)

Figure 3-4 Simulated interferograms with object position shifting from the vertex centre of curvature

The stitching strategy can be described as following. Firstly, two interferograms of the object in two successive positions in space are recorded (Figure 3-5), in such a way that the two pictures have a surface region in common where the fringes are well resolved. Between the two positions, the object under test is shifted along a common optical axis of the interferometer and the aspheric test surface. Secondly, the surface profiles in the two positions are obtained by analysing and calculating the two interferograms. Next, the two surface profiles in the region of overlap are superposed by making use of the transformation between these two positions. Applying this procedure recursively, a completely reconstructed surface can be acquired finally.

The stitching interferometry is different in procedure from all other existing techniques. It firstly interprets the sub-interferograms into geometrical topographies and then stitches the topographic segments up together so as to obtain the overall shape of a surface. This makes it more universal to use, especially for surfaces with steep topographies.

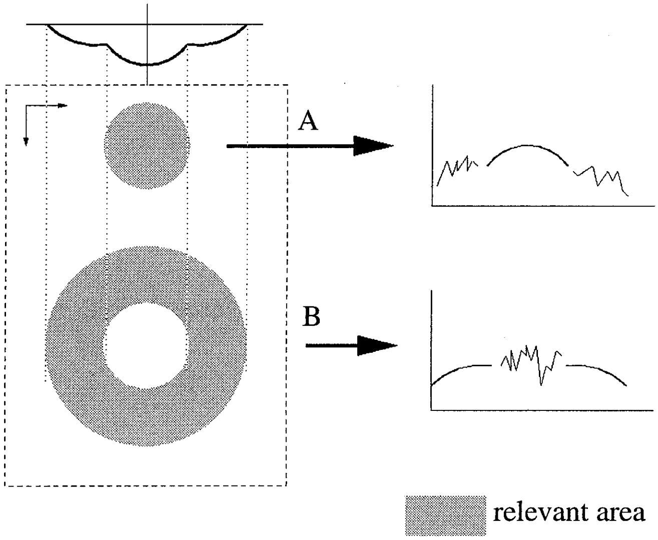

Figure 3-5 Stitching strategy

The individually measured profiles can not be stitched directly because of any possible displacements and/or rotations of the surface during the procedure. To make the things even worse, as the object is shifted during the stitching procedure, the optical path of each point on the object surface changes, too. Chapter 4 will give the treating finesses and solutions to the problems.

4.

Stitching Interferometry

4.1 Stitching procedure

The basic concept of stitching interferometry is composed of three parts. The first one is to split the measurement of an entire aspheric surface in certain different zones. The second one is to obtain topographic pieces of the surface from the series of measurements. And the last one is to stitch the sequence of the topographic profiles up together to acquire the entire surface.

The concept is realised by varying the position or orientation of an aspheric surface from the focus of an interferometric reference sphere. The focus is considered as a source emitting a series of spherical wavefronts that are defined in this chapter as the virtual spherical reference. As the aspheric surface is moved, the radii of the virtual reference wavefronts change, and the matching area of the tested surface increases or decreases in diameter consequently. In such a way, a different part of the tested aspheric surface is matched or compared to the varying reference wavefronts correspondingly. Accordingly, the interferograms obtained at different positions are recorded to acquire profiles of the correspondent surface portions.

Figure 4-1 and Figure 4-2 show respectively the experimental interferograms of an aspheric contact lens inner surface. The interferogram in Figure 4-1 was made to test the central portion of the surface at its vertex centre of curvature in the arrangement shown in Figure 3-2. The interferograms in Figure 4-2 were made to test the outer portion of the surface in two measurements, with the object position shifts from the vertex centre of curvature in respect to the well-corrected spherical reference.

Although only the aspheric surfaces were treated in this thesis, the principles of stitching interferometry can be certainly extended to the measurements of more general types of surfaces, for example the astigmatic and cylindrical surfaces.

The stitching procedure can be described as follows. Firstly, two interferograms of the object in two successive positions in space are recorded, in such a way that the two pictures have a surface region in common where the fringes are well resolved.

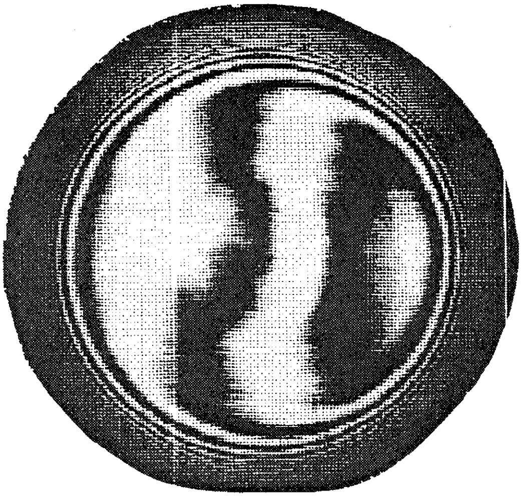

Figure 4-1 Interferogram of a contact lens inner surface, measuring the central portion at its vertex center of curvature

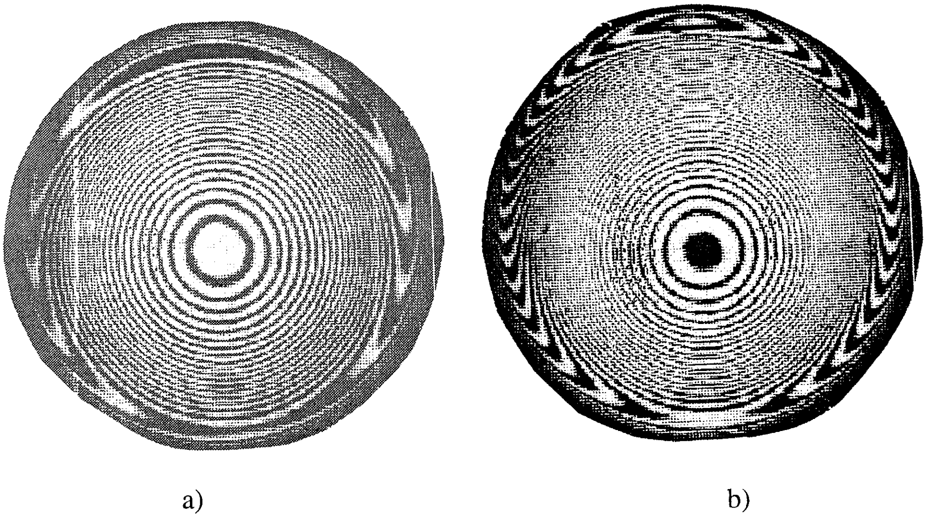

a) b)

Figure 4-2 Interferograms of the same aspheric surface as in Figure 4-1, but measuring the outer portions with different position shifts

Between the two positions, the object under test is shifted along a common optical axis of the interferometer and the aspheric test surface. Secondly, the surface profiles in the two positions are obtained by analysing and interpreting the two interferograms. Next, the two surface profiles in the region of overlap are superposed by making use of the transformation between these two positions. Applying this procedure recursively, a completely reconstructed surface can be acquired finally.

The stitching interferometry is different in the procedure from other existing techniques. Firstly, it interprets the sub-interferograms into geometrical topographies and then stitches the topographic segments up together so as to obtain the overall shape of a surface. This makes it more universal to use. Secondly, whereas the majority of commercial interferometers employs only one fixed reference wavefront, stitching interferometry employs a family of virtual reference wavefronts. This is realised by means of varying the relative position of the tested surface with respect to the reference surface.

An important issue in the stitching interferometry is to shift the aspheric object in respect to the focus of a reference sphere, such that every portion of the measured interferogram should be resolvable in turn. In this way, the entire surface is "swept" with certain predetermined overlapping sectors, for example, outwardly. As a result, a series of measurements of overlapping surface segments is made which is subsequently stitched together to obtain an entire reconstructed surface. It has been implemented by make use of the modification on a commercial Möller-Wedel V-100/P phase shifting interferometer, and of a self-designed precise 5-axis manipulator for shifting and/or rotating the object under test. Successively, interpreting the interferograms of submeasurements, beforehand, to topographical profiles is a necessity. The final task is to stitch the topographical segments together properly and correctly.

4.2 Mathematical models and algorithms

4.2.1 Considerations regarding the stitching algorithms

In the stitching procedure, each pair of interferograms of the tested object in successive positions in space is recorded with an overlap region. Between the measurement positions, the object under test is shifted along a common optical axis of the interferometer and the aspheric tested surface. Such a loop will be repeated until the entire surface is measured and can be correctly reconstructed in terms of topography. It is essential to the stitching procedure that a fixed data area on the aperture, that corresponds to a fixed data recording grid on the CCD, is used.

From the optical test viewpoint of degree of freedom (see Chapter 1.2.3), extra degrees of freedom are introduced externally by means of shifting the object under test and recording more interferograms. However, this causes, too, a kind of trade-off matters. Shifting the object makes it possible to extend the measuring range of aspheric departures from the spherical reference while remaining the desirable high resolution of measurement. On the other hand, however, such an object shift introduces certain supplementary problems or difficulties. It not only introduces a misalignment problem but also worsens further the data misregistration, in addition to the problem of different ray trajectories for incoming and outgoing rays, due to the surface asphericity, mentioned previously in Chapter 2.4.

To realise stitching interferometry for the measurement of curved surfaces routinely, careful analyses must be executed on the following items. One is to correct the errors introduced by the misalignment of the series of measurements. It can be done by using regions of overlap and knowing the transformation between successive measurements. Another item is to rectify the misregistration of the individual data sets introduced by the surface asphericity and by the object position shift that cause optical path variations. This can be accomplished by careful optical analyses based on the theories of geometrical optics, including image formation, optical aberrations and the characteristic functions of Hamilton.

4.2.2 Data sets and measurement frames

The topographical relief of a measured surface is represented on a rectangular image grid of points in the x-y plane. For each point on the surface, the z-coordinate, or the height information, can be deduced from the measurement by means of phase unwrapping, image interpreting and data converting software.

The system of coordinates is defined as the measurement coordinate frame with which the measurement is made, where the z-axis coincides with the common optical axis of the measuring system. In the same way, an object coordinate frame, that describes the shape of the actual surface, is defined, which is independent from its position in the measurement coordinate frame.

Suppose two successive measurements are made respectively of the two surface pieces P and Q, as shown in Figure 4-3 a. Two data sets $\{\mathbf{P}\}$ and $\{\mathbf{Q}\}$ are therefore consequently acquired from the measurements. There is an overlap region between the two surface pieces, corresponding to the acquired data set $\{\mathbf{V}\}$ of the overlap region, showing in Figure 4-3 b. Each element of the data sets $\{\mathbf{P}\}$, $\{\mathbf{Q}\}$ and $\{\mathbf{V}\}$ is referring to a coordinate triple of numbers, (x, y, z), in the measurement frame.

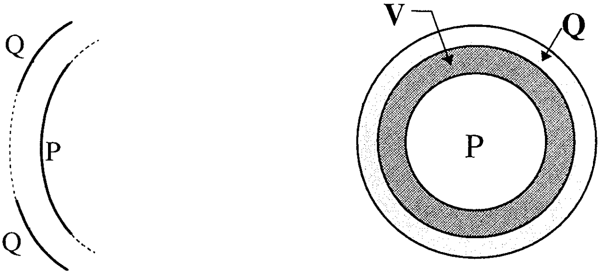

a) the measured pieces of surface b) the corresponding data sets

Figure 4-3 The measurement pair and the corresponding data set pair

Because the measured data grid in the x-y plane is kept to be the same during the two measurements being made in the stitching procedure, the x-y coordinates of each point on the surface should be the same, if there would no data misregistration and misalignment. The z-coordinates represent the surface topography.

Let $\mathbf{P}_i$ and $\mathbf{Q}_j$ denote the elements of the measured data sets of the first and the second submeasurements, acquired respectively from the CCD image grid of the interferometer. Note here $i, j \in \mathbf{N} = [1, 2, ..., n]$, but normally $i \neq j$ due to the above-mentioned data misregistration. In other words, the indexes of $\{\mathbf{Q}_j\}$ are slight different from those of $\{\mathbf{P}_i\}$. After being corrected by misregistration rectification, $\mathbf{P}_i$ and $\mathbf{Q}_j$ are turned to $\mathbf{P}_i'$ and $\mathbf{Q}_i'$ correspondingly with the same data frame and the same order sequence. Furthermore, the misalignment correction is made which results in the corrected data of the new data sets $\mathbf{P}_i''$ and $\mathbf{Q}_i''$ correspondingly. It is supposed that there exists an index set $\mathbf{M}$, such that if $i \in \mathbf{M}$, then $\mathbf{P}_i''$ and $\mathbf{Q}_i'' \in \mathbf{V}$. The corresponding data within an overlap region is denoted as $\mathbf{V}_i$, $i \in \mathbf{M} = [1, 2, ..., m]$, $m < n$. The relationship among the data sets is illustrated intuitively by the block diaphragm in Figure 4-4.

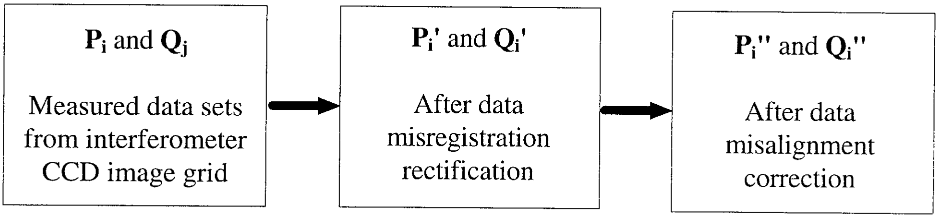

Figure 4-4 Data sets at different stages of treatment

4.2.3 Mathematical formulation

Considering the practical situation of measurement, it is reasonable to make the following assumptions. The first one is that there is no shift for the first submeasurement itself. The second assumption is that the misalignment about the first submeasurement itself is negligible. In other words, the object axis is aligned as precise as possible, such that it is coincident with the optical axis of the interferometer. Therefore the common optical axis of the interferometer and the aspheric tested surface is defined, along that the object is shifted in the stitching procedure. A pair of measured data **within the overlap region**, should represent the same topographic profile. This implies in terms of mathematics that within the overlap region,

$$\mathbf{P}_i'' = \mathbf{P}_i' = \mathbf{Q}_i'' \text{ , } i \in \mathbf{M} = [1, 2, ..., m]. \qquad (4\text{-}1)$$

Assuming that the data misregistration in the image formation has been rectified and therefore the data $\mathbf{Q}_j$ is converted into $\mathbf{Q}_i'$. This means that it is possible to find a kind of transformations, **E**, between each pair of corresponding points regarding the same physical point on the measured surface but from two successive measurements. As a result, each element of the two data sets refers to the same corresponding point. It can be expressed mathematically as

$$\mathbf{Q}_i' = \mathbf{E}\,\mathbf{Q}_j + \varepsilon' \qquad i,\ j \in \mathbf{N} = [1,2,...,n],\ i \neq j, \qquad (4\text{-}2)$$

where ε' is the vector of an error term. This equation can be re-written in matrix format

$$\begin{pmatrix} x_i^{q'} \\ y_i^{q'} \\ z_i^{q'} \end{pmatrix} = \begin{pmatrix} e_{11} & e_{12} & e_{13} \\ e_{21} & e_{22} & e_{33} \\ e_{31} & e_{32} & e_{33} \end{pmatrix} \begin{pmatrix} x_j^{q} \\ y_j^{q} \\ z_j^{q} \end{pmatrix} + \begin{pmatrix} \varepsilon'_x \\ \varepsilon'_y \\ \varepsilon'_z \end{pmatrix}. \qquad (4\text{-}3)$$

In order to obtain the data set $\mathbf{Q}_i''$, a kind of transformation between the data set $\mathbf{Q}_i'$ and $\mathbf{Q}_i''$ must be found to correct the misalignment errors. Such a kind of transformation is referred as to a rotation transformation **R** and a translation one **T**. Mathematically it can be described as

$$\mathbf{Q}_i'' = \mathbf{R}\,\mathbf{Q}_i' + \mathbf{T} + \varepsilon, \qquad (4\text{-}4)$$

or,

$$\begin{pmatrix} x_i^{q\,''} \\ y_i^{q\,''} \\ z_i^{q\,''} \end{pmatrix} = \begin{pmatrix} r_{11} & r_{12} & r_{13} \\ r_{21} & r_{22} & r_{23} \\ r_{31} & r_{32} & r_{33} \end{pmatrix} \begin{pmatrix} x_i^{q\,'} \\ y_i^{q\,'} \\ z_i^{q\,'} \end{pmatrix} + \begin{pmatrix} t_x \\ t_y \\ t_z \end{pmatrix} + \begin{pmatrix} \varepsilon_x \\ \varepsilon_y \\ \varepsilon_z \end{pmatrix}. \qquad (4\text{-}5)$$

where, again, ε is a residual error term.

Finally, the mathematical formulation of the relationships between three date sets $\mathbf{Q_j}$, $\mathbf{Q_i}'$ and $\mathbf{Q_i}''$ can be summarised as

$$\mathbf{Q_i}'' = \mathbf{R}\,(\,\mathbf{E}\,\mathbf{Q_j}\,) + \mathbf{T} + \varepsilon'', \qquad (4\text{-}6)$$

where $\varepsilon'' = \mathbf{R}\,\varepsilon' + \varepsilon$, which is the resultant error term containing the error components of all transformations.

Now, the major tasks to develop the stitching algorithms become in turn to find the transformation **E** for rectifying the data misregistration, and the transformations **R** and **T** for correcting the misalignment.

4.3 Correction of the misalignment

During two successive submeasurements, the position of the tested object changes. Therefore, a kind of misalignment is introduced that spoils the correspondences of orientations and positions in space between the measurements.

In other words, there exists a kind of transformation between the successive measured data, with which the misalignment can be determined. As a result, two measured profiles can not be simply stitched together. The correction of the misalignment must be done beforehand by means of the misalignment transformations.

4.3.1 The principle to find the transformation

The basic criterion for adjusting the measured segments is that they match each other as well as possible in the overlapping region. Therefore, the fundamental way to find the misalignment transformation is to make use of the measured data of the overlap region. Originally, the measured data acquired from any two successive submeasurements should represent the same physical points or topographical profile of the measured surface. As a result, there should exist a rototranslation such that the points of the second surface segment are mapped on the first. In other words, the transformed points must satisfy the equation of a certain surface. The transformation is the unknown we want to find out.

Figure 4-5 illustrates the concept behind the method to correct the misalignment, where $\mathbf{V_P}$ and $\mathbf{V_Q}$ refer to the overlap region between the first and the second measurements **P** and **Q**, $\mathbf{V_P} \in \mathbf{P}$ and $\mathbf{V_Q} \in \mathbf{Q}$ respectively.

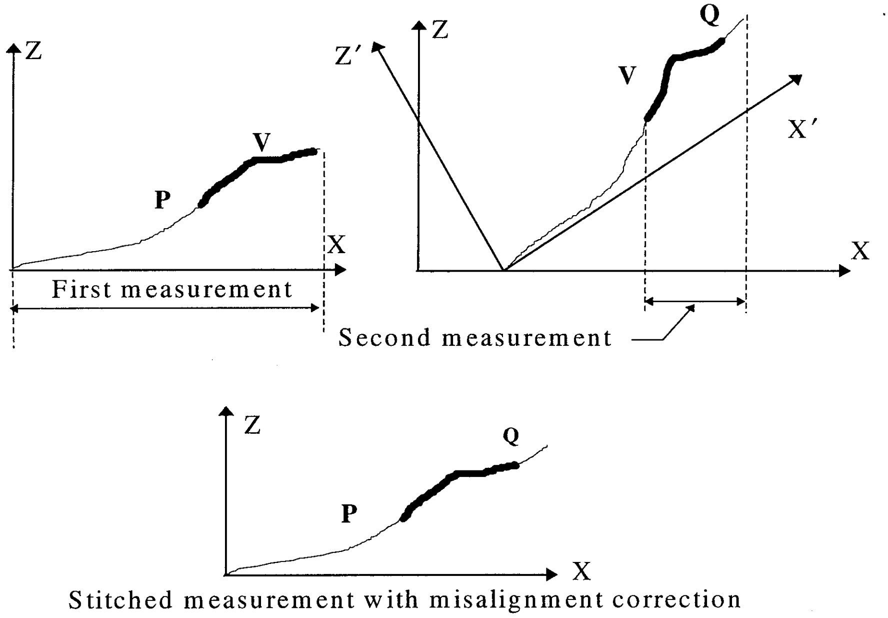

Figure 4-5 Misalignment correction

We are now going to study the correspondences between the two submeasurements in the overlap region.

Based on Equation (4-1) the condition, that the two measured surface segments acquired from two successive submeasurements should represent the same geometry in the overlap region, can be depicted as,

$$\mathbf{Q}_i'' = \mathbf{R}\,\mathbf{Q}_i' + \mathbf{T} + \varepsilon,\ i \in \mathbf{M}. \tag{4-7}$$

In case of the data misregistration has been rectified, the transformations **R** and **T** can be determined in virtue of some kinds of optimisation methods under the condition of letting the error term ε be as small as possible.

4.3.2 The optimization models

As for the data sets **P**$_i$" and **Q**$_i$" within the overlap region, they should represent the same part of the measured surface profile but they happen to be in a different position in the measurement frame because of the misalignment. Due to the measurement uncertainty referring to the error term, ε in Equation (4-7), it is impossible to find a transformation that satisfies the condition (4-1) for every point of **Q**$_i$' for $i \in \mathbf{M}$. We have then to solve an optimization problem, i.e., to find the 'best' transformation or the transformation that brings most points of **Q**$_i$' as close as possible to the points of **P**$_i$'.

An optimization model can be expressed generally [Fletcher, 1990]

$$\underset{\mathbf{X}}{\text{minimise}} \quad f(\mathbf{X}),\ \mathbf{X} = (x_1, x_2, x_3, \ldots, x_n)$$

$$\text{subject to} \quad g_i(\mathbf{X}) \le 0,\ i = 1, 2, \ldots, k, \tag{4-8}$$

where $f(\mathbf{X})$ is called the objective function and $g_i(\mathbf{X})$ are constrains. Both the objective function and the constrains are functions of **X**, an independent variable vector or a matrix.

In terms of the optimization model, the objective function in our case can be written as

$$f(\mathbf{R}, \mathbf{T}) = \sum_i \left\| \varepsilon_i \right\|, \qquad i \in \mathbf{M}. \tag{4-9}$$

Where $\| \cdot \|$ stands for a norm of a vector or a matrix, which is the criterion referring to the converging accuracy or the iteration accuracy of an optimization procedure.

A few kinds of norms can be accepted as a criterion for the iteration quality according to what kind of algorithms is being employed. Perhaps norm 1 and norm 2 are the most widely used options in engineering calculations.

In terms of mathematics the objective function can be written as, when using norm 1, i.e., $\| \cdot \|_1$,

$$f(\mathbf{R}, \mathbf{T}) = \sum_{i \in M} \left| z_i^q - z_i^{q''} \right|, \qquad i \in \mathbf{M}. \tag{4-10}$$

While when using norm 2, i.e., $\| \cdot \|_2$, it can be written as

$$f(\mathbf{R}, \mathbf{T}) = \sum_{i \in M} (z_i^q - z_i^{q''})^2, \qquad i \in \mathbf{M}. \tag{4-11}$$

Either norm 1 or norm 2 can be employed in practice regarding accepted algorithms. The former is in the approach sense to minimise the maximum deviation between two data sets, for example in the Chebyshev approach algorithm. The latter is to minimise the deviation of one data set with respect to the other as reference in the least squares sense.

According to the different way to describe the transformations **R** and **T**, there are two kinds of mathematical models. We shall accept norm 2 as the iteration criterion to find the transformation. This is because that the least squares algorithm is relatively easier to be used in practice. In other words, we shall use Equation (4-11) as the object function $f(\mathbf{X})$ in the optimisation model (4-8).

- **the general model**

According to the general principle of transformation, the unknowns are the nine elements of **R** and the three elements of **T** [Fraleigh 1987]. That means

$$\mathbf{R} = \begin{pmatrix} r_{11} & r_{12} & r_{13} \\ r_{21} & r_{22} & r_{23} \\ r_{31} & r_{32} & r_{33} \end{pmatrix}; \qquad \text{and} \quad \mathbf{T} = \begin{pmatrix} t_x \\ t_y \\ t_z \end{pmatrix}. \tag{4-12}$$

In order to acquire the transformations uniquely and correctly, there might be some constraints subject to the objective function above-mentioned should be taken into consideration. The constraints regarding the translation transformation **T** is

$$\begin{aligned} &| t_x | < \delta \\ &| t_y | < \delta \\ &| t_z | < r_0. \end{aligned} \tag{4-13}$$

Here δ stands for the interval of the CCD grid and r_0 for the nominal radius of the tested curved surface. It is pointed out that in practical cases, $r_0 / t_z \geq 10$, or, $t_z < 0.1\, r_0$.

The first constraint regarding the rotation transformation **R** is that the determinant of **R** should be unitary. The second constrain is that the inverse of **R**, i.e., $\mathbf{R}^{-1}$, should be equal to the transpose of **R**, i.e., $\mathbf{R}^{\mathbf{T}}$. In terms of mathematics, it is read then as

$$\mathbf{R}^{-1} = \mathbf{R}^{\mathbf{T}}. \tag{4-14}$$

The above constrain asks the matrix to be of a rotation, explicitly [Fraleigh 1987]:

$$\frac{r_{22}r_{33}-r_{23}r_{32}}{\Delta} = r_{11}, \quad -\frac{r_{12}r_{33}-r_{13}r_{32}}{\Delta} = r_{21}, \quad -\frac{-r_{12}r_{23}+r_{13}r_{22}}{\Delta} = r_{31},$$

$$-\frac{r_{21}r_{33}-r_{23}r_{31}}{\Delta} = r_{12}, \quad \frac{r_{11}r_{33}-r_{13}r_{32}}{\Delta} = r_{22}, \quad -\frac{r_{11}r_{23}-r_{13}r_{21}}{\Delta} = r_{32},$$

$$\frac{r_{21}r_{32}-r_{22}r_{31}}{\Delta} = r_{13}, \quad -\frac{r_{11}r_{32}-r_{12}r_{31}}{\Delta} = r_{32}, \quad \frac{r_{11}r_{22}-r_{12}r_{21}}{\Delta} = r_{33}, \tag{4-15}$$

where Δ is the determinant of **R**.

Such kind of a general model is rather difficult to be accepted in finding either a numerical or an analytical solution of the problem. This is not only because the objective function with Equation (4-12) is rather complicated, but also because the intricate constrains, e.g., Equation (4-15), must be operated in the computation. Although there is a commercial routine of software available, called E04UCF in the NAG library, it takes much more time and possesses a high degree of complexity, according to our practical experience.

- **the differential model**

In the circumstance of measuring an aspheric surface by the stitching interferometry, most elements of the rotation and translation transformations, **R** and **T**, are infinitesimal comparing with the size of the measured surface, except for the translation shift, t_z, along the z-axis. We call it the infinitesimal hypothesis. Keeping this hypothesis in mind, a kind of differential model had been investigated preferably, in order to simplify the mathematical treatment. Nevertheless, some mathematics for the general treatment should be studied first.

The rotation and translation transformations can be expressed generally as follows [Paul 1982]:

$$Rot\,(x,\psi) = \begin{pmatrix} 1 & 0 & 0 \\ 0 & \cos\psi & -\sin\psi \\ 0 & -\sin\psi & \cos\psi \end{pmatrix}; \quad Rot(y,\theta) = \begin{pmatrix} \cos\theta & 0 & \sin\theta \\ 0 & 1 & 0 \\ -\sin\theta & 0 & \cos\theta \end{pmatrix}; \tag{4-16}$$

$$Rot(z,\varphi)=\begin{pmatrix} \cos\varphi & -\sin\varphi & 0 \\ \sin\varphi & \cos\varphi & 0 \\ 0 & 0 & 1 \end{pmatrix}; \quad T=\begin{pmatrix} t_x \\ t_y \\ t_z \end{pmatrix}. \tag{4-17}$$

Where Rot (x, ψ), Rot (y, θ) and Rot (z, φ) are the rotation transformations about the x, y, and z axis respectively.

The rotation transformation combination of roll, pitch and yaw, RPY (φ, θ, ψ), can be written as

$$\mathbf{R} = \mathrm{RPY}\,(\varphi, \theta, \psi) = \mathrm{Rot}\,(z, \varphi)\,\mathrm{Rot}\,(y, \theta)\,\mathrm{Rot}\,(x, \psi) =$$

$$\begin{pmatrix} \cos\varphi\cos\theta & \cos\varphi\sin\theta\sin\psi-\sin\varphi\cos\psi & \cos\varphi\sin\theta\cos\psi+\sin\varphi\sin\psi \\ \sin\varphi\cos\theta & \sin\varphi\sin\theta\sin\psi+\cos\varphi\cos\psi & \sin\varphi\sin\theta\cos\psi-\cos\varphi\sin\psi \\ -\sin\theta & \cos\theta\sin\psi & \cos\theta\cos\psi \end{pmatrix}, \tag{4-18}$$

Similarly, the unknowns here are the nine elements of **R** and the three elements of **T**.

Now, we are going to investigate the differential transformations. Substitute cosθ, sinθ, t_x and t_y with their first order approximations in Equation (4-18), we have then the differential transformation

$$\mathbf{R_d} = \mathrm{Rot}\,(z, \delta_z)\,\mathrm{Rot}\,(y, \delta_y)\,\mathrm{Rot}\,(x, \delta_x), \tag{4-19}$$

where Rot (z, δ_z), Rot (y, δ_y) and Rot (x, δ_x) are the differential rotation translations about z-, y- and x-axis with smaller differential rotation δ_z, δ_y and δ_x respectively.

That means

$$\mathbf{R_d} = \begin{bmatrix} 1 & -\delta_y & 0 \\ \delta_z & 1 & 0 \\ 0 & 0 & 1 \end{bmatrix} \begin{bmatrix} 1 & 0 & \delta_y \\ 0 & 1 & 0 \\ -\delta_y & 0 & 1 \end{bmatrix} \begin{bmatrix} 1 & 0 & 0 \\ 0 & 1 & -\delta_x \\ 0 & -\delta_x & 1 \end{bmatrix} \approx \begin{bmatrix} 1 & -\delta_z & \delta_y \\ \delta_z & 1 & -\delta_x \\ -\delta_y & \delta_x & 1 \end{bmatrix}. \tag{4-20}$$

Conclusively, the differential transformations $\mathbf{R_d}$ and $\mathbf{T_d}$ can be written as

$$\mathbf{R_d} = \begin{bmatrix} 1 & -\delta_z & \delta_y \\ \delta_z & 1 & -\delta_x \\ -\delta_y & \delta_x & 1 \end{bmatrix} ; \quad \text{and,} \quad \mathbf{T_d} = \begin{pmatrix} d_x \\ d_y \\ t_z \end{pmatrix}. \tag{4-21}$$

It is very favourable that the number of the unknowns has been reduced down to six, the three elements of **R** and the three elements of **T**. This will greatly improve the computational efficiency and reduce the complexity of the problem.

Another advantage of the differential model is the fact that the sequence of each transformation is not important, that affects nothing, although in the general model the sequence of each transformation is important. In other words,

$$\mathrm{Rot}\,(z, \varphi)\,\mathrm{Rot}\,(y, \theta)\,\mathrm{Rot}\,(x, \psi) \neq \mathrm{Rot}\,(x, \psi)\,\mathrm{Rot}\,(y, \theta)\,\mathrm{Rot}\,(z, \varphi), \tag{4-22}$$

$$\mathrm{Rot}\,(z, \delta_z)\,\mathrm{Rot}\,(y, \delta_y)\,\mathrm{Rot}\,(x, \delta_x) = \mathrm{Rot}\,(x, \delta_x)\,\mathrm{Rot}\,(y, \delta_y)\,\mathrm{Rot}\,(z, \delta_z). \tag{4-23}$$

This characteristic allows to simplify the operation and calculation to a certain extent.

- **a short summary**

The criteria to stitch the two measured profiles together is to minimise the data differences of the overlap region, based on the Equation (4-9) and appropriate transformations.

As for the transformations **E** regarding the data misregistration rectification, there exists the following relationship between the raw data $\{\mathbf{Q}_j\}$ and the corrected data $\{\mathbf{Q}_i'\}$, i.e.,

$$\mathbf{Q}_i' = \mathbf{E}\,\mathbf{Q}_j + \varepsilon'. \tag{4-24}$$

In terms of matrix, it is

$$\begin{pmatrix} x_i^{q'} \\ y_i^{q'} \\ z_i^{q'} \end{pmatrix} = \begin{pmatrix} e_{11} & e_{12} & e_{13} \\ e_{21} & e_{22} & e_{23} \\ e_{31} & e_{32} & e_{33} \end{pmatrix} \begin{pmatrix} x_j^q \\ y_j^q \\ z_j^q \end{pmatrix} + \begin{pmatrix} \varepsilon'_x \\ \varepsilon'_y \\ \varepsilon'_z \end{pmatrix}. \tag{4-25}$$

As for the transformations **R** and **T** regarding the misalignment correction, there exits the following relationship between the data with misregistration rectification but without misalignment correction {$\mathbf{Q}_i'$} and the completely corrected data {$\mathbf{Q}_i''$}. The general model leads to

$$\mathbf{Q}_i'' = \mathbf{R}\,\mathbf{Q}_i' + \mathbf{T} + \varepsilon, \qquad (4\text{-}26)$$

or, with matrix expression,

$$\begin{pmatrix} x_i^{q''} \\ y_i^{q''} \\ z_i^{q''} \end{pmatrix} = \begin{pmatrix} r_{11} & r_{12} & r_{13} \\ r_{21} & r_{22} & r_{23} \\ r_{31} & r_{32} & r_{33} \end{pmatrix} \begin{pmatrix} x_i^{q'} \\ y_i^{q'} \\ z_i^{q'} \end{pmatrix} + \begin{pmatrix} t_x \\ t_y \\ t_z \end{pmatrix} + \begin{pmatrix} \varepsilon_x \\ \varepsilon_y \\ \varepsilon_z \end{pmatrix}. \qquad (4\text{-}27)$$

The differential model leads to

$$\mathbf{Q}_i'' = \mathbf{R}_d\,\mathbf{Q}_i' + \mathbf{T}_d + \varepsilon_d\,, \qquad (4\text{-}28)$$

or

$$\begin{pmatrix} x_i^{q''} \\ y_i^{q''} \\ z_i^{q''} \end{pmatrix} = \begin{pmatrix} 1 & -\delta_z & \delta_y \\ \delta_z & 1 & -\delta_x \\ -\delta_y & \delta_x & 1 \end{pmatrix} \begin{pmatrix} x_i^{q'} \\ y_i^{q'} \\ z_i^{q'} \end{pmatrix} + \begin{pmatrix} d_x \\ d_y \\ t_z \end{pmatrix} + \begin{pmatrix} \varepsilon_{xd} \\ \varepsilon_{yd} \\ \varepsilon_{zd} \end{pmatrix}. \qquad (4\text{-}29)$$

This is based on the infinitesimal hypothesis. A further analysis regarding its effects on the accuracy will be done in the following chapters.

4.3.3 Solving the problems

In principle, the objective function $f(\mathbf{R}, \mathbf{T})$ can be exactly determined or computed by a kind of constrained optimization method. However the complexity of $f(\mathbf{R}, \mathbf{T})$ can affect the complexity of the solution. If the overlap region includes too many points and the function $f(\mathbf{R}, \mathbf{T})$ is very complicated, this kind of method is expected to be very time-consuming.

An easy form for $f(\mathbf{R}, \mathbf{T})$ can be obtained in the following approximate way. Let's suppose that the misalignment errors be small compared to the grid interval, after the data misregistration rectification. It is then safe to assume that the points on the two grids correspond to the same physical point on the measured surface. In other words, the indexes of data sets {$\mathbf{Q}_i''$} and {$\mathbf{Q}_i'$} are the same. Therefore, only z-coordinates ($z_i^{q''}$, $z_i^{q'}$ and z_i^{q}) should be taken into consideration. It is then allowed to use the so-called point to point fitting method in Equation (4-26) to express the **Q**$_i$", whose z-coordinate is $z_i^{q''}$,

$$z_i^{q''} = x_i^{q'} r_{31} + y_i^{q'} r_{32} + z_i^{q'} r_{33} + t_z + \varepsilon_{zi}\,, \quad i \in \mathbf{M} = [1, 2, \ldots m]. \qquad (4\text{-}30)$$

The actual expression in terms of matrix should be read as

$$\begin{pmatrix} z_1^{q''} \\ z_2^{q''} \\ z_3^{q''} \\ \vdots \\ \vdots \\ z_m^{q''} \end{pmatrix} = \begin{pmatrix} x_1^{q'} & y_1^{q'} & z_1^{q'} & 1 \\ x_2^{q'} & y_2^{q'} & z_2^{q'} & 1 \\ x_3^{q'} & y_3^{q'} & z_3^{q'} & 1 \\ \vdots & \vdots & \vdots & \vdots \\ \vdots & \vdots & \vdots & \vdots \\ x_m^{q'} & y_m^{q'} & z_m^{q'} & 1 \end{pmatrix} \begin{pmatrix} r_{31} \\ r_{32} \\ r_{33} \\ t_z \end{pmatrix} + \begin{pmatrix} \varepsilon_{z1} \\ \varepsilon_{z2} \\ \varepsilon_{z3} \\ \vdots \\ \vdots \\ \varepsilon_{zm} \end{pmatrix}. \qquad (4\text{-}31)$$

Moreover, based on our infinitesimal hypothesis and its consequence referring to the differential model of Equation (4-29), the above expression can be further simplified as

$$z_i^{q''} = - x_i^{q'} \delta_y + y_i^{q'} \delta_x + z_i^{q'} + t_z + \varepsilon_{3i}\,, \quad i \in \mathbf{M} = [1, 2, \ldots, m]. \qquad (4\text{-}32)$$

This is the result of substituting r_{31}, r_{32} and r_{33} with $-\delta_y$, δ_x and 1 into the Equation (4-30).

There exist a couple of algorithms which can be used to solve our problems [Fletcher 1990, Fraleigh 1987]. This is a kind of non-linear least squares problem because the objective function f (**X**) is not linear. We have solved the problem by applying the algorithm of the Levenberg-Marquardt method with a mixed quadratic and cubic line search procedure. Naturally, the Gauss-Newton algorithm can be accepted alternatively [Fletcher 1990].

As a result, the transformations, **R** and **T**, can be determined by solving the optimization problem of the least squares, based on Equation (4-11) and Equation (4-31) or (4-32).

4.4 Rectification of data misregistration

4.4.1 Data misregistration

In the Fizeau interferometry arrangement shown in Figure 2-4, the focal point of a well-corrected focusing lens is coincident with the center of curvature of the tested curved surface. When the test object is a sphere, the interference pattern on the detector consists of straight lines, of which the spatial frequency is proportional to the tilt of the reference surface.

A spherical object under test sends the rays that emanate from the focus of the well-corrected focusing lens back along the same path. At the same time, a data registration is formed on the CCD grid. Any deviation in respect to this kind of data registration, due to optical path variation, will be called data misregistration. In other words, the data registration formed on the CCD grid under the circumstance of testing spherical surface with ideal optics is set as a reference. Any position variation differing from the reference pattern of data registration is defined as data misregistration.

In case of measuring a steep aspheric surface by stitching interferometry, however, the picture is different from measuring a spherical surface. We have to deal with the misregistration problem.

There are two major factors that can cause the data misregistration in the image formation course. The first one is the surface asphericity that results in different ray trajectories of the incoming and outgoing rays described in Chapter 2. The second factor is the variation of the object position due to the shift in the stitching procedure, which results in optical path changes as well. In either case, the optical aberration of the well-corrected focusing lens may contribute to the data misregistration as well. It is the principal aberration that has been taken into consideration because all other kinds of optical aberrations with the commercial interferometer should be negligible.

Based on the treatment of image formation according to the Hamilton's method of characteristic function, the problem can be solved by means of the so-called eikonal methods [Born & Wolf 1984, Velzel 1987]. These methods deal with the characteristic functions of a surface and enable us to determine uniquely the corresponding image position of a surface. In order to do so, some analysis tools regarding optical image formation treatment are needed.

4.4.2 Image formation and the eikonal method

An optical system is a set of arrangements of refractive, reflective and diffracting surfaces. Geometrical optics is a science of image formation for an optical system. To trace the optical path and locate the image position corresponding to the object point is a must to optical design and optical analyses.

Under the right circumstances, it is possible to simplify the treatment with the concept of light rays. Rather than thinking about waves propagating through space, we think about lines that are normal to the waves, and we call these lines light rays or simply rays. The behaviour of these rays can be modelled by some relatively simple equations. This is called geometrical optics. However, we still keep track of quantum and physical optics effects when needed to get the right answers.

Image formation of an optical system can be characterised by a set of functions of coordinates in both the object and image spaces. Such functions uniquely determine a ray of light travelling through the system. The functional value equals to the optical path length measured along the ray between the two points, determined by the coordinates [Born & Wolf 1984].

In recent years, some research has been done on the theory and methods of characteristic functions of Hamilton, especially on the angle characteristic or angle eikonal as well as its applications on aberration theory [Velzel 1987]. The method enables us to determine uniquely the corresponding image positions of a reflective surface, once the desired characteristic function is known, and vice versa.

The angle eikonal is a function of direction cosines. Let L, M, N be the direction cosines of an incoming ray in object plane, see Figure 4-6, and L′, M′, N′ be those of the outgoing ray in image plane respectively. The same Cartesian coordinate system is used for both the object and image space. Here the incoming and outgoing rays is with respect to S, an optical system or a surface.

The angle eikonal is defined as the optical path along the ray between the points A and B that are the feet of perpendiculars from point O to the incoming and outgoing parts of the ray. Consequently, the angle eikonal is given [Born & Wolf 1984]

$$\mathrm{E}(\mathrm{L}, \mathrm{M}, \mathrm{N}; \mathrm{L}', \mathrm{M}', \mathrm{N}') = \int_A^B n\, ds, \qquad (4\text{-}33)$$

where n is the refractive index.

The relationship among the ray positions in the object and image spaces can be obtained by differentiation of the angle eikonal. In this chapter the eikonal theory is applied in two ways for the purpose of analysing a interferometer for aspheric testing, namely, 1) to define a linear system and, 2) to treat small perturbations.

It is possible to obtain direction cosines of the incident rays, L, M, N, as well as focus offsets, because the surface describing function is known.

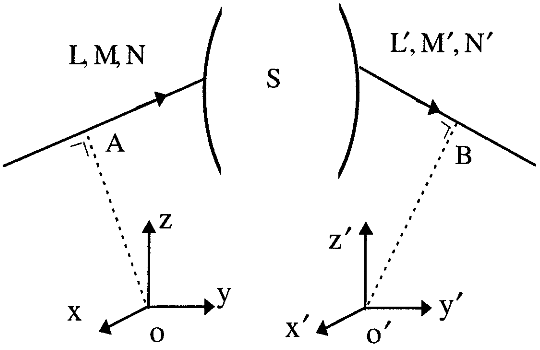

Figure 4-6 Direction cosines in eikonal analysis

Afterwards, the paraxial equations are used with the aid of the eikonal method, to calculate direction cosines of the imaging rays, L′, M′, N′, and then the misregistration on the CCD image plane. As a result, we then finally know the compensation needed for rectification of the misregistration.

Considering the fact that the measuring system of the tested aspheric surface and the optics is of symmetrical arrangement, 2-dimensional analysis is sufficient. In other words, the angle eikonal in our case is a function of two direction cosines L, M and L′, M′.

4.4.3 Misregistration due to the surface asphericity

- **Different ray trajectories**

In the case of an aspheric surface being measured in the scheme of Figure 2-4, the returning beams from the aspheric surface no longer follow the same path as in the case of a sphere. Therefore, the returning rays do not pass through the focal point, but deviate over an angle γ, showing in Figure 4-7, that is given in terms of the asphericity d_r (see Chapter 2.2.4) by

$$\gamma = 2\,(\partial\, d_r) / (r\, \partial\eta), \tag{4-34}$$

where η is the angle that the incoming ray makes with the optical axis, and r is the radius of tested surface.

The reflected ray will make an angle γ' with the reflected ray from the reference. (When the tilt is zero, a concentric circular interference pattern will result.) To the first approximation, the angle is given by

$$\gamma' = -\,\gamma\, r / f, \tag{4-35}$$

where r is the distance from the focal point F to the point P where the ray in question hits the tested object ($r = r_0 + d_r$), while f is the focal distance of the focusing lens. In our case, $f / r_0 = 80$ mm /8 mm =10, and at average, $r/r_0 \cong 1.027$ and r_0 / d_r is of the order of 300, approximately.

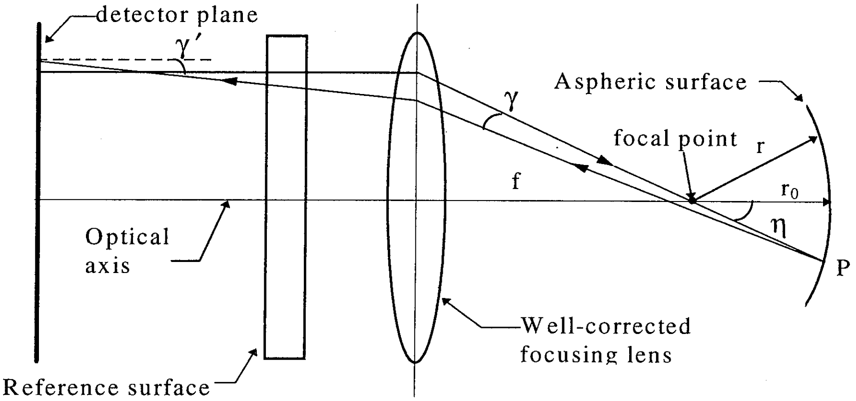

Figure 4-7 Different ray trajectories due to surface asphericity

The interference fringes on the detector have a period

$$p = \lambda / \gamma'. \tag{4-36}$$

When this period is of the order of the pixel interval between the contents of two inter pixels on the CCD array, moiré patterns are formed between the pixel grid and the interferogram [Greivenkamp 1987]. We need at least four pixels to resolve one period of the interferogram adequately, so that we have the condition

$$\gamma' < \lambda / 4p. \tag{4-37}$$

We have a magnification factor M between the detector plane as shown in Figure 4-7 and the CCD, so that p = 10 M μm. With p = 10 M μm and λ= 0.6328 μm, γ' must be smaller than 1.5M milliradians. With M being of the order of 5, r = 8 mm and f = 35 mm, we see that γ' must be smaller than about 6.7 milliradians.

When the aspheric surface is so steep that γ exceeds this value, we can take recourse to stitching interferometry. This means that we obtain the 3D profile of that zone of the aspheric surface where the fringe density is sufficiently low, and then translate the aspheric object to obtain the profile of another zone which has an overlap region with the previous one. Fitting the profiles and continuing the procedure leads to a complete 3D profile of the tested object.

- **Misregistration when using an ideal lens**

The measurement of aspherics by Fizeau interferometer has a disadvantage that becomes serious when the asphericity of the test object is considerable. We describe this problem at the hand of Figure 4-8 . In this section, it is assumed that the beam illuminating the object departs from a perfect focus, although in a later section consideration will be given to the influence of aberrations as well.

When an incoming ray meets the aspheric surface at P, it is in general not reflected in the same direction, as described above in Equation (4-34). This causes a misregistration Δx, between this reflected ray and the corresponding reference ray on the detector. The misregistration is zero when the detector is situated at the point P′ where P is imaged by the focusing lens. Because the image of the aspheric tested object is in general not flat, it is not possible to make the misregistration zero for all points on the aspheric surface. In the next section we analyse the misregistration for the case of an ideal focusing lens.

An ideal lens is a lens without aberration. With an ideal focusing lens, in the sense of eikonal theory [Velzel 1987], the ray transfer equations are given by

$$L = x' / f,$$

$$x = - L' f. \tag{4-38}$$

Where f is the focal distance, x and x′ are coordinates in the front and back focal plane, respectively; L and L′ are direction cosines in object space and image space respectively.

For a ray that leaves a point P of the aspheric surface to be measured, see Figure 4-8, making an angle $\eta+\gamma$ with the optical axis, we have

$$L' = \sin(\eta + \gamma)$$
$$x' = -r \sin\gamma / \cos(\eta + \gamma), \qquad (4\text{-}39)$$

from which L and x follow with Equation (4-38) respectively.

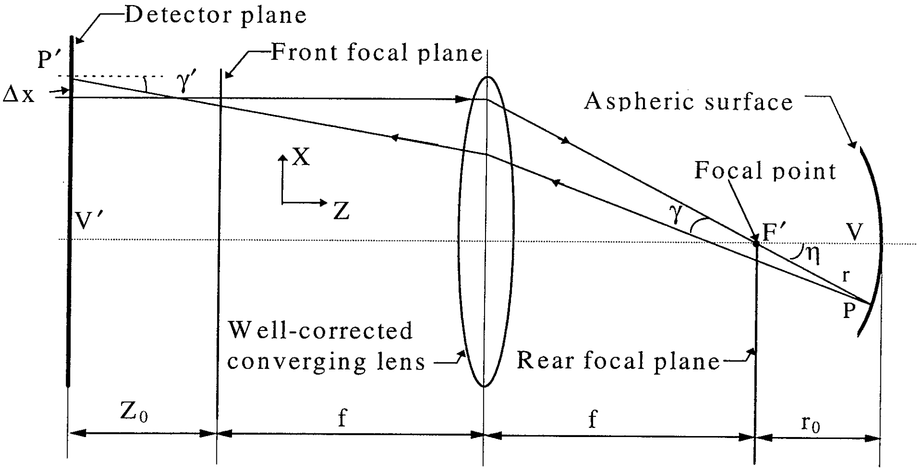

Figure 4-8 Misregistration of the reflected ray in the detector plane

In a detector plane that is situated at a distance Z_0 from the front focal plane, the position x_D of the ray is given by

$$x_D = x + Z_0 L / N, \qquad (4\text{-}40)$$

where $N = (1-L^2)^{1/2}$. The misregistration Δx is given by

$$\Delta x = x_D - x_0 \qquad (4\text{-}41)$$

where x_0 is the ray position of the reference ray, for which we have

$$x_0 = -f \sin\eta \qquad (4\text{-}42)$$

Using Equations (4-39) through (4-42), we can find an expression for Δx that is exact as long as we have an ideal lens. For convenience we introduce the approximation $N \cong 1$ in Equation (4-40).

This is allowed because $L < 1.5$ milliradians (That $M = 5$ results $L < 1.5$ milliradians). With this approximation we find that

$$\Delta x = f\,(\sin\eta - \sin(\eta+\gamma)) - Z_0\ (r/f)\,(\sin\gamma / \cos(\eta+\gamma)). \qquad (4\text{-}43)$$

The corresponding error in the above equation is of the order of

$$f \times \sin\gamma \times (1-N) / \cos(\eta+\gamma)$$
$$= 80 \times (2/\surd 3) \times 0.03 \times 0.5 \times (0.0075)^2 \text{ mm, or}$$
$$\Delta x < 10^{-4} \text{ mm} = 0.1\ \mu\text{m}. \qquad (4\text{-}44)$$

While considering the axial position of the detector in such a way that the vertex V (Figure 4-8) of the aspheric surface is imaged in the detector plane, we have

$$Z_0 = -f^2 / r_0. \qquad (4\text{-}45)$$

According to Newton's image equation, where r_0 is the radius of curvature at the vertex. Now we find

$$\Delta x = f\,\{\sin\eta - \sin(\eta+\gamma) + (r/r_0)\sin\gamma/\cos(\eta+\gamma)\}. \qquad (4\text{-}46)$$

This is the essential formula for calculating the misregistration. Note that r depends on η, with an aspheric surface. The calculation of r and η can be carried out based on the relationship of $Z = Z(x)$, contact lens surface expression, from Equation (2-1).

To show the order of magnitude of the misregistration, the approximations $r \cong r_0$ and $\cos\gamma \cong 1$ are employed, so that

$$\Delta x \cong f \sin\gamma\,(-\cos\eta + (1/\cos\eta)). \qquad (4\text{-}47)$$

With $\gamma \cong 1.5m$ milliradians, and $\eta = 30°$, we find

$$\Delta x \cong f \times m \times 4 \times 10^{-4}. \qquad (4\text{-}48)$$

With $f = 80$ mm, this corresponds to about 4 pixels (32 μm) on the CCD.

- **Misregistration when using a real lens**

Now we study the case of the aberration with the well-corrected focusing lens used. In this section, another result of the eikonal theory will be used [Born 1984]. It can be expressed as follows:

"The wavefront error caused by a small perturbation of an optical instrument is, to a first approximation, equal to the optical path length of the perturbation along the unperturbed rays."

For the situation discussed in the previous section, we can add the wavefront error and then calculate the misregistration due to the aberrations in addition to those caused by the asphericity of the tested object. As for the aberration here, we refer mainly to spherical aberration of the well-corrected focusing lens .

In case there are some spherical aberrations of the well-corrected focusing lens, we can describe the spherical aberration of the wavefront in the focal plane mathematically, based on the wavefront analysis theory and methods. Considering its characteristics of symmetry, it can be expressed as

$$W = ax^2 + bx^4 + cx^6, \tag{4-49}$$

where a, b and c are constants.

In the following, it is assumed that $a \cong 0$ and $W \cong 0$ at the edge of the pupil, x_r, so that $bx_r^4 + cx_r^6 \cong 0$. The maximum value of W is reached, according to differential calculus, when

$b + 3cx_r^2 /2 = 0$ is satisfied, or in other words,

$$x_r^2 = - 2b / 3c. \tag{4-50}$$

This is equal to

$$4b^3 / 9c^2 - 8b^3 /27c^2 = 4b^3 /27c^2 = - 4bx_r^4 / 27 \tag{4-51}$$

This is the maximum form error caused by spherical aberration described by Equation (4-49).

For a diffraction limited objective, bx_r^4 should remain within one wave length [Malacara 1993]. The form error is a factor 4 /27 smaller. It can be removed from the measurement data by calibration.

Generally speaking, the misregistration caused by this aberration is given by

$$\Delta x = (\partial W/\partial x)\, Z_0 = (2ax + 4bx^3 + bcx^5)\, Z_0. \tag{4-52}$$

With $a = 0$ and $b = - c\, x_r^2$, it can be written as

$$\Delta x = (4bx^3 - 6bx^5 / x_r^2)\, Z_0 . \tag{4-53}$$

The maximum value of misregistration Δx is reached at $x^2 = (2/5)\, x_r^2$. The maximum value is

$$\Delta x_{max} = 0.85\, b\, x_r^4\, Z_0 / x_r. \tag{4-54}$$

With $bx_r^4 \cong \lambda = 0.6328$ μm and $(Z_0 / x_r) \cong 20$, this is of the order of 10 μm.

This is the result with one wavelength (λ) aberration. However in the practical situation, the actual aberration of the reference object is 20 times smaller, only $\lambda/20$. Considering another fact also that this is the maximum value of misregistration introduced by optical aberration in the worst situation, such kind of misregistration error is therefore negligible. Actually, the practical aberration with the lens we used is less than $\lambda/20$ ($\cong$ 0.03 μm) that introduces a data misregistration in the order of only several tenth of a micrometre.

4.4.4 Misregistration due to object shift

When the stitching interferometry for the accurate measurement of steep aspheric surfaces is employed, as described in the Chapter 3, a test object is shifted along the axial direction between two successive submeasurements. This shift ΔZ, from position 1 to position 2 in Figure 4-9 , causes a change in the optical path of the reflected rays and therefore results in data misregistration on the CCD grid. Accordingly, it is necessary to rescale the data $\{\mathbf{Q}\}$ acquired in a posterior measurement with respect to those, $\{\mathbf{P}\}$, acquired in a prior measurement. It is of course important to know the object shift ΔZ precisely.

With the aid of Figure 4-9, the ratio of the first magnification M_1 to the second one M_2 can be determined. As the object being shifted with a translation amount ΔZ, the vertical dimension of the half measured area subtending at the same angle η changes from h_1 to h_2, while the image dimension on the CCD plane, h', remains the same.

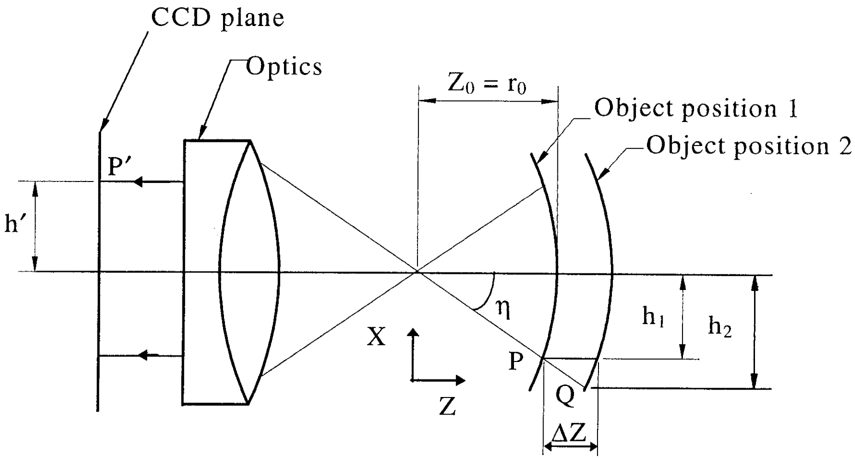

Figure 4-9 Lateral magnification changes due to object shift

It can be seen from figure 5 that the x-coordinate (height) of the point Q is a factor μ lager than the x-coordinate of the point P that is at the original position before shift but in the same direction. To a first approximation, the factor is

$$\mu \cong h_2 / h_1 = 1 + \Delta Z / Z_0 = 1 + \Delta Z / r_0. \qquad (4\text{-}55)$$

By means of the above expression, data of the set {**Q**} acquired in a posterior measurement can be rescaled conveniently, and then treated associatively with the data of set {**P**} acquired in a prior measurement during the stitching procedure.

When γ would approach to zero, i.e., to measure a "mild" aspheric surface, the above equation would be sufficient for the correction of the measurement.

In case of a steep aspheric surface being tested, $\gamma \neq 0$, we should use Equation (4-46) to calculate the misregistration for rectification. Nevertheless, we need in this case some more precise deduction and calculation for the geometric parameters considering the changes due to the object shift.

In addition to Equation (4-34) that can be used directly, we are going to manifest the coordinates (r, η) of the data set {**Q**} after a shift with the coordinates (r', η') of the data set {**P**} before the shift. The latter can be obtained readily by treating the surface expression mathematically.

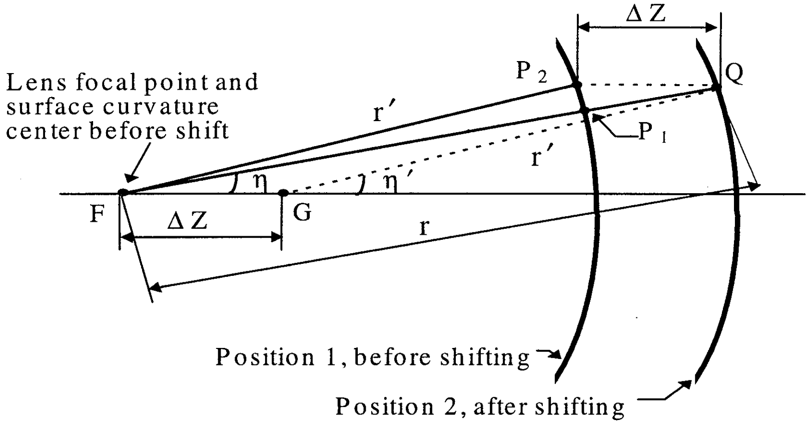

Figure 4-10 Optical path variation due to object shift

With the aid of triangle geometry of Δ FQG about the angle ∠FGQ in Figure 4-10, we have

$$r^2 = r'^2 + 2\, r'\, \Delta Z \cos \eta' + \Delta Z^2, \tag{4-56}$$

and

$$\tan \eta = r' \sin \eta' / (r' \cos \eta' + \Delta Z). \tag{4-57}$$

Let $Z'(X)$ be new z-coordinates of the aspheric surface, we can calculate r and η directly by applying the relationship of $Z'(X) = Z(x) + \Delta Z$ to Equation (2-1).

As an example, we take the shifting of a sphere, so that $r' = r_0$ is a constant. From Figure (4-10) we have directly by applying the cosine rule,

$$r'^2 = r^2 - 2\, r\, \Delta Z \cos \eta + \Delta Z^2. \tag{4-58}$$

Solving this equation about r, we have got

$$\begin{aligned} r &= \Delta Z \cos \eta + (\Delta Z^2 \cos^2\eta - \Delta Z^2 + r'^2)^{1/2} \\ &= r' + \Delta Z \cos \eta - \Delta Z^2 \sin^2\eta / 2r' + O(4), \end{aligned} \tag{4-59}$$

and

$$\gamma = 2(-\Delta Z \sin \eta / r' - \Delta Z^2 \sin \eta \cos \eta / r'^2 + O(3)). \tag{4-60}$$

This shows clearly that with a spherical surface, defocusing gives an extra term $\Delta Z \cos \eta$ in the form function (plus smaller terms). Because of $\gamma \neq 0$ in case of a steep aspheric surface being tested, one can not measure more aspheric departures from a reference sphere limited by the following expression,

$$\sin \eta < (r' / \Delta Z) \times \gamma_{max} , \tag{4-61}$$

where γ_{max} is given by Equations (4-35) and (4-37) and is equal to 0.0067 radian.

4.5 The overlap regions

Yet the primary issues in the algorithm development of the stitching interferometry are dedicated to the correction of misalignment and rectification of the data misregistration. Nevertheless, there still are a few other matters needing to be taken into consideration, too. As the overlap region is so important as discussed in previous sections, the influence of both the minimum size and the optimum size of the overlap region, the latter referring to the number of measurements in a stitching process, should be investigated.

4.5.1 Minimum width of the overlap region

Based on the analysis in Chapter 1.2.3, the least width of the overlap region between two successive interferograms should be kept, theoretically, with respect to 4 pixels on the CCD employed, while a suggested minimum width of the overlap region should go with 8 pixels.

For the entire aperture with a 240 × 240 pixel CCD, more than 15 rings or 30 fringes could, in principle, be recorded.

However, according to our experience, taking more than 6 rings or 12 fringes may strongly affect measurement accuracy, while less than 4 rings is preferable. Unevenness of the fringe density over the whole interferogram might be responsible for that.

If the aspheric surface slope departure from the available reference should not meet the above conditions, the stitching interferometry could still be useful because it might reduce the optical complexity of the compensation lenses.

4.5.2 The optimum size of an overlap region

The measured areas need to overlap in order to adjust the relative misalignment and data misregistration of each measurement. However, here comes again a dilemma or a trade-off problem between the measurement accuracy and efficiency in the stitching interferometry. This mainly has much to do with the overlap region. The larger the overlap region is, the higher the accuracy will be, while the more the number of measurements should be made; vice versa, the smaller the overlap region is, the higher the efficiency will be. As a result, it is needed to find an optimum size of an overlap region for a pair of successive measurements.

The problem can be solved by means of either theoretical calculation or experimental work. We discuss both approaches in the following.

- **theoretical method**

As for the theoretical means, the task to find an optimum shift, which is associated with the optimum size of an overlap region directly, can be fulfilled by applying the so-called "penalty function" algorithms of optimization [Fletcher 1990] to the measuring processing.

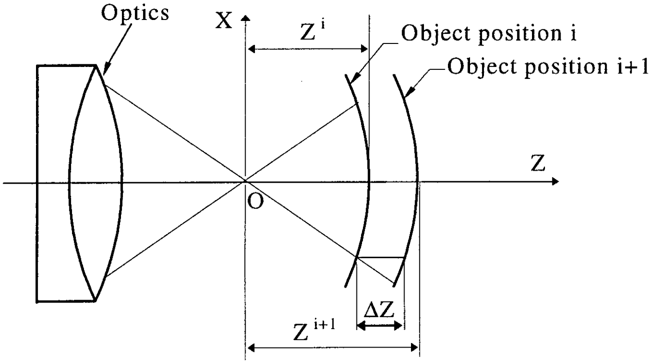

Figure 4-11 Shift between the ith and the (i+1)th measurements

The basic concept behind the method is to maximise the shift ΔZ between the ith and the (i+1)th measurements under certain conditions regarding accuracy required. Let Z^i and Z^{i+1} be the distances from the vertex centre of the surface curvature O to the object position i and the position i+1, respectively, the objective function is then to maximise $(Z - Z^i)$. The constrains are associated with the allowed aspheric departure in the normal direction and required accuracy.

The aspheric departure in normal direction, d_r , given by Equations (2-2) and (2-1) in Chapter 2.2.4, is referred to the surface geometry and mathematical expression of the tested object. Its allowance $d_{r\ \mathrm{allowance}}$ can be determined according to the analysis in the prior section.

In terms of optimisation, the mathematical model is written as

$$\begin{array}{ll} \text{- minimise} & (Z^{i} - Z) \\ \text{subject to} & |\, d_r \,| < d_{r\ \mathrm{allowance}} - \varepsilon \\ & Z^{i+1} \geq Z \geq Z^{i}. \end{array} \tag{4-62}$$

And then the penalty function PF is modelled as

$$\begin{aligned} PF = (Z^{i} - Z) + \tfrac{1}{2}\sigma \{ & \min [(d_{r\ \mathrm{allowance}} - \varepsilon - d_r), 0]^2 \\ & + \min [(d_{r\ \mathrm{allowance}} - \varepsilon + d_r), 0]^2 + \min [(Z^{i+1} - Z), 0]^2 \\ & + \min [(Z - Z^{i}), 0]^2 \}, \end{aligned} \tag{4-63}$$

where ε is a predetermined allowance of accuracy, σ is a parameter so-called penalty factor. It is common to choose a value of σ for each iterative step from a series such as {10, 100, 1000, ...} until a satisfactory result is reached [Fletcher, 1990].

With $d_{r\ \mathrm{allowance}} = 5$ µm that is equivalent to 8 rings or 16 fringes and $\varepsilon = 0.1$ µm, we have gotten a $\{Z^{i}\}$ series of {8.0000, 8.0669, 8.0901, 8.1129, 8.1532,... 8.3419 (mm)}. In fact, only three measurements are necessary to be made to test almost 90% of the contact lens surface. One is made at the curvature centre and other two at the positions with 0.0669 mm and 0.0232 mm relative shifts respectively. In case the outermost part, segment D, being tested, more number of measurements up to 7 will be needed. Fortunately, because such kind of outermost part referring to segment D has nothing to do with optical function, it is therefore not required to be tested at all.

- **experimental method**

As for the experimental means, it can be done by comparing the results of different percentage of overlap with that of a standard sample. Firstly, a measurement was made of a spherical surface in terms of shape inaccuracy PV to set up a comparison standard. Then three groups of measurements were made with different percentages of overlap and varying numbers of measurements.

It has been seen from Table 4-1 that for each percentage of overlap regions, the smallest error was achieved for a small number of measurements, and for the largest overlap region the error was the smallest. Considering the fact that the accuracy in this research is to be required of the order of submicron, the 25% overlap region seems to be a good compromise between accuracy and efficiency. As long as an optimum percentage of overlap region is determined, an optimum size of overlap region can be then readily determined, too.

Table 4-1 Influence of overlap size on the measurement

(comparison standard: 0.232 μm **in PV)**

number of measurements	**10% overlap**	**25% overlap**	**40% overlap**
2	0.84 μm	0.24 μm	0.21 μm
5	1.67 μm	0.32 μm	0.28 μm
average	1.25 μm	0.28 μm	0.25 μm

Greater overlap allows for more accurate fitting, whereas minimal overlap enables fewer measurements to be made. In addition, as the number of measurements increases, the accuracy drops down when the more measured pieces are stitched up together.

Both theoretical and experimental means can be accepted to determine an optimum size or percentage of the overlap region. Although the theoretical one may be more precise, it is much more practical and easy to take advantages of the experimental result.

Furthermore, we point out that for a stitching procedure which takes more than two measurements, the overlap also depends on the number of stitched profiles. Each step of stitching brings errors to the resultant measurement uncertainty.

5.

Realisation and Experiments

5.1 Measuring scheme

Figure 5-1 demonstrates the schematical block diaphragm of the measuring scheme for the accurate measurement of curved surfaces by stitching interferometry.

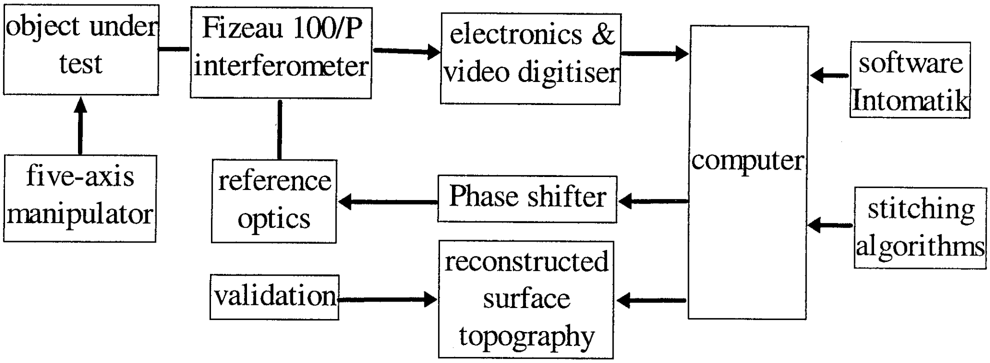

Figure 5-1 The measuring scheme

An Fizeau phase shifting interferometer measures the surface under test according to the stitching procedure described in Chapter 3.3. A series of submeasurements is recorded as phase map information data. After being converted into topographical data sets, the measured data are interpreted into a series of profile pieces. Finally, an entire reconstructed surface is obtained by stitching the series of profile pieces up together, by means of the stitching algorithms described in Chapter 4.

5.2 The interferometer

The heart of the stitching interferometric system consists of a commercial Möller-Wedel V100/P Fizeau phase shifting interferometer. Figure 5-2 shows the optical arrangement of the system.

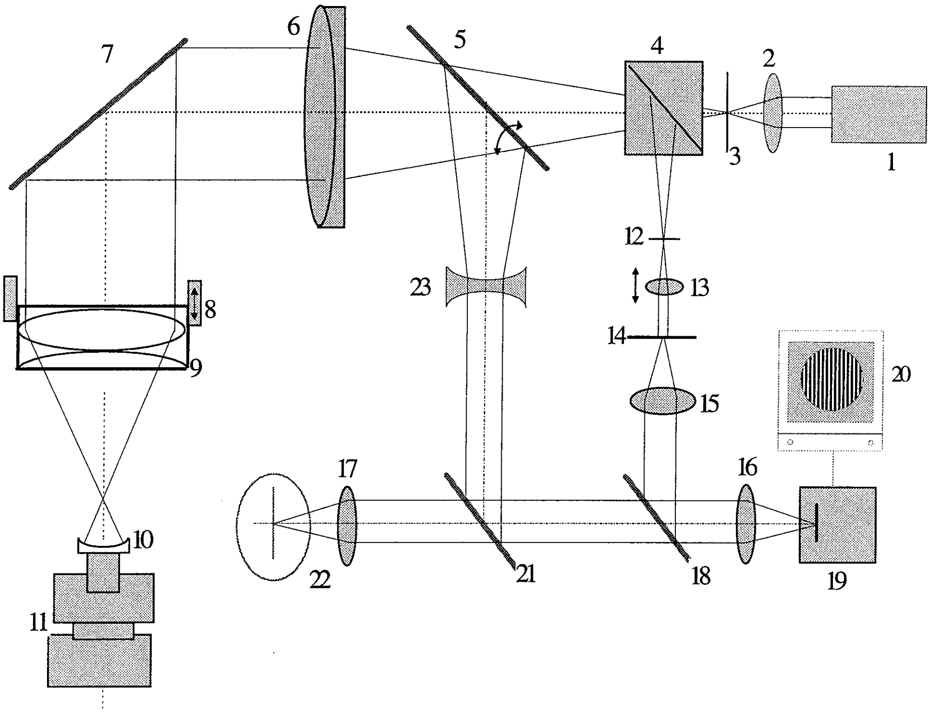

Figure 5-2 Optical schematics of the interferometer

1. Laser 2. Microscope object 3. Pinhole 4. Cubic beam splitter
5. Rotary beam splitter 6. Collimator 7. Mirror 8. Piezo-dived phase shifter
9. Combination of well-corrected focusing lens and plano reference object
10. Object under test 11. Five-axis manipulator 12. Diaphragm
13. Focusing lens 14. Rotating ground glass 18, 21. Beam splitter
15, 16, 17. Combination of zooming and imaging lenses 19. CCD
20. Monitor 22. Rectifying screen 23. Negative lens

A stabilised and unpolarised helium-neon laser (1) with about 1 mw in the single mode power and 632.8 nm in wavelength output is employed. A very well corrected collimating objective (6) serves to collimate the light from the pinhole (spatial filter) (3) that is illuminated by a combination of the laser (1) and a microscope objective (2).

In such a way, the emitting laser light with a beam diameter of 0.6 mm goes through a telescope system and then is expanded by a factor of approximate 200. As a result a typical measuring field of 100 mm through the reference combination (9) in the same size of 100 mm clear aperture is obtained.

The plano reference surface built in the combination (9) is adjusted perpendicular to the vertical optical axis so that the reflected image of the pinhole (3) is autocollimated. Afterwards the surface under test (10) should be also adjusted until the image reflected from it comes into coincidence with the pinhole as well. To facilitate preliminary adjustment, a rectifying screen (21) is used to project the two pinhole images from the two reflecting plane surfaces after the mirror (7). The pinhole image from the reference surface in (9) is at the center of the screen, whereas the one from the surface under test (10) is somewhere on the screen. The two pinhole images can be viewed in the screen (22). To view the Fizeau fringes, the negative lens (21) should be put into function. This is accomplished by virtue of the rotary beam splitter (5). These fringes can be further adjusted in direction and number as required, by adjusting the object under test (10) with the self-designed five-axis manipulator (11).

A part of the beam is diverted by using the cubic beam splitter (4) to a CCD camera (19) for recording the measurement and to the monitor (20) for observing the fringe pattern. This is performed by means of the focusing lens (13), the combination of zooming and imaging lenses (15) and (16), as well as the beam splitter (18). The interference fringes are detected with an area CCD detector of Philips CCD TV camera containing 604 × 576 pixels. However, the effective number of detecting elements is limited actually to 280 × 240 by the resolution of the electronic frame board used.

In the same path, secondary interference and speckle effects occurring due to the coherent nature of laser are diminished by a diaphragm (12) that is located in the focal point of the collimator (6). After being filtered, the interference fringes are projected through the focusing lens (13) onto a rotating ground glass (14) that is the intermediate image plane. It is functional to utilise the rotating ground glass in improving the quality of contrast and signal-to-noise ratio. By operating the focusing lens (13), a best focus or a favourable fringe distribution could be achieved.

A well-corrected focusing lens built in the combination (9) is the one of the key elements of the system in terms of accuracy. It converges the incoming rays to the focus with a 80 mm focal length and 100 mm exit aperture. In terms of optics, the focusing lens has a numerical aperture 0.625 or sin(38.682)°, which allows the measurement of contact lens surfaces to be possible.

5.3 The five-axis manipulator

In order to manipulate the object under test in the stitching procedure, an elaborate five-axis precision manipulator is designed and built up. It is used to shift and/or rotate the object under test during the procedure between successive measurements as well as to adjust and align the object in respect to the vertical optical axis.

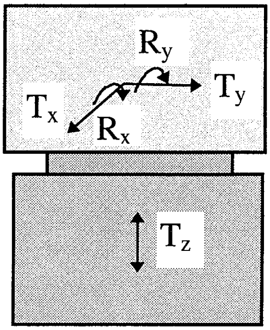

Figure 5-3 Five motions of the manipulator

Five motions are required, see Figure 5-3. Z-translation, T_z, is the principal motion for shifting the object under test between two successive measurements. Other two small translations, T_x and T_y, as well as two rotations, R_x and R_y, are also functioned for adjusting the object to align the Z-translation with the vertical optical axis.

5.3.1 Construction

The picture of Figure 5-4 exposes the mechanical construction of the manipulator. The main motion T_z, precise translation along the vertical axis, is realised by means of three symmetrically structured leaf springs on the lower position. The input of a micrometer screw drives the leaf springs through the horizontal beam contacted. The shift amount is read out from the micrometer screw that was precisely calibrated previously.

On the top position, two offset translations, T_x and T_y, for aligning the manipulator with optical axis are realise by virtue of elastic pivots. Furthermore, the two rotations are accomplished also by means of elastic pivots that coincides with the curvature centre of the tested surface. In this way, vertical translation is designed to be independent to object adjustment and system alignment. For detailed description of the design, please refer to the relevant reference [Crousen 1996].

The manipulator is built up from a few modular parts which are made of aluminium and manufactured by precision wire cutting with an electrical discharge machine (EDM).

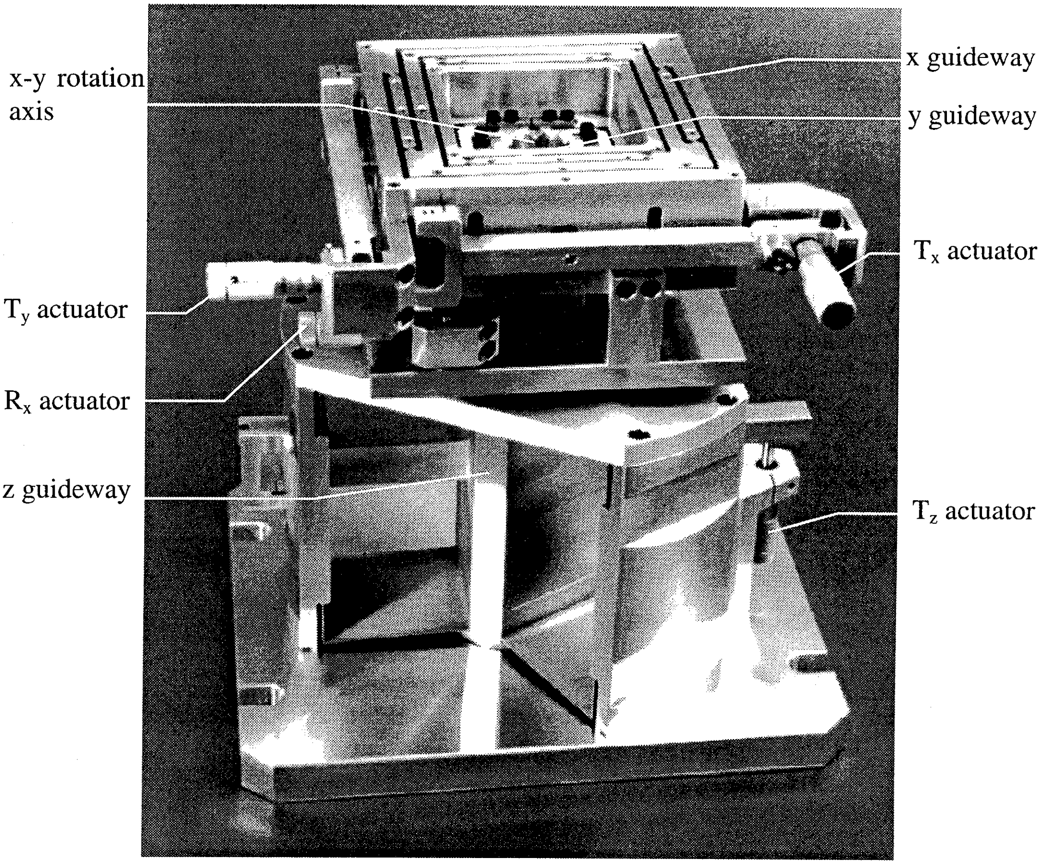

Figure 5-4 Construction of the manipulator

5.3.2 Calibration of accuracy

The measurement accuracy depends on the accuracy and repeatability of positioning of the translational manipulator. Therefore, the manipulator must be calibrated before being put into use.

To calibrate the Z-translation accuracy of the manipulator, two HP (Hewlett-Packard) 5528 laser measurement systems were employed. The method to detect the deviations in X- and Y-directions is based on the measurement principle of the HP laser measurement system for distance measurements. The method to detect the rotational deviations about X-axis and Y-axis is based on the measurement principle of the HP laser angular measurement system. In addition, the amount of the Z-translation was measured by a Heidenhain digital displacement sensor with which the micrometer screw was calibrated accurately.

Figure 5-5.a demonstrates the principle of the distance measurement. The f_1 and f_2 beams that leaves the laser head are aimed at an interferometer which splits f_1 and f_2 via a polarising beam splitter. Component f_1 becomes the fixed distance path, and f_2 is sent to a target which reflects it back to the interferometer. Relative motion between the interferometer, which is mounted on a granite plate table, and the remote retroreflector, which is mounted onto the manipulator to be calibrated, causes a Doppler shift in the returned frequency. Therefore, the measurement receiver photodetector in the laser head sees a fringe difference. This $f_1 - f_2 \pm \Delta f_2$ signal that is returned from the external interferometer is compared in the measurement display unit to the $f_1 - f_2$ reference signal. The difference, Δf_2, is then related electronically to velocity and then to distance. The information is finally processed to obtain the deviations.

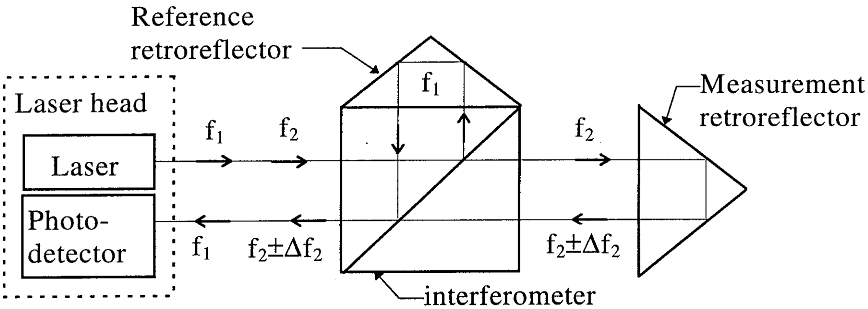

a) distance measurement

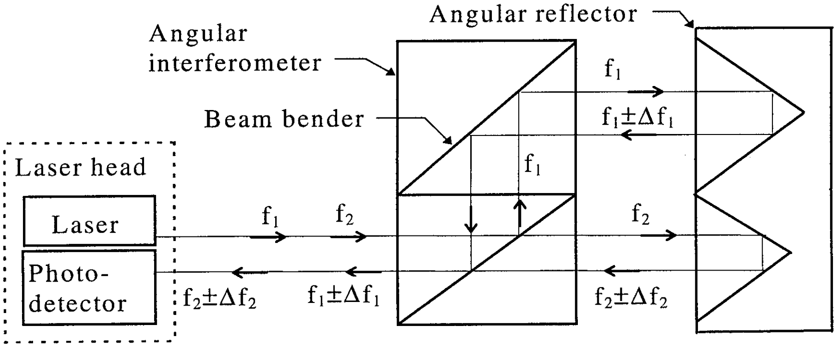

b) angular measurement

Figure 5-5 Measurement principles of the HP laser measurement system

Figure 5-5.b illustrates the principle of the angular measurement. The angular optics create two parallel beam paths between the angular interferometer and the angular reflector; one path is frequency f_1, the second path is frequency f_2. The distance between the two paths is precisely known, since the two retroreflectors are precisely positioned within the angular reflector. Initially, the angle between the angular interferometer, which is mounted on a granite plate table, and the angular reflector, which is mounted onto the manipulator to be calibrated, is assumed to be zero, and the two paths between them have some relative length. If either the angular interferometer or the angular reflector is turned, the relative lengths of the two paths will change; this change will cause a Doppler-shifted frequency change in the beam that is returned from the angular interferometer to the laser head. The electronics hardware of the laser measurement system will calculate and display the angular change, using the new frequency count data and the spacing between the optical paths. In this way, the rotational deviations about X-axis and Y-axis were measured.

Each pre-set motion was calibrated by making a group of eight measurements with a resolution of 10 nm by the HP laser measurement systems. Temperature variation about the manipulator was monitored to be less than 0.1 C° by six thermal sensors employed. The refractive index variation was monitored, too.

As an example, Figure 5-6 gives a pair of measured deviation records from one of eight calibrating measurements for the Z-translation.

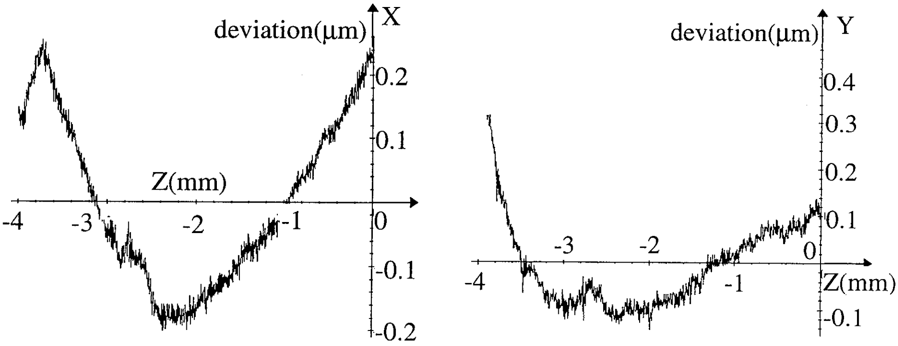

a) in X-direction b) in Y-direction

Figure 5-6 Deviations of Z-translation

Similarly, both X-pre-set and Y-pre-set motions were calibrated based on the equivalent principle and with the corresponding equipment. However, in order to detect the rotation deviations R_x and R_y, an autocollimator was used additionally. For more details on the measurement principles of the HP laser measurement systems, please refer to corresponding service manuals and relevant references [Hewlett-Packard].

Table 5-1 shows the calibration results of the manipulator. It can be concluded that the accuracy of Z-translation, the principal motion, is achieved at 0.1μm/mm in straightness and 1″/mm in rotation deviation over the really used central part of the 2 mm translation stroke, although 1.35μm/mm and 2″/mm are those over the entire stroke of 4 mm stroke. The other two translations of the offset and the two rotations are not being asked to be so accurate. This is because all adjustment and alignment should be done only before starting a stitching procedure. Those translations and rotations, therefore, have no influence on the measurement accuracy.

Table 5-1 Calibration results of the manipulator

Deviation/ /Motion	Z-direction	X-direction	Y-direction	About X-axis	About Y-axis
Z-translation					
(2 mm stroke)	not applicable	0.22±0.07 μm	0.17±0.07 μm	1.9±0.6″	2.0±0.1″
(4 mm stroke)		0.52±0.18 μm	0.56±0.26 μm	3.8±2.2″	4.2±0.4″
X-pre-set					
(0.5 mm stroke)	0.17±0.09 μm	not applicable	0.46±0.11 μm	0.9±0.3″	3±0.1″
(2 mm stroke)	0.56±0.18 μm		12.5±0.31 μm	8.1±0.2″	13.2±0.2″
Y-pre-set					
(0.5 mm stroke)	0.18±0.09 μm	0.60±0.02 μm	not applicable	0.7±0.5″	0.8±0.5″
(2 mm stroke)	0.52±0.26 μm	0.89±0.03 μm		3.5±1.3″	4.0±1.0″

5.4 Experimental setup

A vertical layout setup as shown in Figure 5-7 is employed so that the measurement of objects can be made without clamping deformation. This is especially important to precision surfaces and thin objects.

Considering that mechanical vibration may be one of the most important factors influencing the measurement, the stiffness and dynamic behaviour of the experimental setup must be good enough to reduce the effects from mechanical vibration and ambient noise. In order to improve dynamic behaviours and to prevent the setup from vibration and other variations, each part of the setup is well connected with each other rigidly.

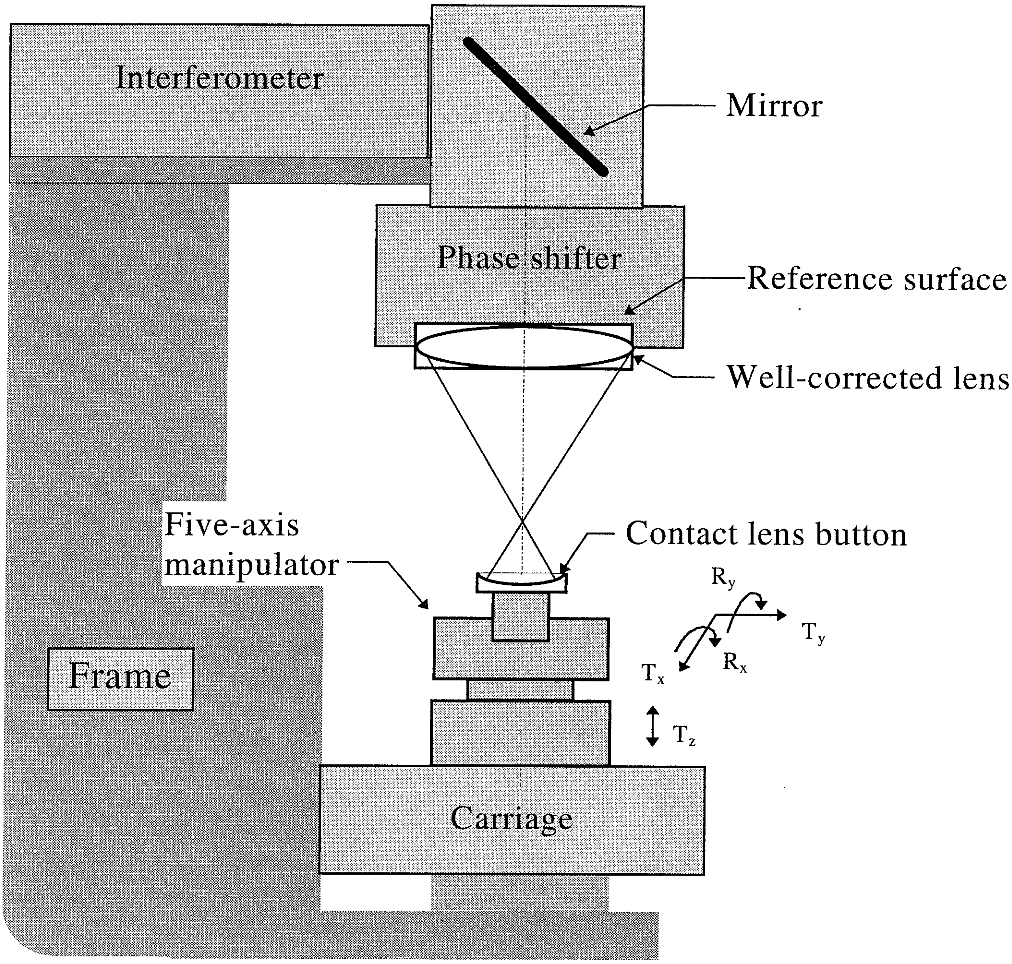

Figure 5-7 The experimental setup

However, the C-shaped structure of the experimental setup may suffer from certain problems with the dynamic behaviour of the setup. Measurements were made to investigate the relative movement or the position variations between the object under test and the phase shifter. An HP 5529 laser measurement system once more was used in an arrangement as shown in Figure 5-8.

It is difficult to identify the frequency components from looking at the original signal in the time domain. The discrete Fourier transform is often employed to convert the signal to the frequency domain. It is common in engineering to choose the power spectral density, a measurement of the energy at various frequencies, as the opponent against frequency to study the signal in frequency domain [Bendat 1986].

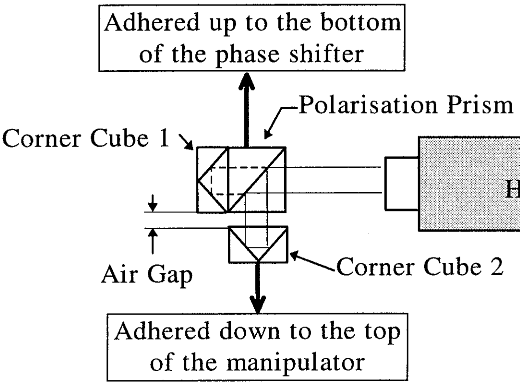

Figure 5-8 Measuring relative vibration

The relative movement between the top and the bottom parts of the opening in the setup construction loop was measured, which is equivalent to the relative vibration between an object under test and the interferometer. The air gap between the polarisation prism and the corner cube 2 (a measuring retroreflector) was smaller than 1 millimetre so that the possible influences of refractive index and air turbulence could be restricted minimally. The polarisation prism was firmly adhered up to the bottom of phase shifter and the corner cube 2 was adhered down to the top of the manipulator respectively.

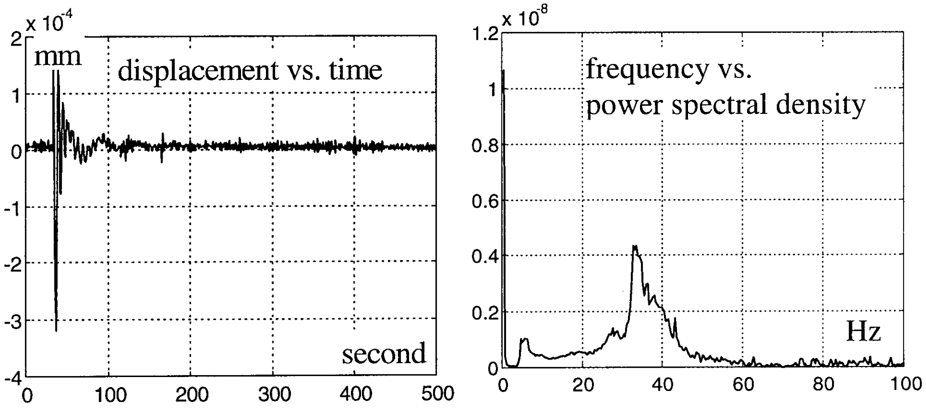

a) the impulse signal b) frequency response of the setup

Figure 5-9 Dynamic behaviours of the setup

Dynamic responses of the setup was tested by means of shock excitation methods. This was done by using a hammer to exert impulses on the frame of the experimental setup and on the floor respectively. Then the frequency responses were recorded. Two groups of five measurements were made respectively at the same resolution of 10 nm. The data were sampled at 200 Hz over 2.5 seconds period of time. Figure 5-9 demonstrates the impulse signal on the frame of the setup and the corresponding frequency response. It can be seen that the main frequency response of the experimental setup is around 34 Hz, much higher than the possible frequency being transferred through the floor which is lower than 1 Hz. On the other hand, there is a small peak at about 5.2 Hz on the graph of Figure 5-9.b, which might allow somehow influence of the mechanical vibration on the measurement accuracy. Analysis on the vibration effects will be carried out in Chapter 6 in details.

In order to investigate the characteristics of the relative movement, a group of six measurements was made. For these measurements, data were sampled at 10 Hz. In other words, the date were collected every 0.1 second during 300 seconds (5 minutes), that corresponds to the maximum time need for a complete stitching measurement of a contact lens button. One of the six measurement results is shown in Figure 5-10.

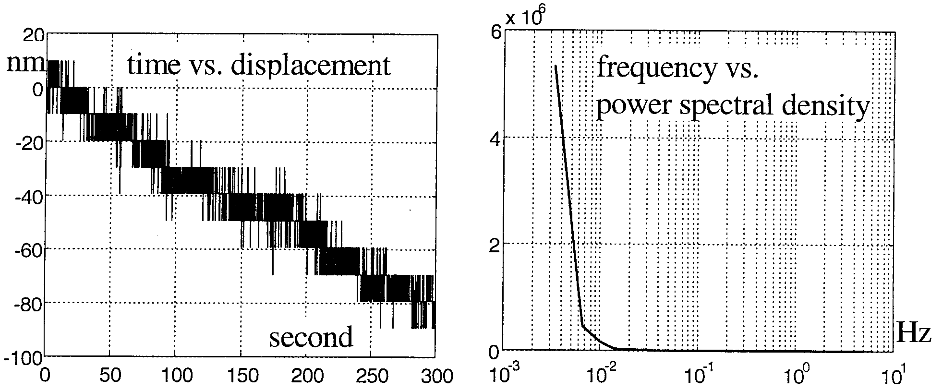

a) in time domain

b) in frequency domain

Figure 5-10 Measurement of relative movement

It can be seen from the measurement that the variation amplitude is approximately on an average of 25 nm in terms of PV. The variation frequency is approximately at 0.02 Hz. This is likely owing to the refractive index variation due to the air turbulence. Furthermore, a drift can been seen from Figure 5-10.a, that varies from 20 to 100 nm over 300 seconds. This drift is caused by the ambient temperature fluctuation. This has been proved by our second group of three measurements over a longer time period

(80 minutes). The influences of the mechanical vibration and the temperature variation on the measurement accuracy will go into detailed analyses in Chapter 6.

5.5 Experiments

5.5.1 Objects under test

The samples measured are mainly buttons of the F. Ellipse contact lenses. Here the term, button, refers to half-completed lenses with the most important interior surface being ready shaped. Their geometrical description have been given in Chapter 2.3 already. Their other parameters are given out in Table 5-2.

Table 5-2 Sample parameters

type	F.Ellipse	**material**	Boston RXD
dioptre	0.120 D	**base radius**	8.000 mm
diameter	≤ 10.000 mm	**eccentricity**	0.4, 0.6, 0.9 mm
refractive index	1.435 (dry)	**code**	47

5.5.2 Measuring procedure

The measuring procedure is comprised of the following steps.

1. placing the object onto the holder of the manipulator;
2. adjusting the distance between the reference and the object so that the focus of the reference focusing lens coincides with the curvature center of the central spherical portion of the object surface;
3. aligning the aspheric surface with the interferometer by examine interferograms at both the highest and the lowest positions of the object;
4. making the measurement of the central spherical portion;
5. shifting the object by the micrometer screw so that overlap region size of the second measured area is about 25% of the whole second measured area size;
6. adjusting the micrometer screw finely so that a non-fringe condition is satisfied in the measured annular; making the measurement and taking reading of the shift;
7. repeating step 6 until the overlap region between two successive measurement is so small that is equivalent to the least width described in Chapter 4.5.
8. reconstructing the sequence of interferograms in topographical pieces of profiles;
9. correcting the misalignment and rectifying the data misregistration;
10. stitching the profile pieces up together to obtain an entire surface profile.

5.5.3 Data acquisition and processing

The interferometric test data were processed by the Intomatik software which is based on a phase shifting algorithm. This software has a "masking" feature that allows designation of circular or other kinds of masks over the image of the whole aperture, and choice of activation or inactivation of the pixels inside or outside of the masked area. This function allows the area where fringes are not resolved on an interferogram of one submeasurement to be ignored [Möller-Wedel 1995]. Zernike and Seidel coefficients can be calculated by the software [Schlewitt 1994]. This enables to remove possible errors from the measured data such as tilt, defocus, spherical, coma and astigmatism aberrations.

The use of solid state detector CCD arrays ensures the geometric precision of the sampling position. As a result, there are no mapping distortions of the measured wavefront and the test surface. Because a uniform sampling of the wavefront is imperative for the sequence of submeasurements, a data area is fixed for all submeasurements in the stitching procedure. It is also important for averaging a group of measurements to reduce the effects of air turbulence and vibration on the wavefront to be measured.

Data collection in each submeasurement endures one second that includes five data acquisition steps of the phase shift method. In this way, the data collection procedure is designed to prevent from the mechanical vibration. An electronic interfacing unit takes the analogue intensity signals and converts them to digital signals which are stored in the memory of a frame grabber board. The four frames of signals are sent to the Intomatik program which calculates the optical path different phase data over the active area which can be stored in a particular format.

Our format converting program is then used to alter the format to be of readable format for ordinary computer viewers. The stitching programs are thereafter run to regenerate the series of topographical pieces of tested surface, correct misalignment and data misregistration and so forth, and finally stitch the profiles up together to obtain a complete reconstructed topography of the whole surface.

5.5.4 Experimental results

A group of experimental results of an aspheric surface by the stitching interferometry is demonstrated in Figures 5-11, 5-12 and 5-13 respectively. The two interferograms in Figure 5-11 were recorded for measuring the inner portion at its vertex centre of curvature in a prior measurement and for measuring the outer portion with position shift in a posterior measurement respectively. Areas where the fringes are unresolvable were masked so that the data in these areas are made inactivate.

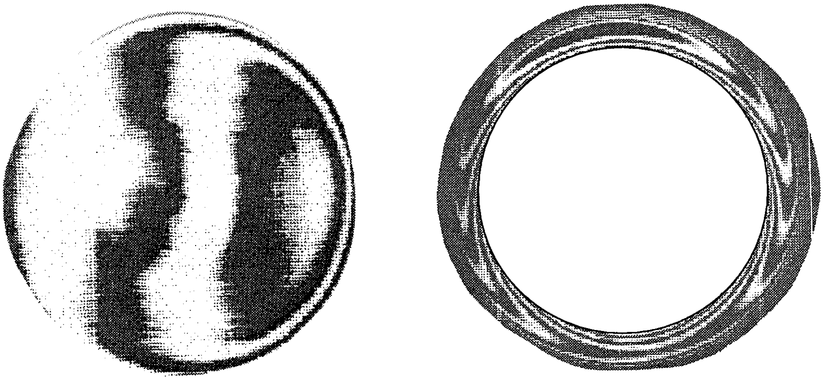

a) measuring inner portion b) measuring outer portion

Figure 5-11 A pair of interferograms

These two measurements of the inner portion and the outer portion were made with a common region of overlap indicated by the dark annular as shown in Figure 5-12 .

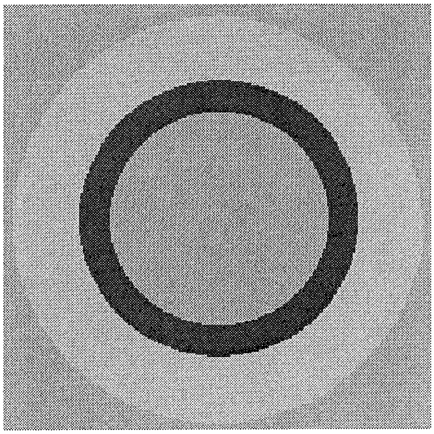

Figure 5-12 measuring two portions with an overlap region

The corresponding profiles of the inner portion and the outer portion of the measured aspheric surface were obtained respectively, which are shown in Figure 5-13.

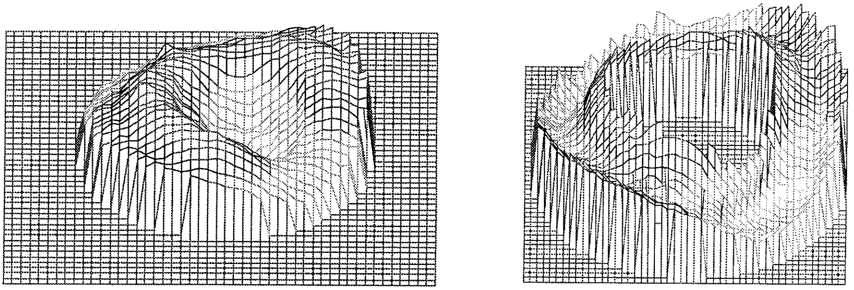

a) inner portion
(PV=176 nm, R_a=34 nm)

b) outer portion
(PV=195 nm, R_a=38 nm)

Figure 5-13 A pair of reconstructed profiles

This pair of profiles cannot be stitched together simply, otherwise a disfigured and unfitting topography is the consequence as shown in Figure 5-14.a. After performing the misalignment correction and the data misregistration rectification, a correct topography of the entire surface (Figure 5-14.b) is acquired by stitching then up together properly.

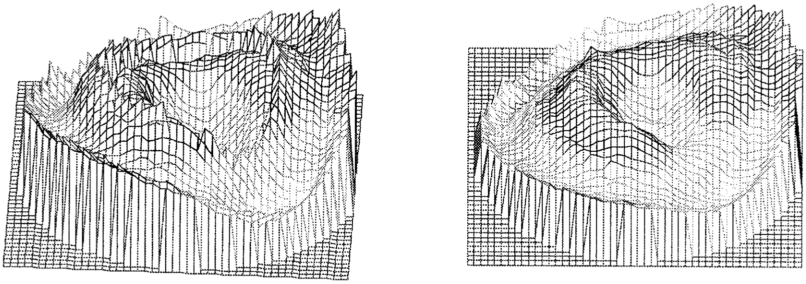

a) without correction
(PV=380 nm, R_a=49 nm)

b) with correction
(PV=232 nm, R_a=39 nm)

Figure 5-14 The stitched profiles of the entire surface

6.

Accuracy Analysis and Validation

6.1 Terminology about accuracy

In the practice of engineering, the term accuracy is widely used to indicate the quality of a measuring machine or an instrument as well as a measurement. In the strict sense of measurement science, however, there are different terms regarding the meaning of accuracy in engineering, more precisely formulated [ISO 1993].

Knowing the distinction between terms such as precision, repeatability, accuracy and uncertainty is necessary. A measuring system that possesses very small random errors has high precision. Accuracy of a measuring instrument is its ability to give responses close to a true value [ISO 1993]. In practice, a system with very small systematic errors is said to have high accuracy because random errors can be reduced by averaging multiple measurements. Repeatability of a measuring instrument is its ability to provide closely similar indications for repeated applications of the same measured under the same conditions of measurement. Therefore, a system that gives almost the same result for consecutive measurements has high repeatability. High repeatability, however, does not imply either high accuracy or high precision.

The particular term uncertainty is introduced with respect to a measurement result with a measuring system. It is a parameter, associated with the result of a measurement, that characterises the dispersion of the values that could reasonably be attributed to the measurement. Uncertainty of measurement comprises, in general, many components. Some of these components may be evaluated from the statistical distribution of the results of series of measurement and can be characterised by experimental standard deviations. The other components, which can also be characterised by standard deviation, are evaluated from assumed probability distributions based on experience or other information [ISO 1993]. A measurement made with small random errors and possible small systematic errors is considered with a smaller uncertainty.

These terms are used when more exact meanings are required in describing the measurement quality from particular points of view, although the word accuracy is most widely used in a more broad sense in engineering .

Errors in stitching interferometry may result from two sorts of sources. One is associated with single measurement error sources in the Fizeau interferometry, another one is associated with the stitching processing error sources. We start the analysis for a single measurement with the Fizeau interferometer and then discuss the stitching processing errors.

6.2 Errors with a single measurement

Error sources of a single measurement with a Fizeau interferometer generally fall into three categories. The first one has much to do with the quality of the optical cavity between the reference surface and the surface to be tested, which is mainly associated with defects of a few key elements. The second one is mainly with the data acquisition process, which has much to do with the signal-to-noise ratio (SNR) on a CCD array employed. The last one is associated with ambient effects including mechanical vibration, air turbulence and temperature variation.

6.2.1 Optical cavity error

The quality of all the optics of uncommon paths in the interferometer is very important. If the two paths, reflecting from the reference surface and from the tested surface respectively, are not equal, then systematic errors will be introduced. Therefore the measurement accuracy for relative measurements depends primarily on the quality of the cavity between the reference surface and the tested surface. defects of the reference surface and of any other surfaces which are present in the interferometer cavity affect the measurement quality greatly. Typically, it is of the order of tenths of a wavelength.

To minimise the possible effects of optical path differences in the uncommon path of the cavity, the highest quality components should be used as the reference objects. For measuring a plano surface, the possible maximum error introduced by the plano reference object is smaller than $\lambda/50$, or 0.012 μm. In the case of measuring a curved surface the combination of the well-corrected condensing lens and the plano reference object is employed which is calibrated by the manufacturer. This key optics of reference may introduce a maximum error smaller than $\lambda/20$, or 0.03 μm, in terms of PV value for measuring surface shape or wavefront [Möller-Wedel 1995].

There are some other error sources with the interferometer, such as spurious reflection, stability of the laser source, and so forth. Because the interferometer manufacturer has restricted the total resultant error to be less than the specified accuracy of $\lambda/100$, or 0.006 μm, such kinds of errors and possible imperfection of other optics in the common path will hardly influence the measurement accuracy.

6.2.2 Data acquisition errors

- **detector noise**

The fundamental limitation to the resolution of the optical phase shifting measurement arises from the signal-to-noise ratio of the measurement. The accuracy of the interferometry depends directly on the CCD signal-to-noise ratio of the intensity measurements for each measured data frame. The noise is comprised of photon noise, detector generated noise and electronic noise.

Phase measuring interferometers reconstructed the wavefront by sampling a large number of pixels across the pupil. This is done by using a CCD array. In addition to the noise above-mentioned, the quality of a CCD array is limited by input noise, amplifier noise, transfer inefficiency, trapping noise and detector uniformity.

The comprehensive detector noise will introduce about 0.5% error of the measured wavefront, in the worst situation it could be 1% [Malacara 1993, Stahl 1990]. In other words, the signal-to-noise ratio (SNR) is about 200 in an ordinary situation. According to Equation (1-1) and Equation (3-3), we have

$$\mathrm{SNR} = 2\pi / \Delta\varphi = (\lambda/2) / \Delta h, \tag{6-1}$$

where $\Delta\varphi$ is the phase resolution and Δh is the corresponding height variation.

Therefore,

$$\Delta h = (\lambda/2) / \mathrm{SNR}. \tag{6-2}$$

With SNR = 200, we have an error of the order of 0.0016 μm in the ordinary case, while with SNR = 100 in the worst situation, we have the possibly maximum error of the order of 0.003 μm.

Experiments and theory have shown that other errors in the phase measurement are systematic errors and therefore can be corrected [Malacara 1993, Möller-Wedel 1995, Massie 1988, Stahl 1990]. This has already been done by the manufacturers of the CCD and the interferometer.

- **phase shifting algorithm errors**

A phase shifting interferometry suffers from two main sources of algorithm errors: phase shifting miscalibration and computational errors. The limited precision of arc tangent lookup tables can be reduced to the point where the phase measurement accuracy is limited solely by the detector noise [Möller-Wedel 1995]. The nonlinearity of phase shifting and computational errors are typically well within $\lambda/20$, or 0.03 μm [Schmit 1995].

Detailed calculation of this kind of errors is quite lengthy but has been carried out by many researchers already [Cochran 1992, Creath 1988, Hariharan 1987, Selberg 1987], which indicates that this kind of error will not exceed $\lambda/20$ in a measurement.

- **quantization errors**

Another form of intensity error in phase measuring interferometry is quantization error introduced by truncating intensity measurement to a nearest integer representation. Considering the fact that in our case each fringe interval, that corresponds to $\lambda/2$ of optical path difference, is scaled by 8 bits electronically, hence the quantization error is of the order of $\lambda/2^9$, or 0.001 μm. It is naturally negligible.

Some more detailed analyses of this kind of errors have been investigated carefully[Cochran 1992, Malacara 1993], indicating the quantization errors are generally negligible.

6.2.3 Errors resulting from ambient effects:

- **mechanical vibration**

An important factor influencing the accuracy of any opto-mechanical system is the environment to which the system is exposed. Because of the high sensitivity of the interferometer, it can be easily effected by mechanical stability of the setup. Mechanical stability is therefore paramount in an interferometry considering the ambient effects. In some instances vibration can not be eliminated completely.

Mechanical vibration is in our case transmitted from the floor through the manipulator. The setup is built up with such construction and stiffness, see Chapter 5, that the natural frequencies of the setup are safely higher than those of the background mechanical vibration.

However, we did suffer from the mechanical vibration problem, although the casting iron base of the frame attenuates the transferred vibration from the floor efficiently. The vibration amplitude was approximately on an average of 0.025 μm in evenings or weekends, see Chapter 5.4, and 0.05 μm in working days. The mechanical vibration may affect the measurement in two ways.

First, it can be considered as a relative position shift between the reference and the tested surfaces, and therefore results a slight variation of optical magnification. With the aid of Equation (4-55), the maximum error on data misregistration due to the corresponding optical magnification changes is only 0.006 μm. This is negligible, when comparing it to our accuracy specification of the order of submicrometres.

However, such a mechanical vibration can damage the measurement seriously when it is considered as the relative changes of the optical path difference between the reference wavefront and the surface under test. Such an equivalent optical path difference leads to some kinds of extra or artefact fringes in the phase measuring process and consequently introduce measurement errors. Unfortunately, this seems to be the case with our experiment. This is because the fact the machine frequency is about 35 Hz (see Figure 5-9.b), while the sampling frequency in the phase measuring procedure is 50 Hz (0.2 second per sampling). The situation could be improved if the machine stiffness of the experimental setup would be enhanced so that the machine frequency could be higher than 50 Hz, better to be 60 Hz.

During working days, the vibration amplitude was approximate 12% per fringe on an interferogram, while during the evenings or weekends, the vibration is fortunately reduced by a factor of two, i.e., 6% of a fringe width. As a result, the errors introduced by the mechanical vibration are of the order of 0.016 μm [5% × ($\lambda/2$) = 0.016] in the weekends, and 0.032 μm in working hours. Consequently, all precision measurements we made and show in this thesis were performed during the evenings or weekends.

- **air turbulence**

The error introduced by air turbulence is usually of a low frequency. To minimise effects of air turbulence, data should be acquired as quickly as possible. This was done at the rate of 20 milliseconds per intensity sampling and one second per single measurement, in the phase shifting measuring procedure. The air path between the reference and the tested object should be as short as possible, and the environment should be as tranquil as possible.

All the measurements were made during weekends or evenings to prevent the measurement from air turbulent effects. The influence of air turbulence should then have been kept less than 0.025 μm which is the noise level of our measurements.

- **other ambient errors**

It is possible that the refractive index of the optical cavity between the reference and the tested objects varies as the temperature and air current change. From the basic relationship between optical path difference (OPD) and the refractive index n, we have

$$\Delta(\mathrm{OPD}) = \Delta n \times s, \qquad (6\text{-}3)$$

where s is the length of the beam path between the reference and tested objects, which is about 2 × (80+8) = 176 mm.

The possible changes of the refractive index, Δn, is 10^{-6} / K°, or, of the order of 10^{-7} in our case less than 0.1°C variation. Therefore, the height changes due to the temperature variation will be of the order of maximum 0.018 μm. However, the measuring time for a single measurement is only 1 second while the air fluctuation time may be 50 seconds (0.02 Hz) for one period, see Figure 5-9, so that only (0.018/50) μm, or 0.0004 μm variation may be detected during the sampling.

Other environmental factors for a single measurement, such as humidity, pressure and possible contamination of the tested surface should also need to be kept under control and not allowed to vary to extreme values of total 0.025 μm. The influence of temperature variation on the manipulator length changes for a series of measurement will be considered later in the next section of this chapter.

Averaging a number of measurements as well as minimising the environmental factors will improve precision of the measurements. In fact, each important measurement was made in a group of at least five measurements that were averaged to obtain a better measurement result.

6.3 Stitching processing errors

Error sources of the stitching process in stitching interferometry may be categorised in four groups. The first group is in regard to the residual defocus errors associated with the non-zero fringe density condition. The second one is in relation to positioning errors of the object shifting as well as residual misalignment errors. The third one is related to the stitching algorithms. The last one has to do with temperature changes during the whole stitching measuring procedure.

6.3.1 Residual defocus errors

One of the problems regarding measuring aspheric surface with stitching interferometry is the defocus errors in the imaging system introduced by non-zero fringe density. Due to the surface asphericity, it is practically hard to obtain the zero fringe density condition for the measurement of each portion of the aspheric surface.

The commercial software Intomatik used has a function to subtract such kind of defocus or non-zero fringe density errors from the measurements, in terms of tilt and defocus errors. Unfortunately, it can not remove these errors completely according to our practical experience. As a result, there exists a problem with the residual defocus errors.

In a commercial interferometer, the interference pattern is focused on a CCD detector and data points are sampled at the corresponding locations [Sullivan 1995]. Also, a zoom lens forms a part of the optical configuration to suitably magnify the test optics to fill the detector. Thus, the spatial sampling conditions may be variable and determined by the magnification of the optical system. Fortunately, focusing errors of the imaging system of a commercial interferometer have already been best minimised.

In case of measuring a curved surface with an optical arrangement shown in Figure 5-2, the nominal magnification of the optical system is fixed to a factor of 10, which is the ratio of focal length (80 mm) of the spherical reference unit to the nominal radius (8 mm) and the surface under test. In other words, the defocus errors introduced by the zooming system could be negligible, provided that the data misregistration due to the object position shift, analysed in Chapter 4.4.4, has been rectified in advance.

However, the residual defocus error still exists. Although it is possible to obtain a zero fringe density in the central part of the measured area, it is almost impossible to obtain the same condition in the outer parts of the measured area, too. The error introduced by not having the image plane conjugate to the surface under test depends upon the aspheric departures between the virtual reference wavefronts and the aspheric surface geometry present.

As in all interferometers, if at all possible the surface being tested should be imaged onto the image or detector plane. If this is not the case, the interferogram being observed is not the interferogram created by interfering the reference wavefront with the wavefront produced by the surface under test, but rather it is the interferogram produced by interfering the reference wavefront with the Fresnel transform of the wavefront coming from the surface under test. Such a fringe localisation problem is actually a kind of small misregistration within certain limited amount.

In order to investigate the residual defocus errors after correction by the commercial Intomatik software, a group of experiments was done. The test object was a plano glass with 0.1 μm PV as its shape inaccuracy over 100 mm surface in diameter. The backside surface was oiled to prevent possible reflection effect.

The experimental procedure was as follows.

1. placing the test object into a self-centring holder, and adjusting the amount of tilt by observing the number of fringes;
2. setting the instrument at minimum zoom, and using the best practice to focus the interferometer so as to minimise focus error;
3. selecting operating conditions to obtain low noise measurements, including doing the experiment in the weekend to minimise air turbulence, isolating the test table from ground vibration by inflated tyres, and making the distance between the transmission flat and the test flat as small as possible (50 mm);
4. Adjusting the interferometer as close to zero tilt as possible, and then recording a series of 10 observations for noise assessment;
5. making each 10 observations at the tilt positions respectively that correspond to the fringe number of 1, 2, 5, and 10 respectively; saving the measurement results;
6. recording the PV values for each measurement and the corresponding errors in terms of tilt and defocus.

It can be concluded from the measurements that the noise level of the measurement precision was of the order of 0.025 μm. Although the residual error in terms of tilt is negligible comparing with the noise level and the mechanical vibration effects, the residual error in terms of defocus is considerable, especially as the number of fringes increases. Table 6-1 gives out the experimental results showing the relationship between the residual errors and the number of fringes.

Table 6-1 Residual errors of PV measurement ($\lambda = 0.6328$ μm)

number of fringes error type	1 fringe	2 fringes	5 fringes	10 fringes
tilt	0.01 λ	0.01 λ	0.03 λ	0.08 λ
defocus	0.01 λ	0.02 λ	0.08 λ	0.2 λ

It is interesting to notice that here comes a kind of coincidence, although not exactly the same, of the results in Table 6-1 with our foregoing analysis on the minimum width of the overlap region. We stated in Chapter 4.5.1 that according to our experience, taking more than 12 fringes may strongly affect measurement accuracy and less than 8 fringes is preferable. Table 6-1 leads to almost the same advice that not taking more than 5 fringes.

As a result, it is desirable to make a measurement when a zero fringe density in the central area measured is obtained. If this would be too hard to realise, it is then desirable to keep the maximum number of fringes over the measured area being less than 5 lines, while keeping the lowest fringe density in the central portion of the measured area. In this way, the defocus error introduced by non-zero fringe density condition can be controlled to be smaller than 0.05 μm.

6.3.2 Alignment and positioning errors

In the operation of making the measurement of an aspheric surface with stitching interferometry, careful alignment for the vertical optical axis and the object Z-translation axis should be done, and the object position before and after each shifting should be also recorded. Any deviation from the perfect situation may result in some kind of errors for the resultant measurement.

- **residual misalignment**

Although misalignment between the object translation direction and the optical axis or the system recording system looks naturally important, it is actually not a serious problem because of the misalignment correction function of the stitching algorithms. Actually, if the misalignment error is kept less than the lateral resolution of the CCD, it will be removed by the stitching algorithms described in Chapter 4.3, with the residual errors determined by the precision of the algorithm correction.

The data grid frame on the CCD for the measured area normally contains 250×250 pixels, which is with respect to the clear aperture of the interferometer with 100 mm in diameter. That means with the optical magnification factor 10, the lateral resolution of the CCD is 0.25 mm/pixel. With the aid of observing the changes of the fringe pattern and the symmetry of an interferogram while aligning the system, it is easy to have a better than $\lambda/2$ (0.3 μm) alignment precision.

- **positioning errors of object shifting**

The object is shifted by driving a micrometre screw onto the manipulator. Due to the inherent backlash imperfection for a micrometre screw, there may be some positioning errors of object shifting although the micrometre screw has been calibrated previously.

Positioning errors due to mechanical uncertainty of the micrometre screw are of the order of ±0.01 mm. It can be considered as a relative position change, ΔZ, between the reference and the tested surfaces. According to Equation (4-55), this may introduce a data misregistration error on an average $\pm 0.12\%$ of the surface PV value. With PV=0.2 μm, it is of the order of ±0.0002 μm, which is negligible.

6.3.3 Stitching algorithm errors

The computational errors associated with stitching algorithms mainly depend on the computational precision or the converging precision of the iteration algorithms.

In our stitching algorithms described in Chapter 4, both the termination tolerance for the independent variable **X** and the termination tolerance for the objective function $f(\mathbf{X})$ were set to 0.05 μm as the termination criteria on the converging precision of the iteration process. This is to match the accuracy of the measurement and obtain a good compromise between the required precision and the computational time.

The computational precision is, naturally, adjustable according to the required accuracy of the practical measurement. However, if a computational precision smaller than the error amount for a single measurement, i.e., 0.07 μm, would be set, it could not improve the measurement accuracy but increase the computational time only.

6.3.4 Errors by temperature changes

The influence of temperature changes on a single measurement is negligible because the sampling procedure for a single measurement completes within only one second. However, the influence on the whole procedure of the stitching interferometry can not be simply neglected because a stitching measuring procedure normally takes approximately four minutes.

It has already been noticed previously from Figure 5-10.a that there is a drift of the relative position between the reference and tested objects. It varies from 0.02 μm to 0.1 μm over 5 minutes. It could be negligible when considering its effects on the data misregistration as a minor change of the optical magnification due to the relative position shift.

However, it has been found out by our observations accordingly that this drift corresponds a fringe density change by 2 lines during 5 minutes. According to Table 6-1, this may introduce a maximum defocus error in the order of 0.02 λ or 0.012 μm in the worst situation. Actually, well focusing was carried out at each measuring step in the stitching measuring procedure. As a result, the maximum error should be reduced by the number of submeasurements during a stitching measuring procedure. As for a 2-step procedure, the error introduced by temperature variation can be reduced to 0.006 μm.

6.4 Short summary

It has been revealed that the accuracy of interferometric measurement with a single measurement is primarily determined by the optical cavity errors, which is of the order of 0.03 μm. Other factors such as detector noise, electronics resolution, phase shifting algorithm error and so forth are secondary for most measurements. They can be kept smaller than $\lambda/20$ (0.032 μm) in terms of PV as long as the measurement conditions and ambient effects are under well control.

However, we must pay much attention to the mechanical vibration that could spoil the measurement if it would not be well controlled. Under a good ambient situation in weekends, the corresponding influence of all ambient factors together on the measurement accuracy can be kept being of the order of 0.04 μm in total. In other words, mechanical vibration was responsible for about 40% of the error amount, i.e., 0.016 μm, and all other factors were responsible for another 60%, i.e., 0.025 μm, which was the noise level of the measurement.

We have pointed out that the residual defocus errors are dependent on the surface asphericity. The residual defocus errors could be serious to the stitching processing when the aspheric departure in certain area goes too large and the slope of the measured aspheric surface changes very sharply. It is desirable to refocus the measured area after the object shift to minimise the fringe density. Under the condition having always as less as possible fringes and keeping the maximum number of fringes smaller than 5 lines, the error introduced by non-zero fringe density condition can be kept of the order of 0.05 μm.

As a result, the measurement uncertainty for a single measurement is on the average of 0.05 μm. The maximum error amount might be of the order of 0.07 μm. The least error amount of 0.03 μm can be achieved when the mechanical vibration is reduced and the optical cavity error is compensated efficiently.

The total error amount for the whole stitching interferometry under the current circumstances is therefore of the order of 0.2 μm. In other words, our goal to achieve a resultant measurement accuracy of the order of submicrometre for the aspheric surface measurement has been realised.

6.5 Validation

In precision engineering it is always advantageous to have multiple ways of making a measurement as a cross check. The quantities measured are so small and the measuring devices so sensitive to errors approaching the magnitude of the object quantities being measured. Hence, it is difficult to know from a single, though perhaps repeatable, measurement that what is being measured represents the "truth". The alternative method for the cross check or validation can be of the same generic class, or can be the mathematical analyses or other compatible measuring methods. We are going to demonstrate three methods and corresponding results as the cross check and validation.

6.5.1 Validation by topographical analysis

A beautiful result was obtained and is shown in Figure 6-1 as an efficiency validation of the misalignment and data misregistration correction of the stitching algorithms.

Two groups of raw measured data sets, {**P**} and {**Q**}, obtained from the first submeasurement and the second submeasurement respectively, should represent, in principle, the same topographical profile of the **overlap region**. The dark annular in Figure 6-1 demonstrates the position of the overlap region between the inner portion and the outer portion which correspond to the date sets {**P**} and {**Q**} respectively.

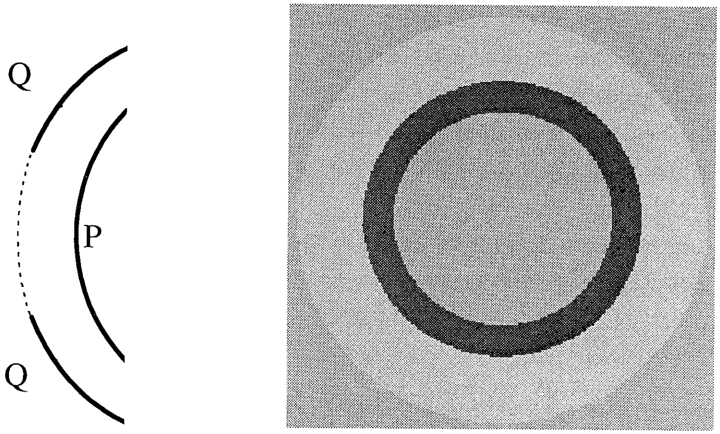

a) the inner and the outer portions b) dark annular indicates the overlap region

Figure 6-1 the overlap region between two measurements

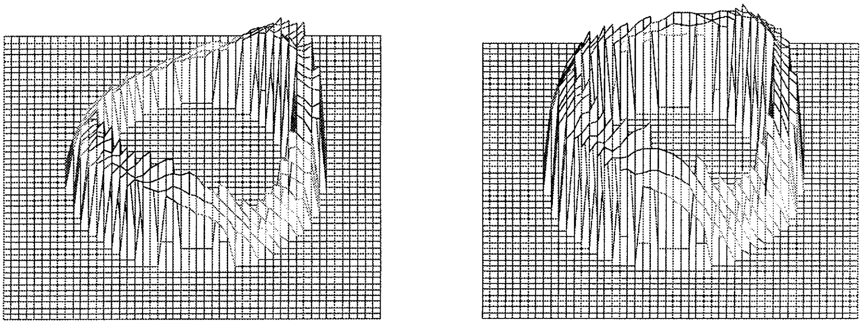

a) via the 1st measurement $\{\mathbf{P}_i\}$
(PV = 0.127 μm);

b) via the 2nd measurement $\{\mathbf{Q}_j\}$
without correction (PV = 0.160 μm);

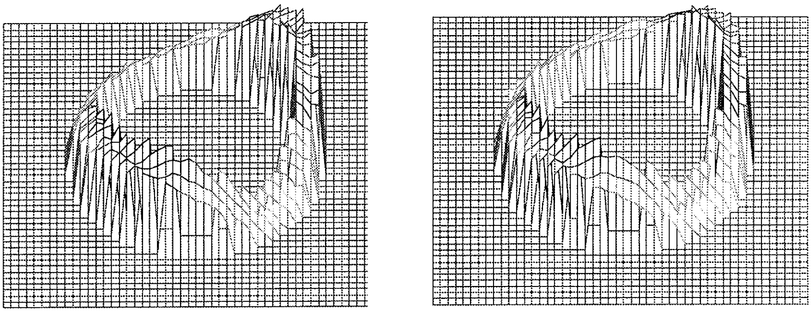

c) via the 1st measurement $\{\mathbf{P}_i''\}$
(PV = 0.127 μm);

d) via the corrected 2nd measurement $\{\mathbf{Q}_i''\}$
after correction(PV = 0.128 μm);

Figure 6-2 Reconstructed topographical profiles of the overlap surface

However, the topographical profile from the second raw data set (Figure 6-2.b) brings us a much different shape from that from the first one (Figure 6-2.a), while the corrected data set, {$\mathbf{Q_i''}$}, does bring us an almost the same profile (Figure 6-2.d).

6.5.2 Data correlation analysis

In order to employ another way to validate the misalignment and misregistration correction by the stitching algorithms, some data correlation analyses were carried out. The same two data sets as in the prior section, representing the same profile of the overlap region but being obtained from two successive submeasurements respectively, were analysed.

The cross-covariance is the cross-correlation function of two sequences with their means removed, which reflects the relationship between the two sequences or the two data sets. The correlation coefficient, r, indicates the degree of correlation between the two data sets.

It is clear that the correlation coefficient between these two data sets, {$\mathbf{P_i}$} and {$\mathbf{Q_i}$} for $i \in \mathbf{M} = [1, 2, \ldots, 7992]$ in **the overlap region**, should approach to one (100%) after the correction treatment. In other words, their correlation graph should be symmetric because the two date sets characterise the same geometry of the overlap region topography. However, a non-symmetric graph, Figure 6-3.a, with a correlation coefficient r=0.81 was got without the correction, whereas a symmetric one, Figure 6-3.b, with a correlation coefficient up to 0.99 was achieved after our correction. The algorithms perform correctly.

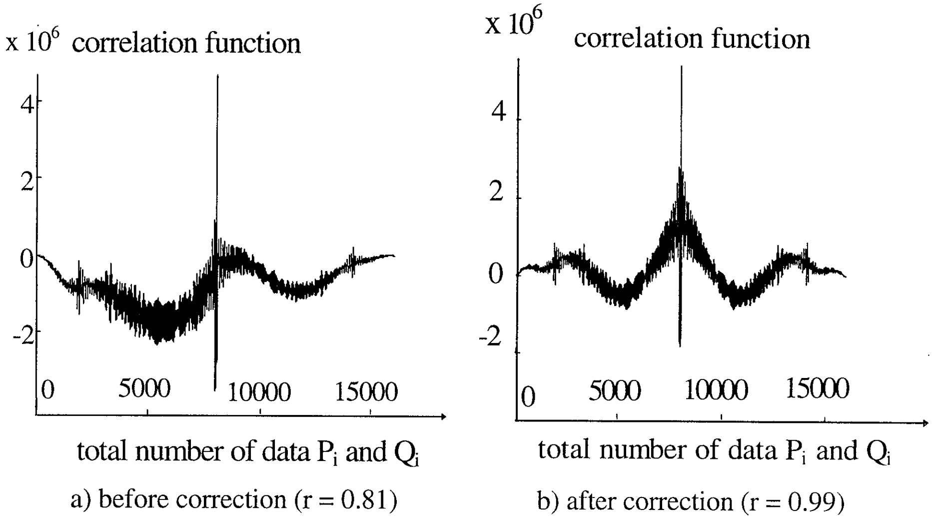

a) before correction (r = 0.81)

b) after correction (r = 0.99)

Figure 6-3 Algorithm validation by correlation analyses

6.5.3 Validation by measurement comparison

In order to test the global validity of the stitching interferometry, two groups of measurements were made and the results were compared, as shown in Figure 6-4.

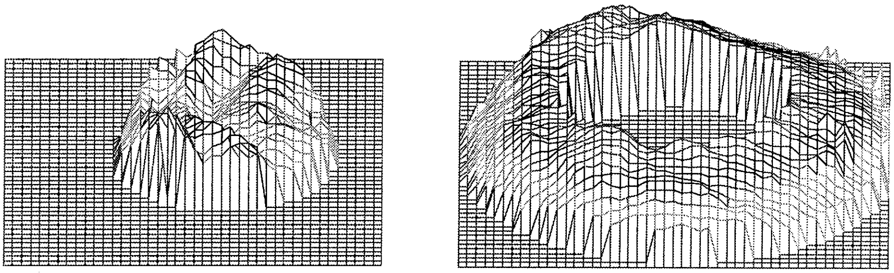

a) profile of the central portion
(PV = 0.117 μm);

b) profile of the outer portion
(PV = 0.108 μm);

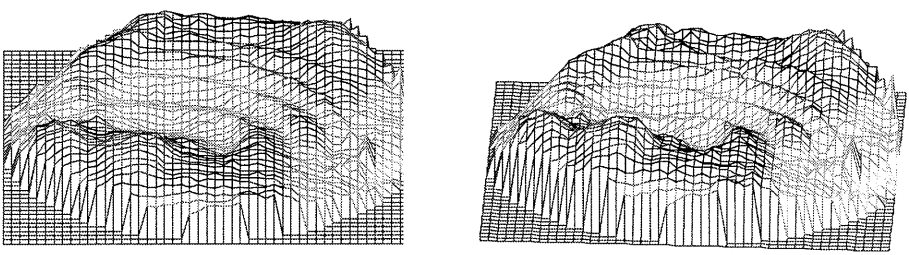

c) whole profile by 2-step stitching method
(PV = 0.153 ± 0. 1 μm);

d) whole profile by one measurement
(PV = 0.176 ± 0.03 μm);

Figure 6-4 Validation by measurement comparison

The first group gives the measurement result in terms of surface topographical profile by means of measuring the whole surface in one measurement, see Figure 6-4.d., as the reference. The second group gives that by means of the 2-step stitching interferometry. The object measured was an F.Ellipse 0.4 contact lens button.

Figures 6-4.a and 6-4.b show the profiles of the central portion and the outer portion respectively, while Figure 6-4.c shows the stitched topographical profile of the whole measured area of the surface.

It can be concluded from the comparison shown in Figure 6-4, that the stitching method works properly at the sense of submicrometre measurement accuracy.

Conclusively, it has been verified by the three cross check methods that the stitching interferometry works correctly for the 2-step measurement of the aspheric sample objects under test.

7.

Conclusions and Recommendations

7.1 Conclusions

A novel technique, stitching interferometry, has been developed which is capable of the precision measurement of complicated surfaces having relatively large aspheric departures. Stitching interferometry is a method which overcomes the problem of limited measuring range and aberrations due to surface asphericity.

In order to correct the misalignment and to rectify the data misregistration between two successive submeasurements, stitching algorithms have been developed. To realise stitching interferometry, careful analyses must be executed on the following items. One is to correct the errors introduced by the misalignment of the series of measurements. This is achieved by using regions of overlap and knowing the transformation between successive measurements. Another item is to rectify the misregistration of the individual data sets introduced by the surface asphericity and by the object position shift that causes optical path variations. This is accomplished by careful optical analyses based on the theories of geometrical optics, including image formation, optical aberration and the characteristic functions of Hamilton.

Stitching interferometry is different in procedure from other existing techniques. It firstly interprets the interferograms into geometrical topographies and then stitches the topographic segments up together so as to obtain the overall shape of a surface. This makes it more universal in use.

A five-axis precision manipulator was designed and constructed to realize three translations and two rotations. A precision translation along the vertical optical axis, the principal motion, is realised by virtue of three symmetric and elastic leaf springs. High accuracy is achieved of the order of 0.1 μm/mm in terms of straightness and 1″/mm in rotation deviation over the 2 mm central part of the translation stroke.

A submicrometre order measurement accuracy or better has been obtained. The total error for the whole stitching interferometry under the current circumstance is of the order of 0.2 μm. In other words, the measurement uncertainty in total is smaller than half of a wavelength.

Experimental results have shown that the stitching interferometry is capable of measuring curved surfaces having large aspheric departures. It has been verified that stitching interferometry works correctly and efficiently by three cross check methods of validation.

7.2 Recommendations

This technique of stitching interferometry offers considerable potential for testing precision surfaces having large aspheric departures. The ability to stitch surfaces to obtain high resolution over a large measurement region should further increase the applications of commercial interferometers. The concept and method may be used to upgrade commercial interferometers.

Similarly it is recommended to apply the principle of stitching interferometry to the measurements of large size plano surfaces and conic surfaces, based on the use of relevant references such as plano reference and conic surfaces and so forth.

It is suggested also to extend stitching interferometry to the asymmetric domain of astigmatic surfaces. However, it is expected to encounter problems with angle magnification changes and misalignment in a polar coordinate frame.

Considering the fact that mechanical vibration could be critical to the measurement accuracy if not well controlled, it would be much better to mount the whole experimental setup on a vibration-isolated platform, and to close the structure loop of the setup by connecting the manipulator platform with the phase shifter.

Finally, it would simplify the control on residual defocusing errors if an automatic focus control method and a corresponding device could be developed and employed in this stitching interferometry technique.

Appendix A

The aspheric surface of a contact lens

The mathematical description of the cross-section curved of an F.Ellipse 0.4 contact lens inner surface can be depicted as follows (see Figure 2-2).

- **segment A**

segment A is a circle part of the base surface, beginning at point 0 (0, 0) and ending at point 1 (1.93538, 0.23763), described by

$$Z = r_0 - (r_0^2 - X^2)^{1/2}, \quad 0 \leq X \leq 1.93538. \qquad \text{(A-1)}$$

Where r_0 is the radium of the base curve. For most commonly used contact lenses, R is 8 mm. In order to do further analyses more conveniently, we re-write it in a normalized expression as

$$X^2 + (Z - r_0)^2 = r_0^2, \quad 0 \leq X \leq 1.93538, \qquad \text{(A-2)}$$

whose tangential line passing through an arbitrary point of tangency M_0 (X_0, Z_0) on the segment curve can be written respectively as

$$(Z - Z_0)(r_0 - Z_0) = X_0(X - X_0), \qquad \text{(A-3)}$$

and

$$X_0(Z - Z_0) = (Z_0 - r_0)(X - X_0). \qquad \text{(A-4)}$$

A normal line passing through an arbitrary contact point on segment A will reach z-axis at point (0, r_0).

- **segment B**

segment B is of the most important piece in the optical zone, which is constituted of many different parts from a family of variable ellipses, starting from point 1 (1.93538, 0.23763) till point 2a (4.11731, 1.12613). It can be expressed mathematically as

$$Z(X, e(X)) = \{r_0 / (1-e^2)\}\{1- [1-(1-e^2)(X/r_0)^2]^{1/2}\}. \qquad \text{(A-5)}$$

By our more complicatedly mathematical deduction, its normalized form can be drawn out as,

$$X^2/\{r_0/(1-e^2)^{1/2}\}^2 + \{Z - r_0/(1-e^2)\}^2/\{r_0/(1-e^2)\}^2 = 1, \tag{A-6}$$

with $0 \le e \le 0.4$ and $1.93538 \le X \le 4.11731$.

Here, the eccentricity e, is not a constant but a function of the feed-displacement of the linear carriage in X-direction. As for an F.Ellipse 0.4 contact lens, we have such a function as

$$e = e(X) = k \times X + e_0 = 0.1831\,X - 0.3544, \tag{A-7}$$

and k is a linear constant for a given surface.

The tangential line of this varying elliptical segment, passing through an arbitrary point of tangency $M_0\,(X_0, Z_0)$ on the segment curve, can then be written as,

$$(X \cdot X_0)/\{r_0/(1-e^2)^{1/2}\}^2 + \{[Z_0 - r_0/(1-e^2)]\cdot[Z - (r_0/(1-e^2)]\}/\{r_0/(1-e^2)\}^2 = 1. \tag{A-8}$$

- **segments C & D**

Both segments C and D are quoted from some kinds of polynomial curves, but with opposite polarity of the curvature. Segment C, from point 2 (4.12030, 1.12784) though point 3a (4.39702, 1.29488), is a transitional piece of the surface and is depicted as,

$$Z = A_3 + B_3X + C_3X^2 + D_3X^3, \qquad 4.12030 \le X \le 4.39702. \tag{A-9}$$

Segment D has nothing to do with the optical function. It is designed to just fit the shape of human eyes. It starts at point 3 (4.40000, 1.29677) and ends at point 4 (4.90122, 1.59077), with the expression of

$$Z = A_4 + B_4X + C_4X^2 + D_4X^3, \qquad 4.4000 \le X \le 4.90122. \tag{A-10}$$

As for the F.Ellipse 0.4 contact lens, the polynomial coefficients in Equation (A-9) are sequentially 1.421374, -0.859805, 0.226894, -0.008618 for segment C, and in Equation (A-10) are sequentially -4.095693, 1.953164, -0.196777, 0.007139 for segment D.

Appendix B

Aspheric departures of the contact lens

Tables B-1, B-2 and B-3 show the aspheric departures of the contact lens surfaces from the reference spheric surface, where d_z and d_r stand for the departures in Z-direction and in the spherical radial direction respectively.

Table B-1 Aspheric departures from the spheric surface (contactlens F.Ellipse 0.4)

POINT	NO.	X(mm)	Z (mm)	D_Z (μm)	D_r (μm)
4	191	4.90122	1.59077	86.411	68.469
middle D	300	4.57602	1.40563	32.355	26.561
3	359	4.40000	1.29677	21.913	18.310
3a	370	4.39702	1.29488	21.841	18.255
middle C	415	4.26313	1.21182	18.710	15.838
2	463	4.12030	1.12784	14.819	12.706
2a	493	4.11731	1.12613	14.733	12.636
middle B	857	3.02634	0.59356	0.951	0.880
1	1221	1.93538	0.23763	0	0
0	1231	0	0	0	0

Table B-2 Aspheric departures from the spheric surface (contactlens F.Ellipse 0.6)

POINT	NO.	X(mm)	Z(mm)	D_Z(μm)	D_r(μm)
4	191	4.90232	1.55365	124.384	98.652
middle D	300	4.57641	1.37612	62.137	51.044
3	359	4.40000	1.27138	47.303	39.547
3a	370	4.39702	1.26957	47.151	39.432
middle C	420	4.24825	1.18145	39.732	33.695
2	463	4.12030	1.11037	32.289	27.694
2a	493	4.11731	1.10876	32.103	27.542
middle B	850	3.04732	0.60085	2.269	2.098
1	1221	1.93538	0.23763	0	0
0	1231	0	0	0	0

Table B-3 Aspheric departures from the spheric surface (contactlens F.Ellipse 0.9)

POINT	NO.	X(mm)	Z(mm)	D_Z(μm)	D_r(μm)
4	191	4.90452	1.48077	198.970	158.105
middle D	300	4.57912	1.31871	121.438	99.875
3	359	4.40000	1.22076	97.923	81.961
3a	371	4.39702	1.21908	97.641	81.749
middle C	420	4.25123	1.13992	83.131	70.542
2	464	4.12030	1.07477	67.889	58.268
2a	494	4.11731	1.07335	67.513	57.960
middle B	850	3.05032	0.59924	5.116	4.730
1	1222	1.93538	0.23763	0	0
0	1231	0	0	0	0

Appendix C

Phase shifting algorithm

Assume that the optical path difference between the two beams in an interferometer is changed in steps of a quarter wavelength (equivalent to a phase step of 90°), and the corresponding values of the intensity at each data point in the interference pattern are recorded in the measurement.

Let the complex amplitudes of the two interfering wavefronts at any point be, respectively,

$$\mathbf{E_A} = a \exp(-i\varphi_A), \qquad (C\text{-}1)$$

and

$$\mathbf{E_B} = b \exp(-i\varphi_B). \qquad (C\text{-}2)$$

The resultant intensity is, therefore,

$$I = I_A + I_B + 2(I_A \bullet I_B)^{1/2} \cos(\varphi_A - \varphi_B), \qquad (C\text{-}3)$$

where I_A and I_B are the intensities due to the two waves acting separately.

The term intensity is widely used as a measure of the energy. However, by international agreement, that term is being slowly replaced in optics by the word irradiance (w/m^2) [Hecht 1987]. The four values of intensity at this point are then

$$\begin{aligned} I_1 = I(0) &= a^2 + b^2 + 2ab\cos(\varphi_A - \varphi_B), \\ I_2 = I(90) &= a^2 + b^2 + 2ab\sin(\varphi_A - \varphi_B), \\ I_3 = I(180) &= a^2 + b^2 - 2ab\cos(\varphi_A - \varphi_B), \\ I_4 = I(270) &= a^2 + b^2 - 2ab\sin(\varphi_A - \varphi_B). \end{aligned} \qquad (C\text{-}4)$$

The original phase difference between the waves at this point can then be calculated from the relation

$$\tan(\varphi_A - \varphi_B) = (I_2 - I_4) / (I_1 - I_3). \qquad (C\text{-}5)$$

For details about the phase shifting algorithms, please refer to the relevant research [Creath, 1988].

BIBLIOGRAPHY

Baier, K. etc., 1994, Interferometrical testing of contact lenses and intraocular lenses, Contact, No.7, 13-16.

Bendat, J. etc., 1986, Random data analysis and measurement procedures, 2nd ed., John Wiley & Sons.

Betend-Bon, J. etc., 1992, Double grating phase stepping interferometry for testing aspherics, Pure & Applied Optics, No.1, 55-69.

Blakley, R., 1994, Testing concave surfaces with a rotating Ronchi grating, Optical Engineering, Vol.33, No.10, 3472-3475.

Born, M. & Wolf, E., 1984, Principles of optics, electromagnetic theory of propagation, interference and diffraction of light, 6th ed., Pergamon Press.

Brown, G., 1993, What industry is looking for in full field optical testing systems, Proceedings of the 2nd international workshop on automatic processing of fringe patterns, 451-500, Akademie Verlag, Bremen.

Chen, F., 1991, Quality control of the milling process using three-dimensional vision, PhD Dissertation, Auburn University.

Chiffre, L etc., 1995, Metrological limitations of optical probing techniques for dimensional measurements, Annals of the CIRP, Vol.44, No.1, 501-504.

Cho, W., etc., 1997, Stable lateral-shearing interferometer for production-line inspection of lenses, Optical Engineering, Vol.36, No.3, 896-900.

Cochran, E. etc., 1988, Combining multiple-subaperture and two-wavelength techniques to extend the measurement limits of an optical surface profiler, Applied Optics, Vol.27, No.10, 1960-1966.

Cochran, E., 1992, Limitations of phase-measuring interferometry for surfaces Characterization and testing, a review, Proceedings of SPIE, Vol. 1776, 151-157.

Creath, K., 1988, Phase-measurement interferometry techniques, in "Progress in Optics", E. Wolf ed., Vol.26, 349-393, Elsevier Science Publishers.

Creath, K. etc., 1985, Contouring aspheric surface using two-wavelength phase-shifting interferometry, Optica Acta, Vol.32, No.12, 1455-1464.

Crousen, R., 1996, Design of a manipulator for testing contact lenses, Master's thesis, Eindhoven University of Technology.

Deck, L.,1996, Vibration-resistant phase-shifting interferometry, Applied Optics, vol.35, No.34, 6655-6662.

Downs, M., 1990, A proposed design for an optical interferometry with sub-nanometric resolution, Nanotechnology, Vol.1, 27- 30.

Durand, E., etc., 1992, Phase detection deflectometry, an industrial solution for three dimensional form measurement of aspheric and spherical surfaces, Proceedings of SPIE, Vol.1781, 249-257.

Evans, C., etc., 1993, Compensation for errors introduced by non-zero fringe densities in phase-measuring interferometers, Annals of the CIRP, Vol.42, No.1, 577-580.

Evans, C., etc., 1995, Visualization of surface figure by the use of Zernike polynomials, Applied Optics, Vol.34, No.34, 7815-7819.

Fan, Y.J., etc., 1994-a, Adaptive sampling method: A new sampling method for the measurement of geometric forms, Journal of Applied Science, Shanghai Science and Technical Publishers, Vol.12, No.4, 423 - 430.

Fan, Y.J., 1994-b, Aspheric testing, Technical Report, Eindhoven University of Technology.

Fan, Y.J., etc., 1996, Stitching interferometry: principles and algorithms, Proceedings of SPIE, Vol. 2778, 1062 - 1063, Published by SPIE, Bellingham.

Fan, Y.J., etc., 1997, Stitching interferometry for the measurement of aspheric surfaces, Annals of the CIRP - Manufacturing Technology, Vol. 46, No.1, 459 - 462.

Fletcher, R., 1990, Practical methods of optimization, Chichester: Wiley-Interscience.

Fowles, G., 1968, Introduction to modern optics, Holt, Rinehart and Winston, Inc.

Fraleigh, J. B., etc., 1987, Linear algebra, Addison-Wesley Publishing Company.

Françon, M., 1966, Optical interferometry, Academic Press.

Gestel, M. van., 1997, Feasibility study on Foucault knife-edge test of aspheric lenses, Master's thesis, Eindhoven University of Technology.

Glatt, T., etc., 1988, Moiré deflectometry - ray tracing interferometry, Optics & Lasers In Engineering, Vol.10, No.8, 277- 320.

Gasvik, K., 1987, Optical metrology, John Wiley & Sons.

Greivenkamp, J., etc., 1987, Sub-Nyquist interferometry, Applied Optics, Vol.26, No.24, 5245-5258.

Greivenkamp, J., 1987, Interferometric measurements at Eastman Kodak company, Proceedings of SPIE, Vol.816, 212-227.

Groot, P. de., etc., 1996, Industrial inspection interferometer having a large equivalent wavelength, ASPE Proceedings, vol.14, 350-352.

Hardy, J., etc., 1987, Shearing interferometry, a flexible technique for wavefront measurement, Proceedings of SPIE, Vol.816, 180-195.

Hariharan, P., 1987, Interferometric metrology, current trends and future prospects, Proceedings of SPIE, Vol.816, 2-18.

Hariharan, P., 1992, Basics of interferometry, Academic Press, Inc.

Hecht, E., 1987, Optics, 2nd ed., Addison-Wesley Publishing Company.

Heimbeck, H., etc., 1995, High-precision surface shape testing by means of an interferometric sensor, Optical Engineering, Vol.34, No.9, 2719-2723.

Hewlett-Packard, 5528 Laser measurement system, User's Guide.

Ho, C. S., etc., 1992, Aspheric surface testing using two-wavelength Shack interferometer, Technical Report, 25-35.

Honda, T., 1987, Measurement of deep aspheric optical surfaces by radial shear interferometer, Proceedings of SPIE, Vol.813, 351- 354.

ISO, 1993, International vocabulary of basic and general terms in metrology, International Organisation for Standardisation.

Igarashi, S., 1992, 3D measurement of shape by projection method using special grating pattern, Int. Journal of JSPE, Vol.26, No.2, 128-133.

Kim, S., etc., 1992, Moiré topography by slit beam scanning, Applied Optics, Vol.31, No.28, 6157-6161.

Komrakov, B., 1994, Method of interference testing of optical components with aspheric surface, J. of Optical Technology,Vol.61, No.3, 251-252.

Kreis, Th., etc., 1993, A comparison of interference phase determination methods with respect to achievable accuracy, Proceedings of the 2nd international workshop on automatic processing of fringe patterns, 51-59, Akademie Verlag, Bremen.

Kreske, K., etc., 1988, Insights on moiré deflectometry, Lasers & Optronics, Vol.7, No.10, 63-66.

Küchel, M.,1991, Advances in interferometric wavefront-measuring technology through the direct measuring interferometry method, Proceedings of SPIE, Vol.1573, 159-162.

Kunzmann, H., etc., 1993, Scales vs. laser interferometers performance and comparison of two measuring systems, Annual of the CIRP, Vol.42, No.2, 753-767.

Lin, D., etc.,1991, Profile measurement of an aspheric cylindrical surface from retroreflection, Applied Optics, Vol.30, No.22, 3200-3204.

Liu, Y., etc., 1988, Subaperture testing of aspheres with annular zones, Applied Optics, Vol.27, No.21, 4504-4513.

Lowman, A., etc., 1993, Interferometer induced wavefront errors when testing in a non-null configuration, Proceedings of SPIE, Vol.2004, 173-180.

Lowman, A., 1996, Calibration of non-null interferometer for aspheric testing, Ph.D. dissertation, The University of Arizona.

Malacara, D., 1993, Optical shop testing, 2nd ed., New York, John Wiley & Sons.

Massie, N. A. ed., 1988, Critical review of optical science and technology: Interferometric metrology, Proceedings of SPIE, Vol. 816, SPIE Press, Bellingham.

Matsumoto, T., etc., 1995, Sensitivity-variable moiré topography with a phase shift methods, Optical Engineering, Vol.35, No.6, 1754-1760.

Melozzi, M. etc., 1995, Vibration-insensitive interferometer for on-line measurements, Applied Optics, Vol.34, No.25, 5595-5601.

Melozzi, M. etc., 1993, Testing aspheric surfaces using multiple annular interferograms, Optical Engineering, Vol.32, No.5, 1073-1079.

Meyer-Arendt, J. R., 1984, Introduction to classical and modern optics, 2nd ed., Prentice-Hall, Inc., Englewood Cliffs, New Jersey.

Möller-Wedel, 1995, Interferometer V-100 / P users' manual, Technical Archive.

Nergo, J., 1984, Subaperture optical system testing, Applied Optics, Vol.23, No.12, 1921-1930.

Nomura, T., 1993, Shape measurement of workpiece surface with one-plate interferometer during machine running, Precision Engineering , Vol.15, No.2, 86-92.

Omura K., 1988, Phase measuring Ronchi test, Applied Optics, Vol.27, No.3, 523-528.

Oreb, B etc., 1993, Contouring the shape of contact lenses by projected fringe profilometer, Proceedings of SPIE Vol.1983, 912-954.

Otsubo, M etc.,1994, Measurement of large plane surface shapes by connecting small-aperture interferograms, Optical Engineering, Vol.33, No.2, 608-613.

Patorski, K., etc., 1993, Handbook of the moiré fringe technique, Elsevier Science Publishers.

Papp, Zs., etc.,1993, Computer aided measuring the shape of aspherical lenses, Proceedings of the 2nd international workshop on automatic processing of fringe patterns, 165-174, Akademie Verlag, Bremen.

Paul, R .P., 1982, Robot manipulators, mathematics, programming, and control, The MIT Press.

Pfeifer, T., etc.,1992, Testing aspherics without rotational symmetry using a Fizeau interferometer with computer generated holograms, Proceedings of SPIE, Vol.1781, 216-223.

Pfeifer, T., etc., 1995, Generalized aspects of multiple-wavelength techniques in optical metrology, Annals of the CIRP, Vol.44, No.1, 493 -496.

Post, D.,1991, Moiré interferometry, advances and applications, Experimental Mechanics, Vol.31, No.3, 276-280.

Prast, G.,1987, Quantitative measurement by the Schlieren method, Philips Technical Review, Vol.43, No.7, 184-191.

Roberts, C.,1994, Characterization of the inherent error in a spherically-biased corneal topography system in mapping a radically aspheric surface, Jl. of Refractive & Corneal Surgery, Vol.10, 103-116.

Sandstorm, T., etc., 1995, Large-area high quality photomasks, Proceedings of SPIE, Vol.2621, 312-318.

Sasaki, K., etc., 1990, Optical aspheric surface profiler using phase shift interferometry, Proceedings of SPIE, Vol. 1332, 97-106.

Sasaki, O., ect.,1995, Exact measurement of flat surface profiles by object shifts in a phase-conjugate Fizeau interferometer, Optical Engineering, Vol.34, No.10, 2957-2963.

Schlewitt, C., 1994, Möller interferometer for optical metrology, Technical Report.

Schmit, J. etc., 1995, Extended averaging technique for derivation of error-compensating algorithms in phase-shifting interferometry, Applied optics, Vol. 34, No. 19, 3610-3619.

Schulz, G., 1988, Aspheric surfaces, in "Progress in Optics", E. Wolf ed., Vol.25, 394- 415, Elsevier Science Publishers.
Selberg, L., 1987, Interferometer accuracy and precision, Proceedings of SPIE, Vol. 749, 8-18.

Sharma, S. K., etc., 1990, The eikonal approximation revisited, Nuovo Cimento D, Vol. 12D, No.6, 719-48.

Simons, C., 1969, The application of eikonal functions in the practice of optical design, PhD Dissertation, Delft University of Technology.

Smirnov, A.P.,1995, Analysis of misalignment-induced aberrations of optical systems within the framework of the Seidel eikonal theory, Optics & Spectroscopy Vol. 78, No.1, 165-171.

Stahl, P.,1990, Aspheric surface testing techniques, Proceedings of SPIE, Vol.1332, 66-76.

Stavroudis, O. N., 1972, The optics of rays, wavefronts, and caustics, Academic Press.
Stedman, M., 1987, Basis for comparing the performance of surface-measuring machines, Precision Engineering, Vol. 9, No.3, 149-152.

Stuhliner, T.,1986, Subaperture optical testing, experimental verification, Proceedings of SPIE, Vol.656, 118-127.

Sullivan, P., etc., 1995, A method for the spatial calibration of a commercial phase measuring interferometer-theoretical aspects, Intl. J. Mach. Tools. Manufacturing, Vol.35, No.2, 293-100.

Sullivan, P., etc., 1996, Stitching of equatorial profiles for extended spatial range assessment, Proceedings of SPIE, Vol. 2775, 67-73.

Suzuki, H., etc. 1995, Development of an on-machine aspheric form measurement system, Journal of the JSPE vol. 61, No. 11, 1594-1598.

Tannock, J.,1992, Automating quality systems, Chapman & Hall.

Tiziani, H., etc.,1996, Dual-wavelength heterodyne differential interferometer for high-precision measurements of reflective aspherical surfaces and steep heights, Applied optics, vol.35,No.19, 3525-3533.

Tolansky, S.,1973, An introduction to interferometry, Longmans, London.

Velzel,C.H.F.,1987, Image formation by a general optical system, using Hamilton's method, J. Opt. Soc. Am. A, Vol.4, No.8, 1342-1348.

Vorburger, T. V., etc., 1997, Industrial uses of STM and AFM, Annual of the CIRP, Vol.47, No.2.

Wan, D., 1992, Decent and defocus for testing aspheric surfaces, Proceedings of SPIE, Vol.1776, 140-150.

Whitehouse, D. J., 1994, Handbook of surface metrology, Institute of Physics Publishing.

Wyant, J. C., 1987, Interferometric testing of aspheric surfaces, Proceedings of SPIE, Vol.816, 19-39.

Wyant, J. C. etc.,1997, Large field of view, high spatial resolution, surface measurements, 7th International Conference On Metrology and Properties of Engineering Surfaces, 294-301.

Yatagai, T., etc.,1984, Aspherical surface testing with shearing interferometer using fringe scanning detection method, Applied Optics, Vol.23,No.4, 357-360.

Yatagai, T., etc.,1987, Interferometric testing technology developments and applications in Japan, Proceedings of SPIE, Vol.816, 58-78.

Yoshizumi, K., etc.,1987, Ultrahigh accuracy 3D profilometer, Applied Optics, Vol.26,No.9, 1647-1653.

Samenvatting

Het bepalen van de vorm van asferische gekromde oppervlakken met behulp van gangbare types interferometers is vaak niet mogelijk. Bij grote afwijkingen van de bolvorm wordt de dichtheid van de interferentielijnen hoger dan het oplossend vermogen van de detector; bovendien treden vervormingen van het interferogram op. Het doel van het onderzoek dat in dit proefschrift wordt beschreven, is het ontwikkelen van een meettechniek die aan deze bezwaren tegemoet komt.

We hebben een nieuwe methode ontwikkeld, "stitching interferometry" genoemd, waarmee sterk asferische oppervlakken nauwkeurig gemeten kunnen worden. De methode wordt in dit proefschrift beschreven.

Het principe van "stitching interferometry' kan als volgt worden omschreven. We maken een reeks metingen van overlappende delen van het oppervlak; deze metingen worden vervolgens aan elkaar gepast om het profiel van het gehele te meten oppervlak te verkrijgen. Dit principe is in de praktijk gebracht met behulp van een commercieel verkrijgbare Fizeau interferometer waaraan een mechanische micromanipulator van eigen ontwerp is toegevoegd, om het voorwerp tussen de deelmetingen te verplaatsen en/of te kantelen.

De bij "stitching interferometry" gevolgde procedure bestaat uit de volgende stappen. Eerst worden twee interferogrammen van delen van het voorwerp in twee verschillende posities opgenomen, zodanig dat de twee interferentie patronen een deel van het oppervlak gemeenschappelijk hebben. De posities worden zo gekozen dat de dichtheid van de interferentielijnen in beide zones laag genoeg is om door de detector te worden opgelost. Tussen de twee posities wordt het voorwerp verschoven; bij een axiaal symmetrisch voorwerp geschiedt de verschuiving langs de gemeenschappelijke symmetrie-as van interferometer en voorwerp. Dan worden de oppervlakteprofielen van de twee overlappende zones berekend uit de interferogrammen. Vervolgens worden deze profielen aan elkaar gepast met gebruik van de transformatie tussen de

twee posities. Door deze procedure meerdere keren toe te passen kan een compleet oppervlakteprofiel worden verkregen.

"Stitching interferometry" verschilt in methodiek van andere bestaande technieken. In onze methode worden eerst de interferentie patronen omgezet in oppervlakteprofielen en pas daarna worden de profielen aan elkaar gepast. De omgekeerde werkwijze zou niet tot het beoogde doel leiden. De meerderheid van de commercieel verkrijgbare interferometers gebruikt een vaste relatie tussen voorwerp en referentie; "stitching interferometry" gebruikt een aantal verschillende voorwerpsposities, elk gerelateerd aan het referentie-oppervlak.

We hebben een vijfassige micromanipulator ontworpen om drie translaties en twee rotaties uit te voeren. De voornaamste beweging, translatie langs de verticale optische as, wordt door drie symmetrische bladveren gegenereerd. Een precisie van 0.1 μm/mm in rechtheid en van 0.005 milliradiaal in karteling over de centrale 2 mm verplaatsing werd gerealiseerd. Twee laterale translaties en twee rotaties worden door elastische scharnieren gerealiseerd.

Proefondervindelijk is aangetoond dat met "stitching interferometry" sterk asferische oppervlakken kunnen worden gemeten met een onzekerheid van 0.2 μm. De asfericiteit kan daarbij variëren van enkele tot enige tientallen micrometres. We hebben de geldigheid van deze methode experimenteel geverifieerd.

"Stitching interferometry" is bruikbaar voor het accuraat meten van sterk asferische oppervlakken. De methode kan worden gebruikt om gangbare types interferometers te verbeteren.

Acknowledgements

This dissertation would never have been completed successfully without the whole-hearted support of my thesis supervisors. I am very grateful to my first promotor, Professor Piet Schellekens, who offered me the opportunity to pursue my PhD program with the Precision Engineering Group and provided valuable technical and personal guidance. My special thanks also go to Dr. Chris Velzel, my copromotor and good friend, for his vital support and generous guidance. I highly appreciate his contributions to my work and our pleasant co-operation.

I would thank all other reading committee members, Dr. Bob Timmermans and Profs. H. F. van Beek, J. E. Rooda and M. J. W. Schouten, who reviewed the manuscript and made valuable suggestions. I am much obliged to Professor Robert Spragg who helped with my English for this thesis as well as offering many technical comments.

In the Precision Engineering group, many people have provided their invaluable help. Many thanks are due to Klaas Struik who spent many hours with me for discussion and who made contributions to the project. Distinctive thanks are due to my good friends and fellows, Wim Weekers, Wouter Pril and Serge Wetzels, who are so kind to offer me continuously a great deal of help, both technically and personally. I am even obliged to other colleagues, Wim van Vliet, Greet Aarts, Harry Sonnemans, Frits Theuws, Leon Levasier and Han Haitjema. Moreover, I should acknowledge the helpful assistance of Jarl Buskop and Roger Crousen.

I am indebted to those who also involved in the research work, especially to Charlotte Groothuis for optical simulation, Jac Cauwenberg for the manipulator, Douwe Overdijk and his students, Alberto Capellini and Arie van de Velde, for the mathematical analyses.

It is a pleasure to thank for the financial and technical support from the Dutch company Procornea and the German company Möller-Wedel. Particularly, I would like to thank

Mr. Ben Wanders and Dr. Carsten Schlewitt for their continuous support and valuable help.

As an overseas Chinese, I would like to thank those who offered their help and encouragement during the course of my stay so far in the Netherlands. I am much obliged to Junmin Wang for his valuable help. Also, I greatly appreciate the friendliness of Leo Janssen and his family. Furthermore, I would offer my thanks to Zhu Li, Xiangqian Jiang, Yaxi Zhou, Dangti Fu, Hualing Chen, Jianzhong Tang, Xuyuan Chen, Xianwen Lou, Zhuoxian Zhao and Yuanzhong Lei.

Furthermore, I consciously understand that I owe my parents my gratitude greatly, since only with their love, concern and understanding was it possible for me to accomplish this research.

Finally, I am most happy to give my cordial thanks to my wife, Sumei, and our daughter, Huanhuan (Bonnie). They left all their relatives, friends and life familiar to them to join me here. Without their love, encouragement and sacrifice, I could not complete this PhD thesis.

Curriculum Vitae

Yu Jian Fan was born on July 19, 1955 in Shaanxi, China.

He had a relatively agreeable time of childhood that was unfortunately terminated by the beginning of the so-called “Great Cultural Revolution" in 1966. Before he could further his secondary school education, he worked first as a mechanical apprentice in a workshop for one year till 1969. After graduating from a secondary school, he lived through a very special experience with farmers and workers in the countryside for three years until 1977. This was owing to the situation at that time. During this period, he undertook both agricultural farm work and mechanical manufacturing work, which taught him a considerable amount about life and engineering.

It was at the end of 1977 when he finally captured an opportunity to enter into Xi’an Jiaotong University, benefiting from the termination of the cultural revolution. In this distinguished university, he received his Bachelor’s degree in Manufacturing and Production Automation in February 1982 and his Master’s degree in Manufacturing Metrology in September 1984, respectively. While working afterwards in the Mechanical Engineering Faculty of that university he was relatively quickly promoted from an assistantship to a lectureship and then to an associate professorship. As either a project leader or a primary worker, he accomplished some 10 projects and won some 10 awards of science and technology with his colleagues. Arranging and delivering three university courses to the students, graduate students and vocational trainees were his major teaching task.

In Autumn 1993, he went to Eindhoven University of Technology in the Netherlands. His multidisciplinary knowledge of mechanical and optical engineering and that of western cultures and behaviours have been enlarged greatly. Under the supervision of Professor Piet Schellekens and Dr. Chris Velzel, he works at the Precision Engineering Group with the subject on “Stitching Interferometry for Accurate Measurement of Curved Surfaces”, which results in this PhD dissertation.

Stellingen
behorende bij het proefschrift

Stitching Interferometry for Accurate Measurement of Curved Surfaces

Yu Jian Fan

1. In order to obtain enough information and perform manufacturing metrology, we make use of all our senses. However, we cannot rely only on our physical senses because of their limitations and unavailability in certain cases.

   this dissertation

2. People develop multiform instruments to improve our detecting abilities. Unfortunately, most of such instruments work in only one sense. It would be very attractive to develop kinds of creative instruments making use of visual, touching and hearing senses comprehensively.

   based on my research experience

3. Precision engineering is the multidisciplinary science underlying the development and realisation of high precision machines, instruments and communication devices. There is an important trend to develop precision engineering as the interdisciplinary integration of precision metrology, precision manufacturing and design for precision, instead of developing each of those fields separately.

   this dissertation

4. The development of traceable nano-metrology is urgently needed. These needs are supported strongly by the fast development of all kinds of nano-measuring equipment such as STM, AFM and nano-displacement sensors.

   based on my research experience

5. From the measurement viewpoint of degree of freedom, the capability of an interferometer is restricted proportionally by the ratio of degrees of freedom available with the instrument to the degrees of freedom needed to perform a measurement.

   this dissertation

6. Engineers solve real-world problems using scientific principles from disciplines that include mathematics, physics, computer science, chemistry, and biology. It is this variety of subjects, and the challenge of real problems, that makes engineering so interesting and so rewarding.

this dissertation

7. It is interesting to recognise the differences between western and eastern philosophies. Westerners emphasise individuality much more than the easterners do. One proof is the fact that a westerner places his own given name in front of his family name while his eastern counterpart puts the family name first.

based on my observation

8. 天下事有难易乎? 为之, 则难者亦易乎; 不为, 则易者亦难乎.

荀子, 中国古代哲学家和思想家

translation:

How difficult is it to do something in the world? If you try to do it, you may make a difficult thing easier. On the other hand, if you never try to do it, you may make an otherwise easy task more difficult.

XunZi, a Chinese philosopher (2000 years ago)

9. It is people who should try their best to take charge of whatever they want to do, whereas it is not only people who can entirely determine whether a good wish can come true or not.

based on my living belief

10. Everything in the world has two sides. Each side may turn to its opposite under certain conditions.

a Chinese proverb